Boston University

OpenBU **http://open.bu.edu**

Theses & Dissertations Boston University Theses & Dissertations

2016

Effects of pharmacological manipulations on activity in the medial entorhinal cortex

https://hdl.handle.net/2144/16727

Boston University

BOSTON UNIVERSITY

SCHOOL OF MEDICINE

Dissertation

EFFECTS OF PHARMACOLOGICAL MANIPULATIONS ON ACTIVITY IN THE MEDIAL ENTORHINAL CORTEX

by

CAITLIN KELLY MONAGHAN

B.S., University of Oregon, 2008
M.S., University of Oregon, 2010

Submitted in partial fulfillment of the

requirements for the degree of

Doctor of Philosophy

2016

© 2016
CAITLIN KELLY MONAGHAN
All rights reserved

Approved by

First Reader _____

Michael E. Hasselmo, D. Phil.

Professor of Psychological and Brain Sciences

Second Reader _____

Shelley Russek, Ph.D.

Professor of Pharmacology & Experimental Therapeutics

Epigraph

"The pursuit of knowledge is hopeless and eternal." -Professor Farnsworth, Futurama

DEDICATION

Dedicated to my mother,

Barbara Jean Monaghan

March 25, 1952 – October 31, 2010

ACKNOWLEDGMENTS

In a way, the acknowledgements section is one of the more difficult parts of a dissertation to write. The citations to corroborate the support I have received are intangible and unquantifiable. I can only attempt to qualitatively express the gratitude I have towards the many people who have been paramount in me reaching this point and I hope that I can adequately express their significance through words instead of numbers.

I have been incredibly lucky to have two amazing advisors throughout my scientific career thus far. First and foremost, Dr. Michael Hasselmo has been an inspiration ever since I joined the lab. His love of science, search for truth, and expansive knowledge has been intellectually motivating and exciting to witness. He has been a role model through his work ethic, somehow finding a way to balance an incredible number of obligations that I cannot begin to representatively list, with always being available to talk and offer feedback on even the most miniscule aspects of the work. His constant support, patience, and kindness have been instrumental to my success and perseverance.

None of this could have even initially happened without the support and encouragement from my undergrad and Masters advisor and PI, Dr. Cliff Kentros. He actually told me no when I first asked to join the lab, teaching me my first lesson about the hard work and determination required to be successful in this field. I eventually convinced him to give me a shot and was given the incredible opportunity to experience the magic of single-unit recordings in behaving animals, something I still sometimes step back and marvel at even after all these years of using this method. I will always be

grateful to him for taking a chance on this eager undergrad and his continued support to this day.

I want to thank my committee members: Dr. Howard Eichenbaum, Dr. Shelley Russek, Dr. David Farb, and Dr. Matthew Wilson for agreeing to serve on my committee and the expansive backgrounds and perspectives they contribute. The comments and feedback I have received from them have shaped the direction of my work and without a doubt, made it much stronger.

I've been incredibly lucky to be surrounded by such amazingly intelligent and supportive lab mates. I've truly enjoyed the opportunity to work with the many lab members throughout the years and my work would be radically different, if even existent, without them. I can't thank Dr. Mark Brandon enough for teaching me his grid cell whispering secrets, and for his patience throughout the years even after he has moved on to build an incredibly successful career to always be available. Without his advice and support from when I first stepped into the lab through now, I would be completely lost. I also especially want to thank my lab mate, Jason Climer, who I've had the joy of entering the program with in the first Graduate Program for Neuroscience class and navigated these six years with. I can't imagine going through this without his friendship, constant support, and intellectual guidance. Huge thanks to our lab programmer Bill Chapman, who has been invaluable in the analyses of these data; I could not have done this without his hard work and seemingly never-ending patience. Thank you to the lab managers/technicians over the years: Tyler Ware, Elijah Petter, Eri Yamaguchi, and Ron DiTullio. They have helped with nearly every aspect of my work, and I am especially

grateful for their help with the time consuming and unavoidably frustrating construction of the recording drives, along with keeping the lab running smoothly and compliantly. Thank you for the support and collaboration of all the current and past Hasselmo lab members, including Dr. Jake Hinman, Dr. Ehren Newman, Dr. Christopher Shay, Dr. Jim Heys, Dr. Eric Zilli, Dr. Nathan Schultheiss, Andrew Bogaard, Dr. Yusuke Tsuno, Dr. Kishan Gupta, and so many others too numerous to list. Lastly, thank you to the two extremely talented undergrads I had the pleasure of working with: Win Gillis and Anna Stopa, who helped tremendously over the years.

Perhaps the most difficult to articulate is my overwhelming gratitude towards all my friends and family who have always supported and believed in me. My friends and teammates have given me so much by the way of confidence, love, support, and periodic reminders that what I do is actually really, really cool and impressive.

I could write pages more just in an attempt to explain how much my family has given me through love and unconditional support but still not begin to adequately express it. My incredibly intelligent brothers forced me into developing a quick wit and intellect just to keep up with them, along with the ability to tune out never-ending political discourses, which I will be forever grateful for. Lastly but most importantly of all, my parents always believed in me and very firmly attested that I could achieve whatever I set my mind to. Their unwavering support and absolute assuredness of this gave me the confidence to explore whatever areas I happened to be interested in. Because of this I never grew up thinking I didn't belong in science or math or even sports, it was always established as a ground truth that I was capable of achieving what I wanted to. My

parents had always been my #1 supporters, even when I gave them reasons not to be, and because of this constant love I know how proud my mother would have been to see me achieve this. My father has been a rock throughout my life and taught me the work ethic that has allowed me to reach this point. Cliché or not, words cannot express the amount of love and respect I have for him, and for all he has given and taught me throughout my life.

Without all of these influences and forces in my life, this would be nothing.

EFFECTS OF PHARMACOLOGICAL MANIPULATIONS ON ACTIVITY IN THE MEDIAL ENTORHINAL CORTEX

CAITLIN KELLY MONAGHAN

Boston University School of Medicine, 2016

Major Professor: Michael E. Hasselmo, D. Phil., Professor of Psychological and Brain Sciences

ABSTRACT

Animal research involving the effects of anxiolytics on theta oscillations has focused on changes in theta frequency in the hippocampus, rather than effects in medial entorhinal cortex (MEC), which provides the cortical input to the hippocampus and is the source of Type I (movement-related) theta rhythm. Neurons coding spatial location, including "grid cells," are found in the MEC and aspects of their spatial modulation have been linked to theta rhythm in different ways. Theta frequency recorded in the local field potential (LFP) is also strongly correlated with running speed and is used in specific computational models of grid cell firing.

Manipulating theta frequency through administration of anxiolytics offers a unique method of examining regulation of the LFP frequency in the MEC, along with the effects of changes in theta frequency on grid cells and other cell types in the region. In addition, the role of the medial septum (MS), which is necessary for theta rhythm in both the MEC and hippocampus, can be investigated by infusing anxiolytics directly into the MS. In this thesis, two separate anxiolytic drugs were tested: a serotonin 1A receptor agonist, 8-OH-DPAT, and a classic benzodiazepine, diazepam, the results of which are

described in chapters 2 and 3, respectively. Systemic injections of either drug caused a reduction in theta frequency across all running speeds, resulting in a decrease in the y-intercept of the linear fit to the plot of theta frequency over different running speeds. However, only MS infusion of 8-OH-DPAT, not diazepam, significantly decreased the y-intercept in the MEC.

Together, these results expand detection of anxiolytic drug action on theta frequency to a new structure, the MEC, when drugs are given systemically, but demonstrate a dissociation between drug types in their ability to produce effects when infused into the MS. Grid cell firing patterns were unaffected and very few effects were found in single unit firing across different cell types. Overall, these results support predictions made by specific computational models and highlight the involvement of the MEC in the anxiolytic-induced decrease in theta frequency phenomenon uniquely tied to the action of these drugs.

TABLE OF CONTENTS

LIST OF TABLES

LIST OF FIGURES

LIST OF ABBREVIATIONS

5-HT – 5-hydroxytryptamine (serotonin)

ACh – Acetylcholine

BDZ – Benzodiazepine

CA – Cornu Ammonis

CAN – Continuous Attractor Model

CDP – Chlordiazepoxide

CSD – Current Source Density

dbB – (vertical limb of the) diagonal band of Broca

DG – Dentate Gyrus

GABA - Gamma-Aminobutyric acid

HD – Head Direction

K+ - Potassium

LEC – Lateral Entorhinal Cortex

LFP – Local Field Potential

MEC – Medial Entorhinal Cortex

MRL – Mean Resultant Length

MS – Medial Septum

OIM – Oscillatory Interference Model

SI – Spatial Information

VCO – Velocity Controlled Oscillator

CHAPTER 1: Introduction

1.1. Spatially modulated activity

The ability to track where one is in an environment and maintain numerous mental representations of space is not only necessary for survival but also adds to the richness of one's experience. The first examples of spatially modulated cells were reported by O'Keefe and Dostrovsky (1971) when they recorded from individual units in the hippocampus in awake, behaving rats as they traversed an environment. They found that some of the isolated units would only fire action potentials when the rat was in a specific location of the environment, cells later deemed "place units" (O'Keefe and Dostrovsky, 1971; O'Keefe, 1976). Since then, research has expanded to look for navigation-related neuronal activity in other areas of the brain, such as finding cells that fire when an animal is facing a certain direction ("head direction," or HD, cells) in the presubiculum (Taube et al., 1990) and many other locations including the medial entorhinal cortex (MEC) (Sargolini et al., 2006).

More recently, spatially modulated cells were found that fire in multiple, but very specific locations in an environment ("grid cells"), residing in the dorsocaudal area of the MEC (Fyhn et al., 2004; Hafting et al., 2005) and pre- and parasubiculum (Boccara et al., 2010). Specifically, as a rat visits locations in an environment, these cells fire in a grid-like pattern corresponding to the corners of tightly packed equilateral triangles tessellating the entire traversed environment. Lastly, another type of spatially modulated cell was found that fires along borders of an environment ("border cells," in MEC and parasubiculum) (Solstad et al., 2008) or in response to boundaries ("boundary vector cells," in subiculum) (Barry et al., 2006; Lever et al., 2009). Remarkably, all of these

cells (place, grid, HD, and border/boundary cells) track changes to and across environments, by "remapping" or changing their firing rate and/or receptive fields in new environments or by matching directions of rotations made to an environment (Bostock et al., 1991; Hafting et al., 2005; Leutgeb et al., 2005; Fyhn et al., 2007; Solstad et al., 2008). All of these types of cells are found throughout the hippocampus, pre- and parasubiculum, and MEC areas of the brain; regions that unsurprisingly form a highly interconnected circuit.

1.2. Circuit of brain regions involved in representing space

The entorhinal cortex is thought to be the gateway between cortical areas of the brain and the hippocampus. Its six layers are often referred to as superficial (I-III) or deep (IV-VI). Layer IV (lamina dissecans) is largely devoid of cell bodies. The MEC is located in the caudal portion of the temporal lobe and provides almost all of the neocortical input to the hippocampus. The entorhinal cortex is commonly divided into two main regions: the caudomedial portion and the rostrolateral portion, or the MEC and the lateral entorhinal cortex (LEC), respectively (Witter et al., 1989). The MEC contains many spatially modulated cells of interest, while the LEC provides largely non-spatial and "item-oriented" input to the hippocampus (Hargreaves et al., 2005; Deshmukh and Knierim, 2011). The dorsocaudal region of MEC, where grid cells are found, receives the most cortical input from the occipital regions, with other strong innervation coming from parietal, temporal, cingulate and frontal regions as well (Burwell and Amaral, 1998). In terms of subcortical input it receives projections from mainly the claustrum and dorsal

thalamus, with a smaller percent from the amygdala, olfactory areas, medial septum, hypothalamus, ventral thalamus, and basal ganglia (Kerr et al., 2007).

1.2.1. Entorhinal-Hippocampal circuit

Superficial layers of the MEC receive the above sensory input and cells in these layers send projections targeting the hippocampus primarily via the perforant pathway. Through this pathway, the middle one third of the molecular layer of septal (dorsal) dentate gyrus (DG) and Cornu Ammonis 3 (CA3) stratum lacunosum moleculare receive a large portion of MEC projections, arising from layer II cells (Steward and Scoville, 1976; Witter and Amaral, 1991; Dolorfo and Amaral, 1998; Witter et al., 2000). Furthermore, MEC layer III cells project to the molecular layers of the proximal part (relative to the DG in the transverse plane) of CA1 and distal part of subiculum (Steward, 1976; Witter and Amaral, 1991). While deeper layers of the entorhinal cortex do make up a component of this hippocampal innervation as well, they comprise a vastly smaller portion (Witter and Amaral, 1991; Witter et al., 2000).

Within the hippocampus, information is passed from DG to CA3 to CA1, which is then passed out to the entorhinal cortex directly or through the subiculum. The DG granule cell axons (mossy fibers) provide glutamatergic input to the dendrites of CA3 pyramidal cells of the molecular layer (Blackstad and Kjaerheim, 1961; Terrian et al., 1990). CA3 then projects to CA1 via Schaffer collaterals, closing out this classic "trisynaptic loop."

In contrast to the extensive entorhinal projections throughout all hippocampal fields, projections from the hippocampus to entorhinal cortex are much more selective in

origin, arising exclusively from CA1 and subiculum. The proximal area of CA1 projects to the distal area of the subiculum, both of which project to mainly deeper layers (layers V-VI) of MEC (van Groen et al., 1986; Witter et al., 1989, 2000; Tamamaki and Nojyo, 1995; Naber et al., 2001).

The subiculum also projects to the pre- and parasubiculum (Witter et al., 1989). These areas send projections to principal neurons in all layers of the MEC (Canto et al., 2012), likely passing on head direction information from the vestibular system to the MEC through this pathway (Taube, 2007; Boccara et al., 2010).

Within the MEC, the deeper layers complete this circuit by sending mostly (but not exclusively) excitatory projections back to principal cells and interneurons in the superficial layers (Witter et al., 1989; Dolorfo and Amaral, 1998; van Haeften et al., 2003), and out to the rest of the cortex, mainly through layer V (Insausti et al., 1997).

1.2.2. Septal projections

The MEC is strongly innervated by the medial septum (MS). The MS and vertical limb of the diagonal band of Broca (dbB) provide the cholinergic input into the MEC (Alonso and Köhler, 1984), along with providing γ-aminobutyric acid (GABA)-containing (GABAergic) (Köhler et al., 1984) and glutamate-containing (glutamatergic) (Manns et al., 2001) projections. These axons from the MS/dbB project mainly to layers II and V of the MEC and the LEC, and cells in these layers also project back to the MS (Alonso and Köhler, 1984; Gaykema et al., 1990; Canto et al., 2008).

Similarly, projections from the MS also strongly innervate the hippocampus and stem from mainly cholinergic and GABAergic neurons (Köhler et al., 1984; Wainer et al.,

1985; Freund and Antal, 1988), with the cholinergic projections making up under half of the hippocampal innervation (Baisden et al., 1984; Wainer et al., 1985). GABA-containing neurons in the MS/dbB innervate GABA-containing interneurons throughout the hippocampus; activation of these afferents likely causes disinhibition of the principal cells in the hippocampus (Freund and Antal, 1988; Krnjević et al., 1988). These GABAergic projections were predominantly found in strata oriens and radiatum layers of CA3 and the hilus and granule cell layer of dentate gyrus, though some contacts were seen in all layers (Freund and Antal, 1988). Non-GABA-containing (presumably cholinergic) axons from the MS are reported to contact mostly (though not exclusively) non-GABA-containing dendritic shafts of pyramidal and granule cells though sometimes were seen in the stratum lacunosum moleculare of CA1 and CA3 (Freund and Antal, 1988).

Additionally, the hippocampus sends projections back to the MS. This pathway is made up by a majority of GABAergic projection neurons from CA1 that innervate mostly GABAergic (few cholinergic) MS cells (Toth et al., 1993) along with some MS cholinergic projection cells (Gaykema et al., 1991). Overall, these brain regions form a strongly interconnected circuit, giving rise to characteristic rhythms throughout these areas.

1.3. Prominent theta rhythmicity is found throughout these regions

Throughout the MS and hippocampal formation is a prominent 6-10 Hz oscillation, or theta rhythm, which can be found in the local field potential (LFP) and rhythmicity of single unit firing. It is particularly striking throughout the hippocampus

(Green and Arduini, 1954; Vanderwolf, 1969; Bland, 1986), MEC (Mitchell and Ranck, 1980; Alonso and García-Austt, 1987a), and MS (Petsche et al., 1962; King et al., 1998).

1.3.1. Local field potential

The LFP reflects the fluctuations in summed currents across a large number of extracellularly recorded cells. The main source of this is thought to be through the synaptic currents from many cells active during overlapping times, producing a measurable current (Buzsáki et al., 2012). Hippocampal theta rhythm is especially prominent in the LFP when rodents perform "voluntary" (as opposed to automatic) behaviors, such as walking, and during REM sleep (Vanderwolf, 1969; Whishaw and Vanderwolf, 1973; Leung, 1984). It is strongest around the hippocampal fissure, and both amplitude and phase of the oscillation change across different depths but not along the long axis of the hippocampus, ultimately resulting in a 180 degree phase difference between theta in CA1 and theta in dentate gyrus (Buzsáki et al., 1983; Bullock et al., 1990; Buzsáki, 2002). In line with the projections from MEC to hippocampus, MEC layer II theta rhythm is similar in phase to dentate theta while layer III theta aligns with CA1 theta phase, with a phase reversal occurring between layers II and III (Mitchell and Ranck, 1980).

Two types of theta rhythm with distinguishing characteristics have been identified and named based on their response to anticholinergics: Type 1 (atropine-resistant) and Type 2 (atropine-sensitive). Atropine-sensitive theta (Type 2) is slightly slower in frequency (4-7 Hz), can be found when the animal is immobile or while under urethane anesthesia, and is abolished by administration of the anticholinergic drug, atropine.

Conversely, atropine-resistant theta (Type 1) is abolished under urethane anesthesia and is found while the animal is mobile (Kramis et al., 1975). The precise mechanisms underlying Type 1 theta remain unclear (Vertes and Kocsis, 1997; Buzsáki, 2002), though extensive research on the phenomenon has provided many clues.

Current source density (CSD) analysis uses high-density recording probes to measure the currents that give rise to the LFP, by localizing current sinks (areas where positive charge enters the cells from the extracellular space) and sources (locations where positive charge leaves the neuron). In the hippocampus, recordings demonstrate a strong sink in CA1 stratum lacunosum-moleculare (which receives perforant path input) coupled with a strong source in the pyramidal layer (through somatic inhibition), along with an additional sink in stratum radiatum (mediated by CA3 Schaffer collaterals) (Leung, 1979; Buzsáki et al., 1983). Under urethane anesthesia or after bilateral removal of the entorhinal cortex, the stratum lacunosum-moleculare sink is attenuated or disappears, respectively, whereas the source-sink in the pyramidal layer and stratum radiatum are retained (Ylinen et al., 1995; Kamondi et al., 1998; Buzsáki, 2002). While deafferentation of the entorhinal cortex cortical inputs does not overtly disrupt hippocampal theta, it does render it atropine-sensitive as atropine administration abolishes the rhythm (Buzsáki et al., 1983). Furthermore, lesions of CA3 pyramidal cells do not affect hippocampal theta in CA1, even after atropine administration (Whishaw and Sutherland, 1982). Overall, these data suggest the involvement of the entorhinal cortex in specifically Type 1 theta.

The MS also plays a large role in the production of theta rhythm and is often regarded as a rhythm pacemaker. It is the common input to the hippocampus and MEC, putatively providing the atropine-sensitive theta still present after entorhinal deafferentation or lesions. MS lesions disrupt theta oscillations in both the hippocampus (Andersen et al., 1979; Rawlins et al., 1979; Sainsbury and Bland, 1981) and the MEC (Mitchell et al., 1982). Temporarily inactivating the MS pharmacologically also suppresses theta oscillations in the hippocampus (Mizumori et al., 1989) and MEC (Brandon et al., 2011; Koenig et al., 2011). Simultaneous hippocampal infusions of carbachol, a non-selective cholinergic agonist, and bicuculline, a GABA-A receptor antagonist, reverses the effect of MS inactivation in the hippocampus (Colom et al., 1991), highlighting the importance of both cholinergic and GABAergic roles in the circuit.

1.3.2. Single unit rhythmicity

Theta rhythmicity can also be found in the rhythmic firing of action potentials by single neurons. Cells in the MS (Petsche et al., 1962; King et al., 1998), hippocampus (Ranck, 1973), and MEC (Mitchell and Ranck, 1980) show theta rhythmicity in the autocorrelations of their spiking. This rhythmic spiking coincides with phases of theta recorded in the LFP. In the hippocampus in urethane anesthetized animals, CA1 pyramidal cells fire around the trough of CA1 pyramidale theta (peak of dentate theta) while interneurons show the inverse relationship, firing at opposite phases unless driven recurrently by sharp waves (Buzsáki et al., 1983; Fox et al., 1986; Skaggs et al., 1996). However, in the dentate gyrus, granule cells and most interneurons fired at the peak of

dentate theta, leading CA1 pyramidal cells by about 90 degrees (Buzsáki et al., 1983). In the MS, putative GABAergic pacemaker cells fire synchronously with hippocampal theta, albeit with different phase relationships in comparison to other nearby MS theta cells (Petsche et al., 1962; Gogolák et al., 1968; King et al., 1998). Neurons in the MEC also fire phase locked to theta oscillations (Mitchell and Ranck, 1980; Alonso and García-Austt, 1987b; Chrobak and Buzsáki, 1998). Theta rhythmic cells in layers II and III demonstrate phase locking to the negative phase of CA1 theta (positive peak of dentate theta) (Quirk and Stewart, 1988; Stewart et al., 1992).

Some cells fire action potentials progressively earlier in relation to theta phase across successive cycles as the animal travels through a given cell's receptive field, deemed phase precession. This was first reported in place cells (O'Keefe and Recce, 1993; Skaggs et al., 1996) and has been found in grid cells as well (Hafting et al., 2008; Climer et al., 2013). Evidence suggests that the MEC plays a critical role in this firing pattern since grid cells still phase precess after hippocampal inactivation (Hafting et al., 2008) whereas MEC inactivation disrupts this phenomenon in place cells (Schlesiger et al., 2015). Furthermore, resetting the phase of hippocampal theta by briefly inhibiting recorded cells via electric shock led to the cells returning to fire at appropriate phases of theta for the given location of the animal, suggesting the involvement of extrinsic mechanisms (Zugaro et al., 2005). MS inactivation greatly diminishes theta rhythmicity in hippocampal (Koenig et al., 2011) and MEC (Jeffery et al., 1995; Brandon et al., 2011; Koenig et al., 2011) neurons, highlighting its role in pacemaking these two anatomical targets.

1.4. Theta rhythm is also involved with representing space

Theta rhythm has been linked to aspects of navigation in a number of ways. In order to effectively track changes in position, for example as reflected in the precession of theta rhythmic spikes to earlier phases of LFP theta as an animal passes through a spatial firing field, it must be able to account for changes in speed. In fact, LFP theta frequency is strongly correlated with running speed in both the hippocampus (Sławińska and Kasicki, 1998) and MEC (Jeewajee et al., 2008). Furthermore, different types of cells that track aspects of navigation, such as place cells, grid cells, head direction cells, and border/boundary cells show theta rhythmicity in their firing and are often phase locked or precess in relation to LFP theta (O'Keefe and Recce, 1993; Skaggs et al., 1996; Hafting et al., 2008; Solstad et al., 2008; Mizuseki et al., 2009; Boccara et al., 2010). Temporarily inactivating the MS pharmacologically reduces MEC theta power and disrupts the spatially periodic firing pattern of grid cells in the MEC (Brandon et al., 2011; Koenig et al., 2011).

1.4.1. Grid scale and theta rhythm

The receptive fields, or grid fields, of grid cells increase in size and spacing (grid scale) along the dorsal to ventral axis of the MEC (Brun et al., 2008). This scale increase along the axis correlates with the period of the subthreshold membrane potential oscillation recorded in layer II MEC stellate cells *in vitro* (Giocomo et al., 2007). Furthermore, the frequency of the rhythmicity of grid cell firing is inversely correlated with increasing grid field sizes (Jeewajee et al., 2008). Grid scale also increases in response to a novel environment, while the rhythmicity of firing decreases in frequency

(period increases) (Barry et al., 2012). MEC theta frequency is positively correlated with running speed (Jeewajee et al., 2008); the slope of this relationship decreases in the hippocampus when an animal is introduced to a new environment (Wells et al., 2013). This could be in response to increased acetylcholine (ACh) levels as novelty has been linked to increased hippocampal release of this neuromodulator (Inglis et al., 1994; Acquas et al., 1996). Furthermore, muscarinic ACh receptor activation decreases the frequency of subthreshold oscillations and membrane potential resonance of MEC layer II stellate cells (Klink and Alonso, 1997; Heys et al., 2010). Similar to the novelty-induced decrease in slope, multiple same day exposures of a rat to a familiar environment can produce small increases in slope of MEC firing to running speed with each exposure, in both the hippocampus and the MEC (Jeewajee et al., 2008; Newman et al., 2013; Wells et al., 2013).

1.5. Computational models

A number of computational models exist that offer explanations of mechanisms underlying spatial representation in the brain, offering testable hypotheses to potentially support their theories. In the grid cell literature, two classes of models were borrowed from place cell models to explain this phenomenon: oscillatory interference models (OIMs) (O'Keefe and Recce, 1993; O'Keefe and Burgess, 2005) and continuous attractor network (CAN) models (Samsonovich and McNaughton, 1997). While they tend to be contrasted against each other, these models are not necessarily mutually exclusive as they approach the phenomenon through different but not inherently contradictory methods. In fact, the addition of features from CAN models to OIMs could improve aspects of OIMs

(Burgess, 2008; Bush and Burgess, 2014). Iterations of models within each class have attempted to explain biological data to varying degrees of success, and more recently have inspired different, hybrid models to emerge.

1.5.1. Oscillatory interference models

OIMs take advantage of the prominent theta oscillations present throughout the hippocampus and entorhinal cortex, found in both the LFP and in the rhythmicity of single units. The general principle behind these models is that two slightly different oscillations, for example found in the LFP and in a given cell's subthreshold membrane potential oscillations, produce constructive and deconstructive interference when the peaks of their oscillations align or cancel out, respectively. During times of peak alignment, this drives the given neuron to spike, producing a grid like pattern (via various mechanisms depending on the model). Importantly, both oscillations must increase in frequency with running speed in order to maintain consistent firing patterns regardless of velocity (though at different rates of increase), matching biological data (Jeewajee et al., 2008). Specifically, the general model states that LFP theta reflects the mean theta frequency of all velocity controlled oscillators (VCOs), or cells in which the membrane potential oscillation increases with movement velocity in a preferred direction (Burgess et al., 2007; Burgess, 2008; Jeewajee et al., 2008). Therefore, while LFP theta increases with running speed, the intrinsic theta rhythmic frequency of grid cells increases faster as it is driven by the currently active VCOs that have a preferred direction aligned with the current running direction of the rat (Burgess, 2008; Jeewajee et al., 2008). These models use these different oscillation frequencies to produce the different scales of grid cell

firing found along the dorsoventral axis, and predicted the later finding that frequency of intrinsic subthreshold membrane potential oscillations decreases in cells along this axis (O'Keefe and Burgess, 2005; Giocomo et al., 2007).

Based on the OIM, Burgess (2008) suggested that the different mechanisms underlying the two components of theta, Type 1 (atropine-resistant) and Type 2 (atropine-sensitive), are also separately involved with the slope and intercept, respectively, of the relationship between theta frequency and running speed (Burgess, 2008). A change in the slope, but not the intercept, of this relationship is predicted to produce a change in grid scale, relating to specifically atropine-resistant theta. While the MS plays a role in both components, the MEC is involved in atropine-resistant as well. This prediction is supported by the findings that exposure to a novel environment increases grid scale and decreases the slope of hippocampal theta frequency plotted across running speeds (Barry et al., 2012; Wells et al., 2013).

1.5.2. Continuous attractor network models

The finding that nearby grid cells share similar scale and orientation but offset phases suggests the possibility of local recurrent connections influencing activity. Broadly, CAN models utilize this through modeling a sheet of connected cells with a traveling activity bump activating specific cells, tracking the animal's running speed and direction (Fuhs and Touretzky, 2006; McNaughton et al., 2006; Guanella and Verschure, 2007; Burak and Fiete, 2009). Each of these sets of grid cells would be independent from the other, a notion that could be supported by the evidence that different modules exist

throughout the MEC dorsoventral axis and respond differently to environmental manipulations (O'Keefe and Burgess, 2005; Stensola et al., 2012).

1.5.3. Hybrid models

Hybrid models often utilize aspects of both CAN models and OIMs to generate grid cell firing patterns. Bush and Burgess (2014) explicitly combine the two models, while another model uses an interaction of traveling waves, using feedback from the grid cell population to the individual traveling wave inputs to produce attractor dynamics (Hasselmo and Brandon, 2012; Hasselmo and Shay, 2014). One criticism of CAN models has been the inability to inherently produce phase precession, which was obtained using a hybrid model by Navratilova et al. (2012) through rebound activity from an afterdepolarization effect from previous spiking activity. Hasselmo (2014) combined rhythmic input from the MS to generate rebound spiking activity in the MEC with the different resonance properties found in MEC neurons to produce spatially periodic firing with different grid field scales.

1.6. Anxiolytic effects on theta frequency

While grid field spacing and mean theta frequency have been correlated, evidence suggests it is not simply the decrease in mean that is important, but the effect on the dissociable components of theta frequency: the intercept and slope of the relationship of theta frequency across running speeds. Type II theta is present during arousal and anxiety (Sainsbury et al., 1987), which Burgess (2008) links to the intercept. Since the OIM predicts that slope influences grid field scale, a decrease in mean theta frequency

through effects on the intercept would not affect grid field scale. This can be directly tested through the use of anxiolytics. Systemic administration of anxiolytics, such as benzodiazepines (BDZs) and serotonin 1A receptor (5-HT1A) agonists reduces the frequency of theta rhythm recorded in the hippocampus (McNaughton et al., 1986; Coop and McNaughton, 1991; Wells et al., 2013). Specifically, they both reduce the y-intercept of the relationship between theta frequency and running speed (Wells et al., 2013). Based on predictions by Burgess (Burgess, 2008; Wells et al., 2013), systemic administration of anxiolytics should impact only Type II theta because Type II theta is altered by arousal and anxiety, and therefore Burgess predicts that anxiolytics should reduce the intercept of the theta frequency correlations across running speeds and leave grid field scale intact.

The mechanisms underlying the effects of anxiolytics on theta frequency are still unclear. It is difficult to pinpoint exactly what produces the decrease in frequency, considering different classes of anxiolytics work through entirely different neurotransmitter systems. Furthermore, they are independent in that antagonists preventing effects within their own class have no effect outside their type. The 5-HT1A antagonist, pindolol, reduces the effect of 5-HT1A agonists, 8-OH-DPAT and buspirone, but not the benzodiazepine, chlordiazepoxide (CDP) (Coop and McNaughton, 1991; Coop et al., 1992). Similarly, the benzodiazepine receptor antagonist, flumazenil, decreases the effect of CDP, but has no effect on the 5-HT1A agonist, buspirone (Coop et al., 1992).

Despite working through entirely different neurotransmitter systems, both classes of anxiolytics have similar effects on hippocampal theta (McNaughton and Coop, 1991), though it is not known if they similarly impact activity in the MEC or if these effects are mediated through the MS, which provides theta rhythmic input to the MEC and hippocampus. In the experiments presented here, the potential influence of anxiolytics on the physiology of the MEC will be tested by infusing anxiolytics directly into the MS and comparing changes in MEC activity to effects of systemic injections of the same anxiolytics.

CHAPTER 2: Effects of systemic administration and MS infusion of a serotonergic anxiolytic on MEC activity[1]

[1]Monaghan CK, Chapman IV GW, Hasselmo ME. In prep.

2.1. Introduction

Research involving the effects of anxiolytics on theta oscillations has focused on changes in theta frequency within the hippocampus, with very little on the effects on medial entorhinal cortex (MEC) activity, which provides the cortical input to the hippocampus and is reportedly the source of Type I theta oscillations (Buzsáki et al., 1983). Furthermore, strikingly spatially modulated cells, grid cells, are found in the MEC and have been correlated in many ways to theta frequency (Hafting et al., 2005; Giocomo et al., 2007; Jeewajee et al., 2008; Barry et al., 2012). The serotonin (5-hydroxytryptamine, 5-HT) 1A receptor agonists make up a separate class of anxiolytics that work through a completely different system than the classic BDZs. While they offer the same benefits of the standard anxiolytics and also reduce hippocampal theta frequency, they do so through non-GABAergic mechanisms (McNaughton and Coop, 1991; Coop et al., 1992).

5-HT1A receptors appear in high concentrations throughout the medial septum (MS), which provides theta rhythmic input to both the MEC and the hippocampus, as well as within the MEC and hippocampus (Pazos and Palacios, 1985; Kia et al., 1996; Lüttgen et al., 2005). Activation of 5-HT1A receptors mediates inhibitory transmission through G-protein-coupled potassium (K+) channels (Hoyer et al., 2002). In the raphe nuclei, which provide serotonergic innervation throughout the brain, 5-HT1A receptors are somatodendritic and activation of these autoreceptors has an inhibitory effect on the presynaptic neuron (Vergé et al., 1985; Sprouse and Aghajanian, 1987). 5-HT1A receptors are also located postsynaptically on different neuron types throughout the brain,

including cholinergic and GABAergic cells in the MS, and activation of these receptors has a hyperpolarizing effect (Kia et al., 1996; Hoyer et al., 2002; Lüttgen et al., 2005).

The MS, hippocampus, and MEC receive dense innervation from the median raphe nuclei, through both serotonin- and non-serotonin-containing processes (Köhler and Steinbusch, 1982; Köhler et al., 1982). Furthermore, the same neuron in the raphe may influence downstream activity in both the hippocampus and the MEC simultaneously, suggesting potential similarities in modulation of activity (Köhler and Steinbusch, 1982). Infusion of serotonergic agonists into the median raphe disrupts theta oscillations in the hippocampus (Kinney et al., 1994; Vertes et al., 1994) while inhibiting the median raphe enhances hippocampal theta (Kinney et al., 1995). Administration of serotonergic anxiolytics has been extensively shown to reduce hippocampal theta frequency elicited via reticular formation stimulation in anesthetized animals and after administration in awake behaving animals (Coop and McNaughton, 1991; McNaughton and Coop, 1991; McNaughton et al., 2007; Wells et al., 2013). However, it is not known how this might affect activity in the MEC—both in terms of LFP effects and on the firing of single units, such as grid cells, which show spacing of firing fields that is correlated with theta frequency and fire theta rhythmically as well (Giocomo et al., 2007; Brun et al., 2008; Jeewajee et al., 2008; Barry et al., 2012).

2.2. Materials and Methods

2.2.1. Subjects

Male Long-Evans rats (Charles River Laboratories) weighing between 350-450 grams at surgery were used for these studies. All experimental procedures were approved by the Institutional Animal Care and Use Committee for the Charles River Campus at Boston University. Rats were housed individually in plexiglass cages, maintained on a 12-hour light/12-hour dark cycle (testing always occurred during the light cycle), and were maintained at ~85% of their ad libitum weight. Prior to surgery, rats were habituated to the experimenter and testing room. The animals were trained to forage in an open field environment (1 m by 1.5 m) for pieces of Froot Loops (Kellogg's). One wall of the otherwise black painted environment was white to provide stable landmark information; cues surrounding the environment were present to provide distal information as well.

2.2.2. Implant

Rats were implanted with recording drives housing up to 16 individually moveable tetrodes (four 12.7 μm nichrome wires spun together) and 4 reference tetrodes, aimed at the MEC. Tetrodes were gold plated to bring down the impedance to <150 kOhm. The exit of the drive was angled at ~25 degrees in the posterior direction in order to implant just anterior of the transverse sinus.

2.2.3. Surgery

Rats were anesthetized with isoflurane and given an injection of a ketamine/xylazine/acepromazine cocktail and buprenorphine; depth of anesthesia was monitored at least every 15 minutes by checking breathing and confirming lack of response to a toe pinch. An injection of atropine was given to prevent fluid buildup in the lungs. After the initial incision, the skull area was cleared of fascia and approximately 10 holes were drilled to attach anchor screws into the skull; 1-2 ground screws were placed over the cerebellum. Two craniotomies were performed: one to implant a drug delivery cannula (from Bregma: 0.5 mm anterior, 3.0 mm lateral; implanted at 25 degrees medially, lowered 6.0 mm from brain surface) and the second as the implant site (left hemisphere; most lateral and posterior corner grazes where the left bone ridge and lambda suture meet). The implant was secured in place using Kwik-Sil and dental acrylic. Tetrodes were lowered 2-3 mm from the dorsal surface at surgery. Animals were allowed one week to fully recover after surgery before experiments began.

2.2.4. Neural recordings

Animals were tested daily in the open field during recordings to search for grid cells, conjunctive grid-by-head-direction cells, border cells, and theta rhythmic cells. Once theta rhythmic cells and theta oscillations in the LFP were recorded, tetrodes were lowered a maximum of ~35 μm/day; experiments were never done on days tetrodes were turned in order to maximize the likelihood of recording the same cells across sessions. Neural signals were preamplified by unity-gain operational amplifiers located on the head of the animal. Signals were linked to digital amplifiers and amplified (5,000-20,000X)

and bandpass filtered (1-500 Hz) by the 64-channel Cheetah Digital Lynx acquisition system (Neuralynx Corp., Bozeman, MT). When a signal crossed threshold all four channels of the tetrode were digitized at 32 kHz and recorded. Position, head direction, and velocity data were calculated from a red (front) and green (back) diode positioned on the recording head stage and sampled at 30 Hz. Position was determined as the centroid of the diodes. LFP activity was collected at 32 kHz and downsampled to 508 Hz. LFP traces obtained from the MEC were recorded from a single lead of a tetrode and referenced to the animal ground or to a cortical electrode that did not show theta oscillations when referenced to ground.

2.2.5. Histology

When possible, final tetrode positions were marked before sacrificing the animal by passing current through tetrodes that had recorded grid cells. Animals were overdosed with isoflurane and perfused intracardially with saline followed by 4% paraformaldehyde. Brains were extracted and stored in 4% paraformaldehyde at 6 degrees C for at least 24 hours. Approximately 72 hours before slicing, brains were transferred into a 30% sucrose solution. The brain was cut to separate the MS and MEC portions; the MEC was sliced along the sagittal plane to visualize tetrode tracks, while the MS was sliced along the coronal plane to confirm cannula placement. Sections were mounted on gelatin-subbed glass slides and stained with cresyl violet.

2.2.6. Experimental design

One to two 20-minute pre-drug recording sessions were performed prior to drug injection or infusion. After drug administration, recording sessions were performed up to 45 minutes in duration to ensure adequate coverage of the environment. This session began within 10 minutes following drug administration, except in the case of muscimol infusion (15 minutes post). A twenty-minute recovery session was recorded 3-6 hours post-drug administration and 24 hours later, to confirm return to normal activity. Multiple experiments, including administration of different types of drugs, were performed in a rat for as long as a given grid cell could be well-isolated, however there was a minimum of 48 hours between all drug and vehicle administrations. When single units of interest could no longer be isolated, tetrodes were moved down and screening for cells of interest began again.

2.2.7. Drugs and drug administration

Drugs were administered either systemically through intraperitoneal injection or intracranially into the MS via the implanted guide cannula. Prior to an infusion, the dummy cannula was removed to allow access to the guide cannula. An injector cannula (33 gauge), extending 1 mm beyond the guide cannula, was filled with the drug or vehicle and lowered through the guide cannula and into the MS. A microinfusion pump infused 0.3-0.5 μL of the solution (depending on the experiment) at a rate of 0.125 μL/min. The injector cannula was left inserted for two minutes after the infusion to allow the drug to diffuse throughout the tissue. The injector cannula was then removed and replaced with a sterilized dummy cannula.

Volume-matched vehicle controls were performed for both systemic injections (1 mL/kg) and infusions (0.5 μL). The 5-HT1A receptor agonist, 8-OH-DPAT (Sigma), was mixed in sterile phosphate buffered saline (PBS) to make a concentration of 100 μg/mL and administered at 75 μg/kg systemically or infused at 2.4 μg or 4 μg of an 8 μg/uL concentration. Before commencing the first infusion experiment in a rat, a muscimol infusion (0.5 μL of 0.5 μg/μL) was performed once a grid cell was recorded and/or when theta oscillations were present in the LFP to confirm loss of theta power and grid cell spatial periodicity (when grid cells were being recorded) in order to verify correct cannula placement. If spatial periodicity and theta power were not disrupted, an injector needle with a 2 mm (instead of 1 mm) projection was tried, at least 48 hours later. If this was not successful either, the rat was not used for collecting infusion data.

8-OH-DPAT systemic

Effective doses of 8-OH-DPAT given via intraperitoneal injection reported in the literature range from 15 μg/kg up to 2.5 mg/kg (Table 2.1). Different doses were tested for this work (50, 75, 100, and 150 μg/kg) and 75 μg/kg was found to be the highest dose that could be given without disrupting ambulation in most cases. Injections were given within a range of 15 minutes to 30 minutes before the given experimental session began, in most cases. When tested and reported, peak effects were achieved 30 or 45 minutes post administration (Klancnik et al., 1989; Coop et al., 1992) but in both experiments, near maximum levels were reported 15 minutes post-injection. In this work, recordings typically began within 10 minutes post-injection.

8-OH-DPAT infusion

Infusion amounts that produced effects range in the literature from 0.5 to 10 μg (Table 2.2). Two amounts were tested in this work: 2.4 and 4 μg (0.3 μL and 0.5 μL of 8 μg/μL concentration). Similar to systemic administration, 2.4 μg was chosen because it impacted ambulation the least. In all examined journal articles when it was reported, the experimental task began 10 minutes after infusion, which was the same for the experiments performed for this research.

2.2.8. Analyses

Cluster cutting across sessions

After the completion of each recording session, single units were isolated using cluster cutting software (Offline Sorter, Plexon Inc.). Single units were distinguished using peak amplitude and principal components for each waveform. Stability of units was confirmed by tracking waveform profiles across the four leads of the tetrode and cluster position across recording sessions, comparing to the baseline session.

Measurement of theta rhythm and running speed

LFP activity was collected at 32 kHz and downsampled to 508 Hz. Downsampled LFP was filtered using a second order butterworth bandpass filter with cutoff frequencies of 6-10 Hz for theta band. Phase was estimated using the angle of the Hilbert transform of the filtered signal and instantaneous amplitude was estimated as the amplitude of the Hilbert transform. The LFP channel used for analyses was chosen on an animal-by-animal basis for each set of four recording sessions based on spectral properties from the baseline recording (Brandon et al., 2013). For each channel the spectrum of LFP power was found, the peak within theta range determined, and divided by the mean signal,

giving the relative power within the theta band. The LFP channel was then chosen as the channel with maximum theta to noise ratio for each rat's baseline session. Theta frequency, amplitude, and power were calculated for 2.5 cm/s running speed bins and plotted from 5-30 cm/s. Each rat's LFP signal was normalized to aid comparison between animals per Wells et al. (2013). In brief, for each measure (frequency, amplitude, and power), the overall mean across all animals during baseline was calculated. A normalization factor was determined on an animal-by-animal basis as the mean difference in the animal's baseline signal from the population mean. This normalization factor was applied across all sessions for each animal, giving a normalized signal. This method accounts for a mean difference, but not speed modulated difference, in theta measures between animals.

Measurement of single unit properties

Spatial rate maps were constructed for a given unit by taking the number of spikes in 3.6 cm by 3.6 cm spatial bins and dividing by the amount of time spent in that bin. Rate maps were smoothed using a 5x5 bin pseudo-Gaussian kernel with a one-pixel standard deviation. The spatial periodicity of grid cells was quantified with a "gridness" score and computed from the spatial autocorrelation of the smoothed rate maps. For the gridness score calculated, "gridness 3," the center peak was removed from the autocorrelation and if present, the six surrounding peaks found and cut out to make a donut. If the grid shape was elliptical, it was distorted to create a circle. The correlation was calculated for each 3 degree rotation of the donut to itself. The gridness score is the difference between the correlation at the minimum peak of 60 or 120 degrees and the

maximum trough at 30, 90, or 150 degrees. The grid field distance was determined from the spatial autocorrelation by calculating the average distance between the middle and six surrounding peaks, checked manually to ensure the proper fields were being detected and measured.

Head direction firing properties of units were calculated by constructing a polar histogram of firing rates by head direction. Spikes were put into bins of 6 degrees and divided by the amount of time spent facing that direction. The mean resultant length (MRL) of the directionality of spiking was then calculated.

The spatial information (SI) score reflects the degree to which a cell's spiking can be used to predict the animal's location. It was calculated as in Cacucci et al. (2007) and expressed in bits/spike. Correlation of the spatial rate maps for cells were calculated by finding the Pearson's correlation coefficient between the baseline rate map and the following sessions for a given cell.

Spike time autocorrelograms were created with time bins of 10 ms and normalized and clipped to the peak in the theta range (6-10 Hz). Autocorrelograms were then fit with the equation:

$$y(t) = [a*(\cos(\omega*t)+1)+b]*\exp(-|x|/\tau_1)+c*\exp(-t^2/\tau_2^2))$$

Where y(t) is the normalized autocorrelogram value, t is the time lag, a is an amplitude of rhythmicity, τ_1 and τ_2 are fall off constants, b and c are coefficients for theta rhythmicity and theta skipping, and ω is the intrinsic frequency of the cell. The theta

index was then defined as (a+b) over the mean of y, representing the relative amount of power in the theta range.

Classification of cells

Single units were classified as grid cells, head direction cells, spatially modulated non-grid cells, theta rhythmic cells, or interneurons. Grid cells were further divided into conjunctive (additionally head direction modulated) and non-conjunctive grid cells. To determine gridness, head direction, and spatial information thresholds, shuffling was performed as in Bonnevie et al. (2013), for gridness 3, MRL, and SI content, respectively. Briefly, the sequence of spikes from a given cell was time shifted along the rat's path by a random interval between 20 s and 20 s minus session length, with the end wrapped to the beginning. A single unit was deemed a given cell type if the value exceeded the 95th percentile of all shuffled permutations. The thresholds for gridness3, MRL, and SI were 0.2178, 0.3244, and 3.0176, respectively. Cells not showing significant gridness, directionality, or SI content but were significantly theta rhythmic based on the measure described above, were deemed theta rhythmic cells. Cells with firing rates greater than 10 Hz were classified solely as putative interneurons (Savelli et al., 2008; Buetfering et al., 2014; Zheng et al., 2015). Somewhat surprisingly, shuffling to determine the SI threshold resulted in a very high number, suggesting the ease to which cells can be classified as spatially modulated, considering a common threshold used is 0.5, regardless of whether the cell's firing is based on actual spiking or shuffled data. Given this, and that few cells could be classified as spatially modulated, analyses were limited to grid cells, HD cells, theta rhythmic cells, and interneurons.

Data exclusion

If an animal did not cover at least 80% of the total number of position bins (3.6 cm x 3.6 cm) in the environment in the first 20 minutes of the recording session (length of most recordings) immediately following drug administration, that set of experiments were excluded from analyses (Bjerknes et al., 2014). Histology was used to verify recording tracks to ensure they were positioned to record from the MEC area; in one animal the recording drive was positioned too anteriorly and data from that animal were excluded. Single units were used for analyses if they were stable enough to be recorded across the first three recording sessions (Baseline, post-Drug/Vehicle administration, and 3-6 hour recovery), otherwise data for that cell were excluded and not analyzed.

Statistical tests of significance

All comparisons between baseline and other conditions used a Bonferroni correction for multiple comparisons with an alpha value of 0.05. This resulted in a p-value of 0.0016 for both LFP and single unit tests (0.05/(4*4*2)) using an ANCOVA or repeated measures ANOVA, a p-value of 0.025 (0.05/2) for post-hoc t-tests, and a p-value of 0.05 for median speed tests.

For single unit analyses, a repeated measures ANOVA was performed for different measures (e.g. firing rate) to look at potential changes between baseline and after drug/vehicle administration, and tested for differences in the amount of change that occurred between the two groups. A significant result from this test suggests that the change that occurred from baseline to post-administration was different for the drug compared to the change that occurred after the vehicle. A non-significant result from this

suggests that any change that might have occurred from baseline to post-administration for the drug was not significantly different from the potential change occurring after vehicle administration.

If the repeated measures ANOVA yielded a statistically significant result then a post-hoc paired t-test was performed to test for changes in the measure from baseline to post-administration. A significant result from this suggests that after administration, the given measure changed significantly. A non-significant result implies that after administration, it cannot be rejected that the values are from the same distribution.

For LFP analyses, ANCOVAs were performed to examine changes in the intercept and slope of the relationship between LFP theta frequency, amplitude, and power across running speeds. Comparisons were made to vehicle, looking at potential differences in the change in the given measure from the baseline to second session (the recording following drug or vehicle administration). If an ANCOVA result was significant, a post-hoc ANOVA was performed to test for drug effects on the slope and intercept.

2.3. Results

2.3.1. Systemic administration of 8-OH-DPAT: LFP

Systemic administration of the 5-HT1A agonist, 8-OH-DPAT, produced changes in MEC theta frequency that resemble those reported in the literature for recordings in the hippocampus. ANCOVAs were performed to examine changes in the intercept and slope of the relationship between LFP theta frequency, amplitude, and power across running

speeds. Comparisons were made to vehicle, looking at potential differences in the change in the given measure from the baseline to second session (the recording following drug or vehicle administration). If an ANCOVA result was significant, a post-hoc ANOVA was performed to test for drug effects on the slope and intercept.

Systemic administration of 8-OH-DPAT reduced the intercept of the relationship between theta frequency and running speed compared to vehicle ($F(1,66)=869.92$, $p<1e-10$) (Figure 2.1 A1-2). There was a drug effect in that 8-OH-DPAT injection reduced the intercept from baseline ($F(1,96)=73.09$, $p<1e-10$). Slope increased significantly more during the second session after vehicle administration compared to after drug ($F(1,66)=11.31$, $p=0.0013$) (Figure 2.1 A1-2). When comparing the slope during baseline and after drug administration, no significant differences were seen ($F(1,96)=0.39$, $p=0.53$).

Drug administration produced a significant decrease in theta amplitude across running speeds compared to vehicle when looking at the intercept ($F(1,66)=92.25$, $p<1e-10$) but not slope ($F(1,66)=1.66$, $p=0.2$) (Figure 2.1 B1-2). However, looking at the effect of 8-OH-DPAT injection on the intercept of the amplitude, it did not reach significance ($F(1,96)=8.95$, $p=0.0035$).

No changes were seen in theta power across running speeds after 8-OH-DPAT injection in comparison to vehicle for intercept ($F(1,66)=1.38$, $p=0.24$) or slope ($F(1,66)=0.58$, $p=0.45$) (Figure 2.1 C1-2).

2.3.2. Systemic administration of 8-OH-DPAT: single units

Repeated measures ANOVAs were performed to examine changes between baseline and the second recording session (following drug or vehicle administration), testing for differences in this change when comparing drug and vehicle. If the repeated measures ANOVA was significant, a post-hoc paired t-test was performed to test for drug effects on the given measure from baseline to the post-administration second session.

In brief, no significant differences were seen in single unit firing properties after 8-OH-DPAT systemic injection, other than in the rhythmicity of firing of grid cells. After 8-OH-DPAT injection compared to vehicle administration, no significant differences were found in the change in firing rates from baseline to the second session for grid cells ($F(1,13)=0.13$, $p=0.72$), head direction cells ($F(1,34)=0.004$, $p=0.95$), theta rhythmic cells ($F(1,9)=0.01$, $p=0.93$), or interneurons ($F(1,7)=0.30$, $p=0.60$) (Figure 2.2).

Comparing drug and vehicle groups, there were no significant differences in the change from baseline to the second session for MRL in HD cells ($F(1,34)=1.81$, $p=0.19$) (Figure 2.3, right) or for conjunctive cells ($F(1,9)=0.03$, $p=0.87$) (Figure 2.3, left).

No differences were seen from baseline to second session between the groups for grid cells for gridness score ($F(1,13)=0.10$, $p=0.76$) (Figure 2.4, left) or for grid field distance ($F(1,11)=0.63$, $p=0.44$) (Figure 2.4, right).

The change in SI between the two sessions when comparing the groups for grid cells did not reach significance ($F(1,13)=5.13$, $p=0.04$) (Figure 2.5, left). Spatial correlations between baseline rate maps of grid cells compared to every other session were calculated. Because the correlation of the baseline to itself is always 1, differences

in correlation to baseline between the drug or vehicle session were compared to the 3-6 hour recovery session. No difference in the change was seen in spatial correlation when comparing drug and vehicle ($F(1,13)=1.07$, $p=0.32$) (Figure 2.5, right). Overall, median running speed was not affected by 8-OH-DPAT injection ($t(6)=-1.50$, $p=0.19$) or vehicle ($t(2)=0.07$, $p=0.95$) (Figure 2.6).

There was a difference found in the change in grid cell intrinsic rhythmicity frequency ($F(1,13)=18.17$, $p<9.24e-4$) from baseline to second session when comparing the drug and vehicle groups (Figure 2.7, left). A drug effect on intrinsic rhythmicity was found after 8-OH-DPAT injection ($t(9)=-3.83$, $p=0.004$) and not after vehicle ($t(4)=2.33$, $p=0.08$).

No significant differences were found in the change between groups for theta index ($F(1,13=0.01$, $p=0.92$) from baseline to second session (Figure 2.7, right).

2.3.3. MS infusion of 8-OH-DPAT: LFP

MS infusion of 8-OH-DPAT produced largely similar results to systemic administration. Namely, after drug infusion, the intercept of the relationship between LFP theta frequency across running speeds robustly decreased compared to vehicle ($F(1,66)=54.53$, $p<3.34e-10$) (Figure 2.8, A1-2). This was true looking within the drug group as well, the intercept decreased from baseline after infusion of 8-OH-DPAT ($F(1,96)=23.27$, $p<5.27e-6$) (Figure 2.8, A1). No differences were found in the change in slope between baseline and the second session, comparing drug and vehicle ($F(1,66)=0.04$, $p=0.85$) (Figure 2.8, A1-2).

The intercept of the amplitude of LFP theta across running speeds significantly decreased after drug administration in comparison to vehicle ($F(1,66)=20.71$, $p<2.36e-5$), whereas no difference was found in slope ($F(1,66)=0.31$, $p=0.58$) (Figure 2.8, B1-2). Within the drug group, the decrease from baseline after MS infusion was not significant ($F(1,96)=3.68$, $p=0.06$) (Figure 2.8, B1).

Drug administration did not significantly change theta power across running speeds in comparison to vehicle for either intercept ($F(1,66)=1.49$, $p=0.23$) or slope ($F(1,66)=0.21$, $p=0.64$) (Figure 2.8, C1-2).

2.3.4. MS infusion of 8-OH-DPAT: single units

In brief, no significant differences were seen in single unit firing properties after MS infusion of 8-OH-DPAT. After 8-OH-DPAT infusion compared to vehicle infusion, no significant differences were found in the change in mean firing rates across cells from baseline for grid cells ($F(1,12)=2.27$, $p=0.16$), head direction cells ($F(1,43)=0.03$, $p=0.86$), theta rhythmic cells ($F(1,23)=0.71$, $p=0.41$), or interneurons ($F(1,7)=0.71$, $p=0.41$) (Figure 2.9).

The change in MRL comparing drug and vehicle was not significant for conjunctive grid cells ($F(1,8)=0.59$, $p=0.47$) or HD cells ($F(1,43)=0.41$, $p=0.53$) (Figure 2.10).

There were no differences in the change of gridness scores ($F(1,12)=0.12$, $p=0.73$), field distance ($F(1,8)=0.39$, $p=0.55$), or SI ($F(1,12)=0.25$, $p=0.63$) in grid cells when comparing drug and vehicle (Figure 2.11 and Figure 2.12, left). No difference was seen in the change of spatial correlation when comparing drug and vehicle spatial rate map

correlations to the baseline for the second session and the 3-6 hour recovery ($F(1,12)=0.004$, $p=0.95$) (Figure 2.12, right).

Running speed of the animal did decrease significantly after 8-OH-DPAT infusion ($t(9)=-4.03$, $p=0.003$, non-Bonferroni corrected p-value threshold used) but not after vehicle infusion ($t(1)=-6.58$, $p=0.1$) (Figure 2.13).

No significant differences in the change in intrinsic rhythmicity ($F(1,12)=0.08$, $p=0.79$) or theta index ($F(1,12)=1.07$, $p=0.32$) in grid cells from baseline to second session were found when comparing drug and vehicle groups (Figure 2.14).

2.4. Discussion

These data show that systemic administration of a serotonergic anxiolytic decreased theta frequency found in the LFP of the MEC. Specifically, it decreased the y-intercept of the linear fit to the plot of theta frequency across a range of different running speeds. These results strongly corroborate the previously reported effects of anxiolytics on hippocampal LFP theta (Wells et al., 2013), expanding detection to a new structure, the MEC. A small decrease in the slope of this relationship as compared to the vehicle condition was also found, where it has been previously shown to increase with multiple same-day exposures to the environment (Jeewajee et al., 2008; Newman et al., 2013; Wells et al., 2013). A decrease in slope from baseline after drug administration would suggest a potential increase in grid scale similar to what has been reported in rats exposed to novel environments (Barry et al., 2012) and in the hippocampus (Wells et al., 2013). However, when comparing the degree of decrease in slope to the previously reported effects of novelty, the decrease shown here appears to be much smaller. This negligible

decrease in slope could explain why there were no significant changes in grid cell firing field distances after drug administration. Even if a change did occur from this decrease it might have been too small to detect or not significant enough of a perturbation to the gain of the relationship between theta frequency and running speed to grossly affect grid scale.

To examine the role the MS might play in modulating theta frequency, MS infusions of 8-OH-DPAT were also performed. The intercept of the relationship between theta frequency and running speed significantly decreased as compared to vehicle, similar to the systemic administration results. While the magnitude of the decrease appeared to be less than systemic administration, dose effects were not systematically tested so it is unclear if infusing a larger amount could produce a similar sized decrease in frequency. This result suggests that the MS could be involved in the decrease in theta frequency seen after systemic injections of serotonergic anxiolytics, but whether it is required to produce the effects is beyond the scope of these experiments.

Similar to theta frequency, both systemic injection and MS infusion of 8-OH-DPAT reduced the intercept of theta amplitude across running speeds. Qualitatively, these findings mean theta oscillations in the LFP were slower and smaller in amplitude after either administration method of the serotonergic anxiolytic. This could be achieved through the inhibitory effects of the neurotransmitter on postsynaptic receptors and autoreceptors. Serotonin generally plays more of a modulatory role in the brain and as such activation of these receptors could produce less or lower probability of recruitment of neurons. This could decrease the overall summed synaptic conductances producing theta rhythm in the LFP without eliminating it entirely, resulting in smaller amplitude

oscillations as fewer neurons are able to overcome the hyperpolarizing effect of 5-HT1A receptor activation. The reduction in theta frequency produced by serotonergic anxiolytics has also been modeled in a septohippocampal system through increasing the time constant, thus slowing the oscillation (John et al., 2014).

While median running speed was significantly lower after drug infusion, it is unlikely this affects the interpretation of the results. For one, the manner of examining changes in LFP theta minimizes the effects of differences in running speed across sessions by looking within bounded speed windows. Even given that a slower running speed would reduce theta frequency, the effect would be limited to lowering the average within a 2.5 cm/s bin, which is negligible. Furthermore, not only was an effect on theta frequency and amplitude found for both systemic administration and MS infusion, the effect appeared larger after systemic administration, despite running speed only being significantly altered during infusion trials.

No effects on theta power were seen after administration of the drug either via systemic injection or MS infusion when looking at power across running speeds. This is in line with what was reported in the hippocampus after systemic injection of a similar anxiolytic when looking at theta power during median running speed-matched epochs (Wells et al., 2013). The relatively flat or negative slope of theta power across running speeds also corroborates hippocampal data (Belchior et al., 2014).

No changes were seen in the firing rates of any of the principal cell types or putative interneurons after systemic injection, similar to what was reported in principal cells in the hippocampus (Wells et al., 2013). Furthermore, MS infusion did not elicit

change. The only significant change across all single unit firing measures tested was in grid cell intrinsic rhythmicity of firing after systemic administration of 8-OH-DPAT. This finding highlights the resiliency of grid cells and other types of MEC cells in general to local perturbations in LFP frequency and the importance of the inputs the cells receive from other areas that pass on different information. While the histology makes it difficult to pinpoint exactly what layer the grid cells were recorded from, due to the approach of the tetrodes traveling through deeper layers first, the multitude of conjunctive grid-by-head-direction cells, and lack of phase precession, this suggests it is very likely that the recordings were from cells in deeper layers of the MEC (Sargolini et al., 2006; Hafting et al., 2008). Further studies could examine the response of grid cells located more superficially, especially in terms of phase precession. Given that the only single unit effect was on intrinsic rhythmicity, and none of the grid cells significantly phase precessed (data not shown), the decrease in the frequency of the rhythmic firing could reflect the maintenance of grid cell phase locking to LFP theta phase. As theta frequency decreased in the LFP, the firing may have slowed slightly to maintain this locking to a constant phase, resulting in a decrease in the grid cell's rhythmicity frequency. It is possible that this slight decrease is too small to significantly affect mean firing rates across the entire session, and requires a larger decrease in LFP theta frequency than seen in the infusion data. Future studies specifically analyzing theta phase locking and phase precession could clarify this possibility.

2.5. Tables

Table 2.1. Literature review of 8-OH-DPAT doses given via intraperitoneal injection.

Doses	Task	Effect	Timing	Citation
12.5, 25, 100 μg/kg	Effects of IP injections in anesthetized rats on population responses in dentate gyrus evoked by perforant path stimulation.	25 and 100 μg/kg produced substantial increase in amplitude of population spike, but not 12.5 μg/kg.	Recorded 30 min post injection, when maximum was achieved (reached 87.5% of peak increase at 15 minutes); higher dose (100 μg/kg) prolonged effect.	Klancnik et al. (1989)
100, 200, 500 μg/kg	Radial arm maze. Examined working memory (defined as re-entry into arms previously chosen) and reference memory (entry into arms never baited).	200 and 500 μg/kg produced deficits in working but not reference memory; 100 μg/kg did not produce any effects.	Behavioral testing began 15 minutes after injection.	Isayama et al. (2001)
30 μg/kg	Passive avoidance task.	Passive avoidance performance was impaired when tested 72 hours later.	Task began 15 minutes post injection.	Santucci & Shaw (2003)
62 μg/kg	Pavlovian/instrumental autoshaping learning task.	62 μg/kg increased conditioned response percent, suggested to be enhancement of memory consolidation.	Drug administered after first autoshaping task; memory tested 24 hours later (specifically testing memory consolidation).	Manuel-Apolinar & Meneses (2004)
0.05, 0.1, 1 mg/kg	Delayed non-matching-to-position task.	1 mg/kg decreased percent correct across delays and increased response bias. No effect with lower doses. May be more motivation related.	Behavioral test began 30 min post administration.	Warburton et al. (1997)
2.5 mg/kg	Measured reticular-elicited hippocampal rhythmical slow activity.	Greatly reduced frequency of rhythmical slow activity.	Max effects 45 min post injection (near maximum at 15).	Coop et al. (1992)

Table 2.2. Literature review of 8-OH-DPAT doses infused into the medial septum.

Doses	Task	Effect	Timing	Citation
1 or 4 μg	Assessed spatial learning using a water maze task and emotional learning in a passive avoidance task.	Neither dose affected spatial learning, 4 μg dose impaired emotional learning. Retention was tested 24 hr after last training session.	Training began 10 min post infusion.	Elvander-Tottie et al. (2009)

4 μg	Water maze. Elevated plus maze.	Infusion before task prevented learning/retention of platform. When infused 2 hrs post acquisition (but not immediately, 1 hr, 4 hr, or 6 hrs) retention was disrupted. Infusion pre-probe trial, retrieval not affected. Did not affect elevated plus maze behavior (anxiety).	10 min prior to testing.	Koenig et al. (2008)
0.5 or 4 μg	Water maze, injected before test phase.	4 μg dose impaired performance, 0.5 μg dose showed trend but not significant.	10 min prior to testing.	Jeltsch et al. (2004)
0.2, 0.5, or 2 μg	Tested MS infusion on elevated plus maze.	Only the intermediate dose (0.5 μg) had an effect; increased anxiety behavior as measured by entries into open arms (but locomotion overall also decreased).	10 min prior to testing.	De Almeida et al. (1998)
0.1, 0.25, 5 and 10 μg	Shock probe test and elevated plus maze.	5 and 10 μg decreased burying behavior in shock probe test. No doses affected elevated plus maze behavior.	--	Menard & Treit (1998)

2.6. Figures

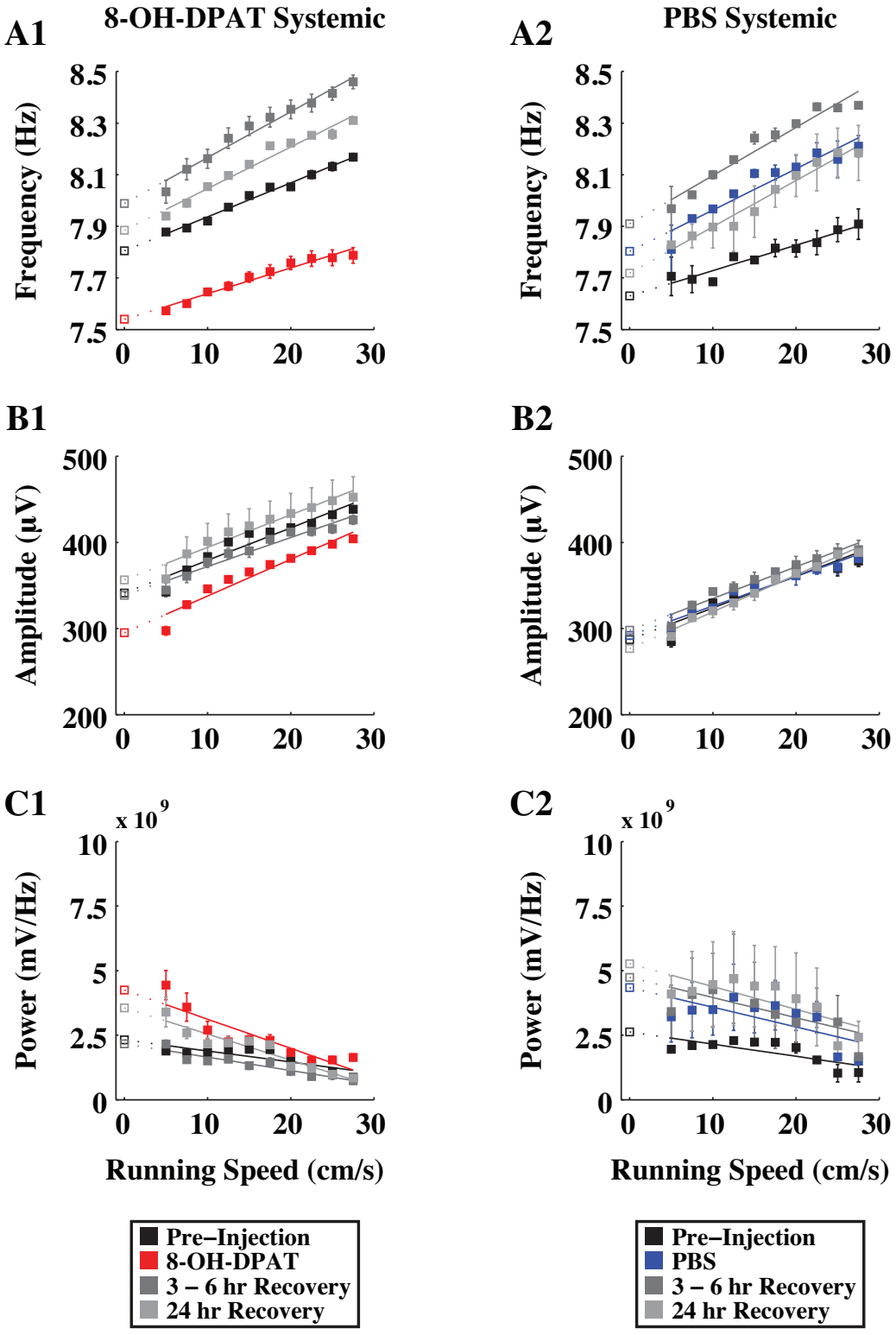
A1
8-OH-DPAT Systemic
A2
PBS Systemic
Frequency (Hz)
8.5
8.3
8.1
7.9
7.7
7.5
0
10
20
30
B1
B2
Amplitude (µV)
500
400
300
200
C1
C2
x 10^9
Power (mV/Hz)
10
7.5
5
2.5
0
Running Speed (cm/s)
Pre–Injection
8-OH-DPAT
3 – 6 hr Recovery
24 hr Recovery
Pre–Injection
PBS
3 – 6 hr Recovery
24 hr Recovery

Figure 2.1. Systemic injection of 8-OH-DPAT reduces the intercept of theta frequency and amplitude.

A. Effects of systemic injection (A1, red line) compared to baseline (black line) and recovery sessions (grey lines) on LFP theta frequency plotted across running speeds, and the same for vehicle (A2, blue line). B, C. Same as A but for theta amplitude and power, respectively.

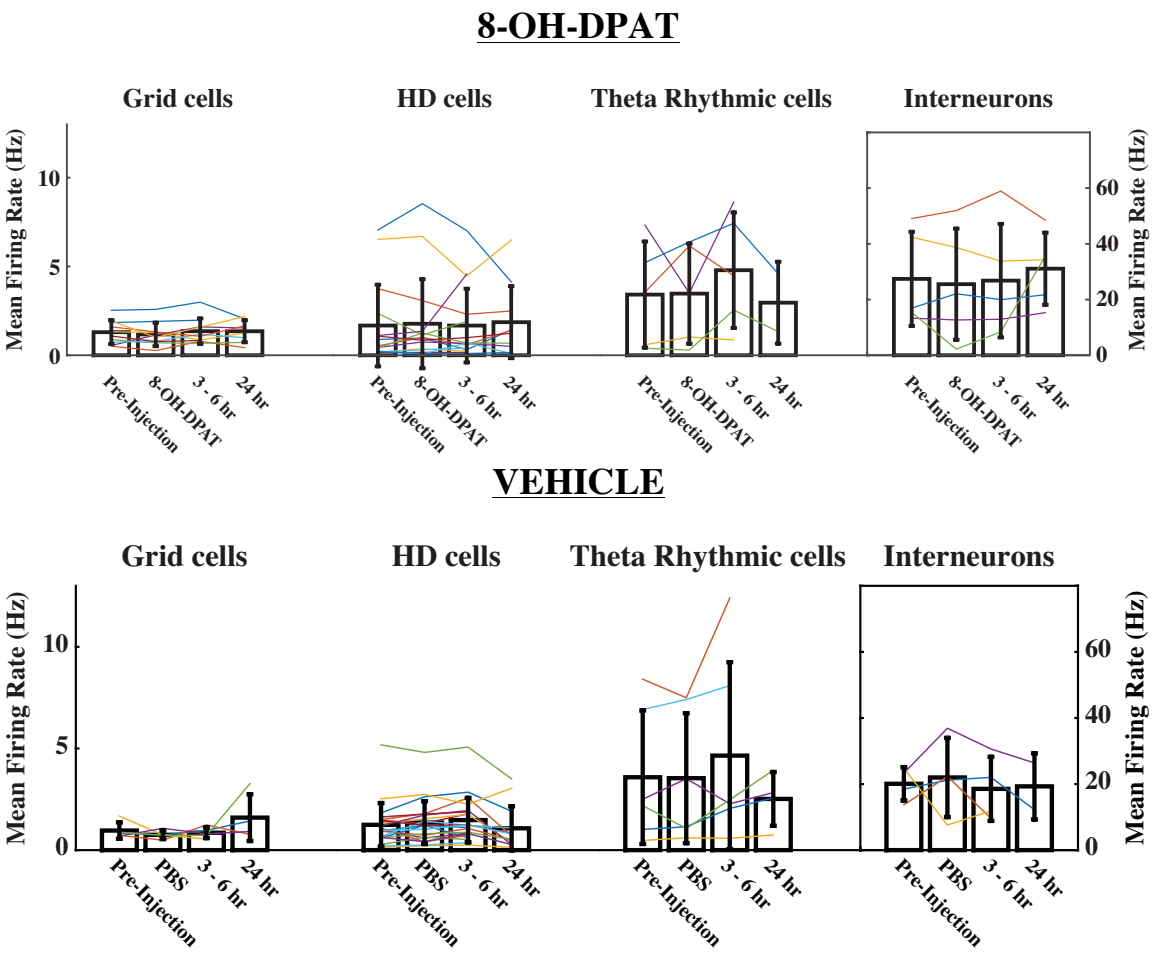

Figure 2.2. Mean firing rate for grid cells, HD cells, theta rhythmic cells, and interneurons across sessions after systemic administration of 8-OH-DPAT.

No drug effects on mean firing rate were seen across multiple cell types.
Effects of systemic injection of 8-OH-DPAT (top) and vehicle (bottom) on mean firing rate of grid cells, HD cells, theta rhythmic cells, and interneurons. Each cell recorded across sessions is marked by a single colored line. The vertical black line represents the standard error of measurement.

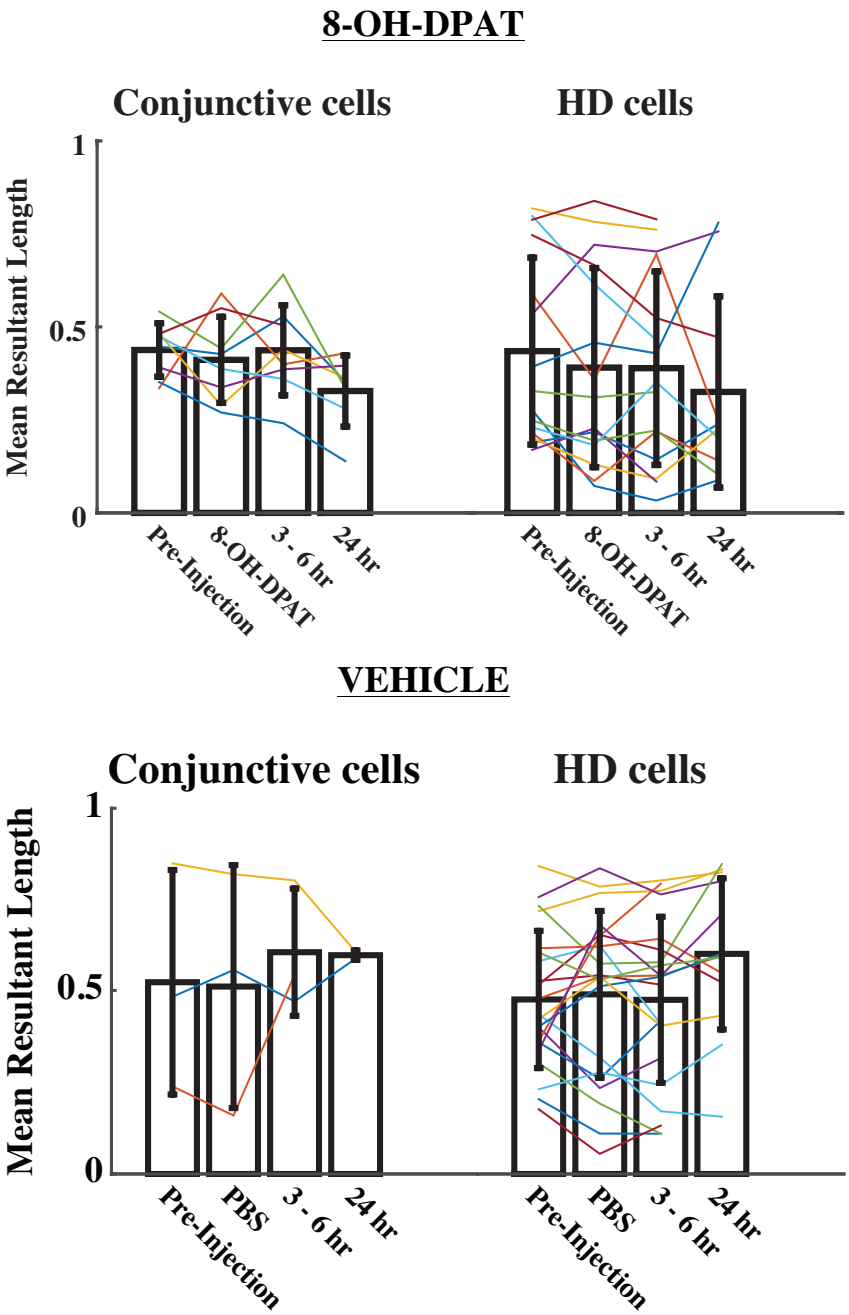

Figure 2.3. Mean resultant length of conjunctive and HD cells across sessions.

Directionality of cell firing across sessions for conjunctive grid cells (left) and head direction cells (right) after systemic injection of 8-OH-DPAT (top) and vehicle (bottom). No drug effects on directionality of firing for conjunctive head by grid cells or HD cells were seen. Each cell recorded across sessions is marked by a single colored line. The vertical black line represents the standard error of measurement.

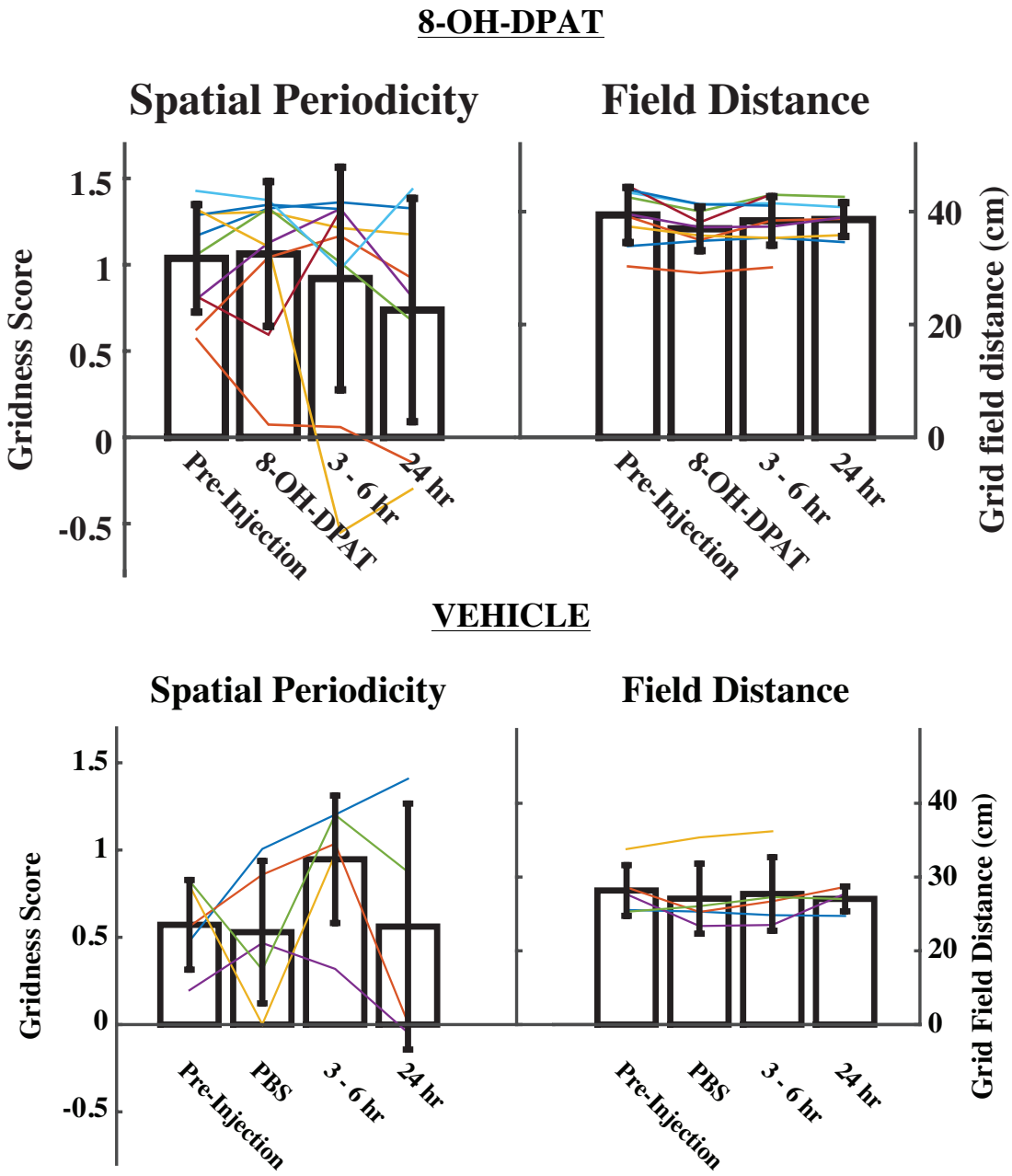

Figure 2.4. Spatial periodicity and grid field distances were not affected by 8-OH-DPAT systemic administration.

Gridness score (left) and grid field distance (right) of grid cells after systemic injection of 8-OH-DPAT (top) and vehicle (bottom). Each cell recorded across sessions is marked by a single colored line. The vertical black line represents the standard error of measurement.

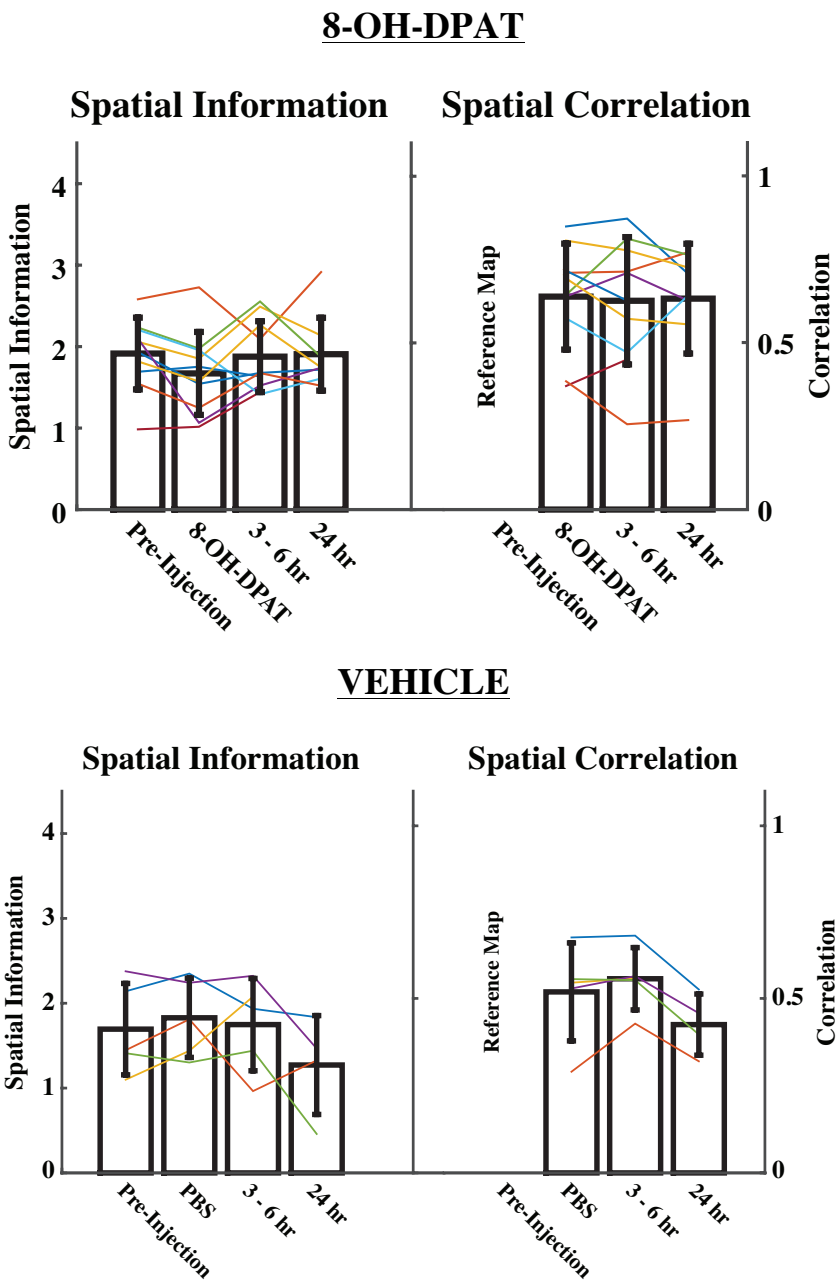

Figure 2.5. Spatial information score and correlation of rate maps of grid cells maintained after drug and vehicle administration.

Measures of spatial firing after systemic injection of 8-OH-DPAT (top) and vehicle (bottom) for spatial information (left) and spatial correlation of rate maps (right). Each cell recorded across sessions is marked by a single colored line. The vertical black line represents the standard error of measurement.

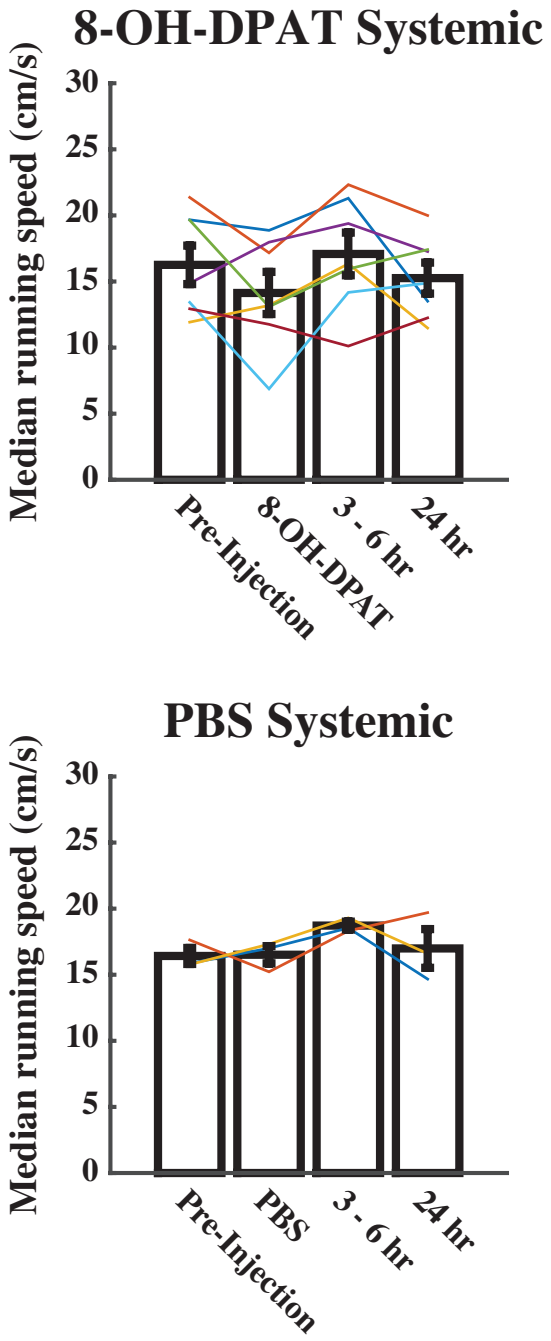

Figure 2.6. Median running speed (cm/s) across recording sessions.

No significant changes in median running speed from baseline to the second recording session were seen after administration of 8-OH-DPAT systemic (top) or PBS (vehicle) systemic experiments (bottom). Each session's median speed is marked by a single colored line. The vertical black line represents the standard error of measurement.

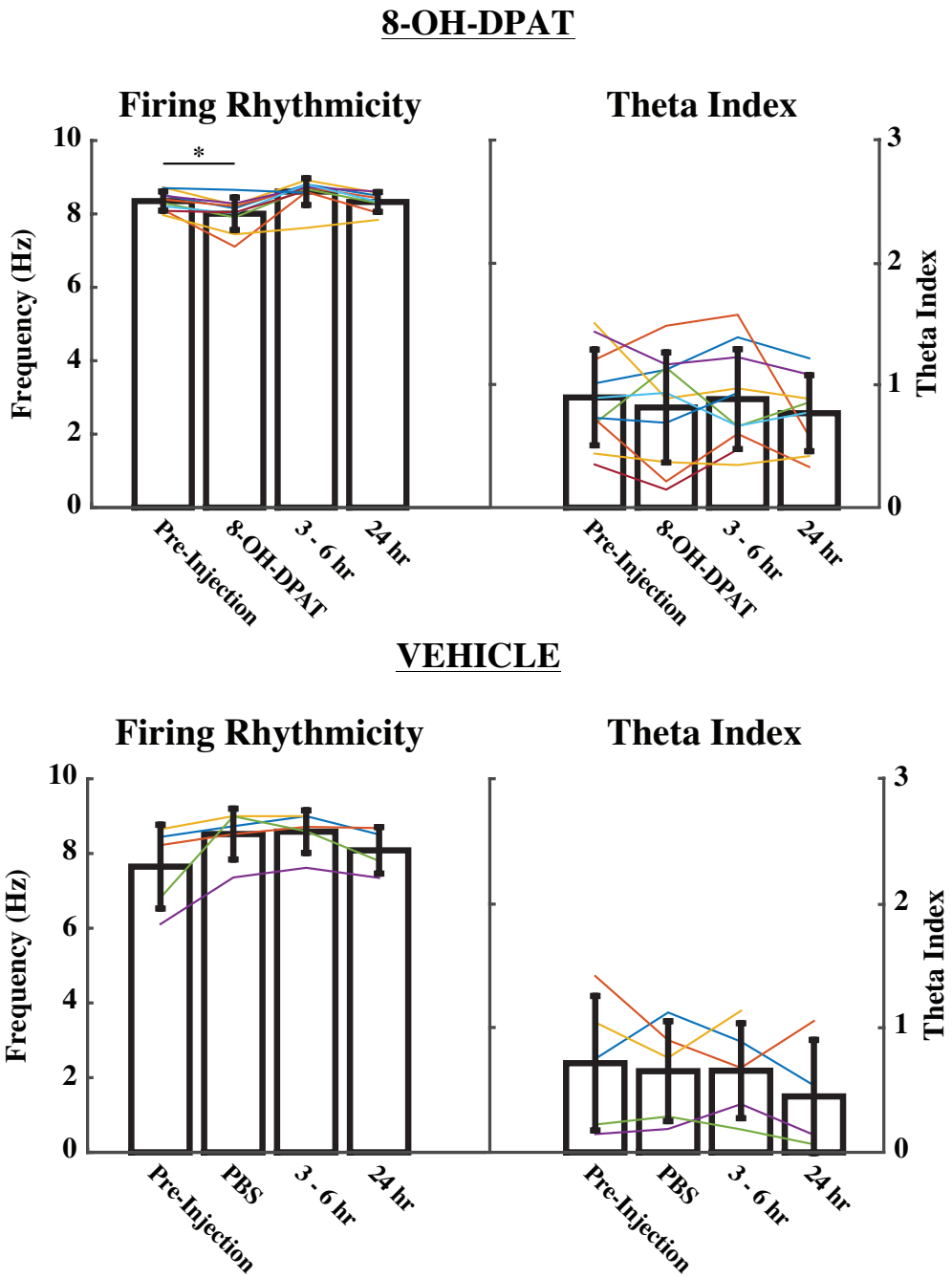

Figure 2.7. A significant difference in intrinsic rhythmicity was found after 8-OH-DPAT systemic injection.

Firing rhythmicity (left) and theta index (right) for systemic injections of 8-OH-DPAT (top) and vehicle (bottom). Each cell recorded across sessions is marked by a single colored line. The vertical black line represents the standard error of measurement.

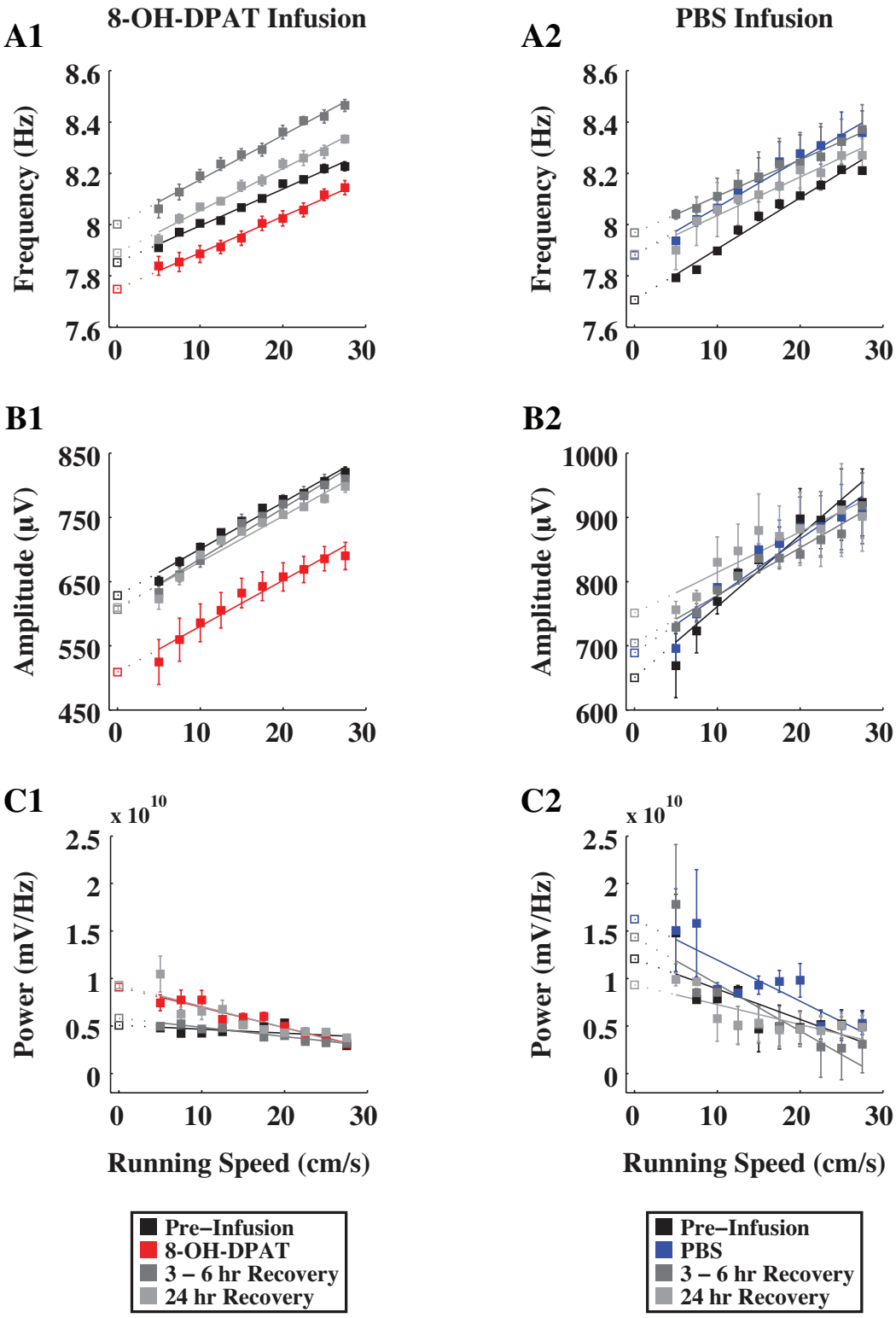
A1
8-OH-DPAT Infusion
A2
PBS Infusion
Frequency (Hz)
8.6
8.4
8.2
8
7.8
7.6
0
10
20
30
B1
B2
Amplitude (µV)
850
750
650
550
450
1000
900
800
700
600
C1
C2
x 10^10
Power (mV/Hz)
2.5
2
1.5
1
0.5
0
Running Speed (cm/s)
Pre−Infusion
8-OH-DPAT
3 – 6 hr Recovery
24 hr Recovery
Pre−Infusion
PBS
3 – 6 hr Recovery
24 hr Recovery

Figure 2.8. MS infusion of 8-OH-DPAT reduces the intercept of theta frequency and amplitude.

A. Effects of MS infusion (A1, red line) compared to baseline (black line) and recovery sessions (grey lines) on LFP theta frequency plotted across running speeds, and the same for vehicle (A2, blue line). B, C. Same as A but for theta amplitude and power, respectively.

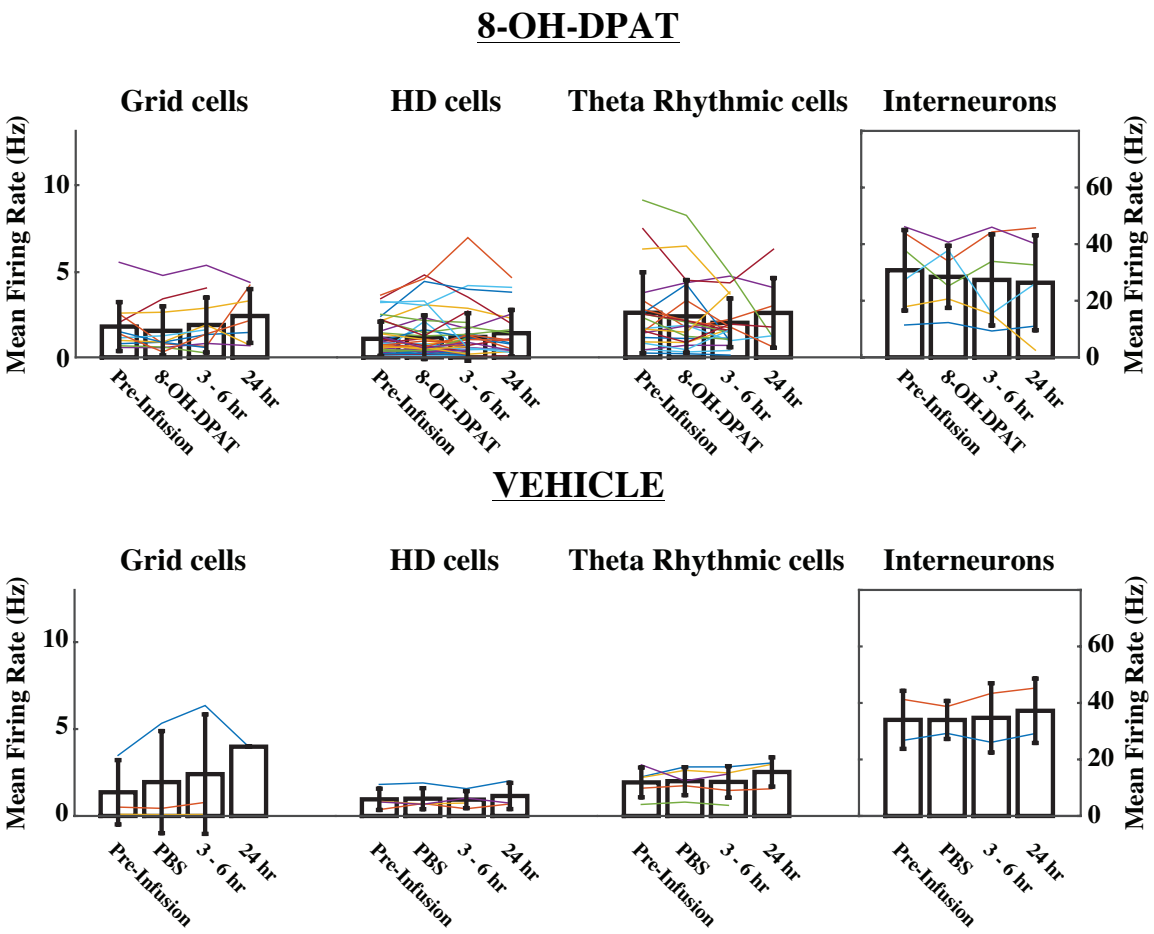

Figure 2.9. Mean firing rate for grid cells, HD cells, theta rhythmic cells, and interneurons across sessions after 8-OH-DPAT infusion and vehicle.

No significant effects found from MS infusion of 8-OH-DPAT (top) and vehicle (bottom) on mean firing rate of grid cells, HD cells, theta rhythmic cells, and interneurons. Each cell recorded across sessions is marked by a single colored line. The vertical black line represents the standard error of measurement.

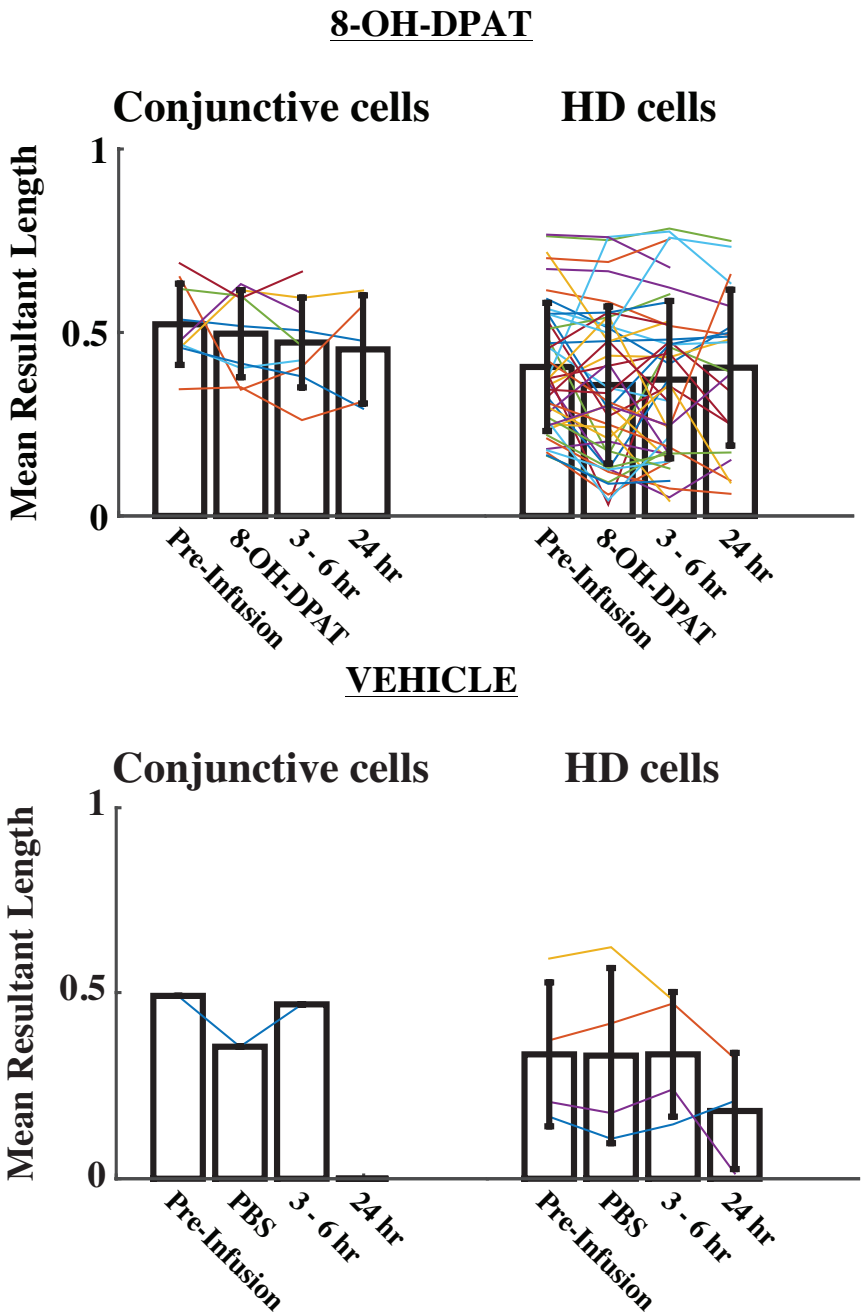

Figure 2.10. Mean resultant length of conjunctive and HD cells across sessions.

Directionality of cell firing across sessions for conjunctive grid cells and head direction cells after MS infusion of 8-OH-DPAT (top) and PBS (bottom). Each cell recorded across sessions is marked by a single colored line. The vertical black line represents the standard error of measurement.

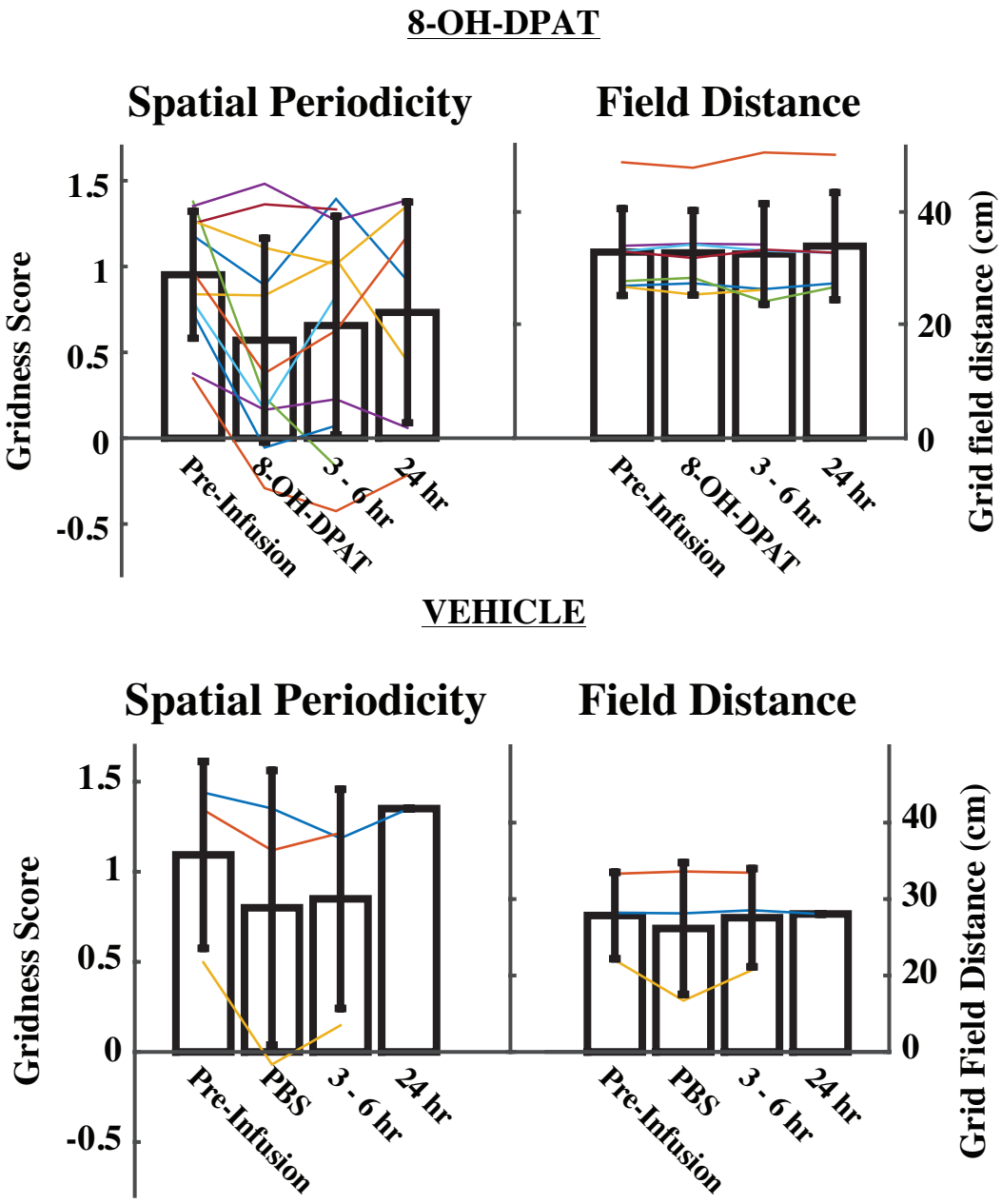

Figure 2.11. Spatial periodicity and grid field distances were unaffected by 8-OH-DPAT infusion.

Gridness score and grid field distance of grid cells after MS infusion of 8-OH-DPAT (top) and vehicle (bottom). Each cell recorded across sessions is marked by a single colored line. The vertical black line represents the standard error of measurement.

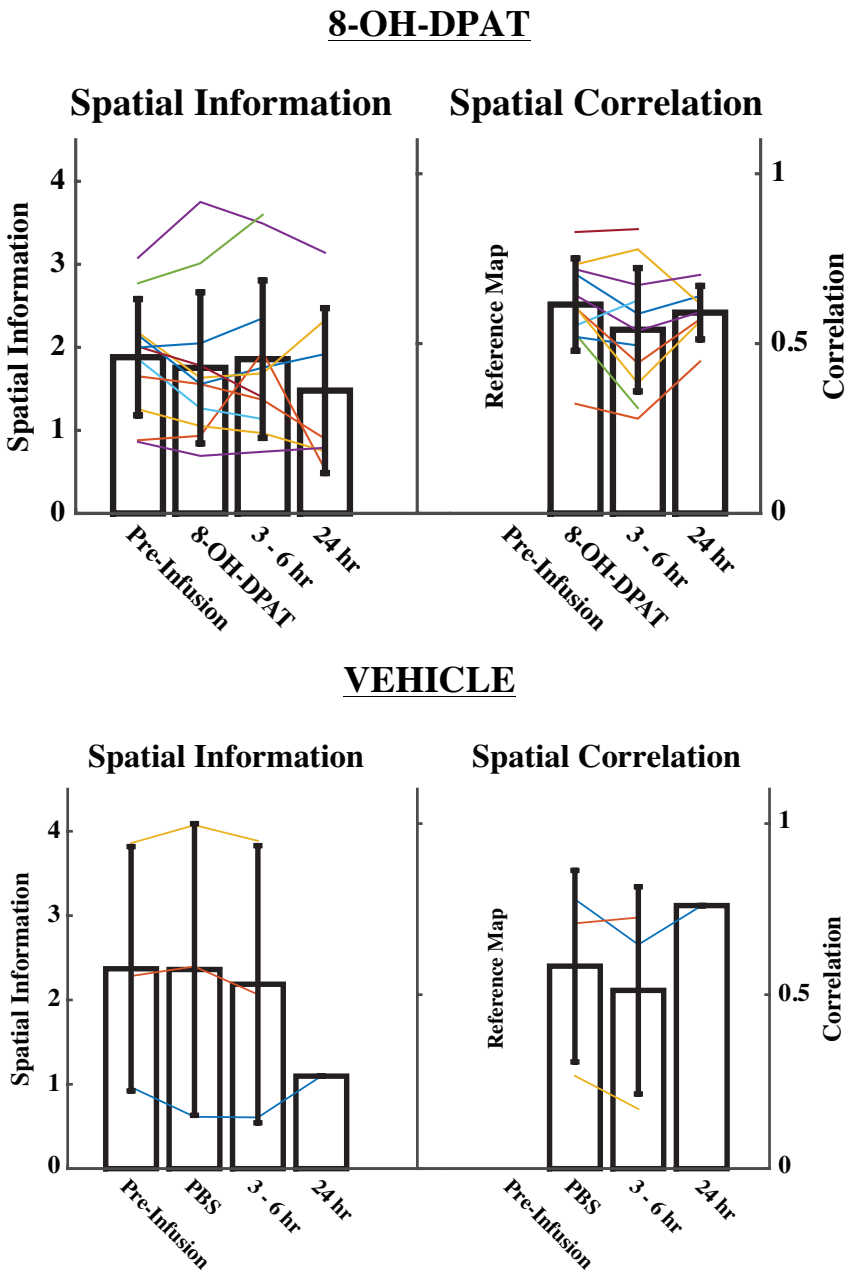

Figure 2.12. Spatial information score and correlation of rate maps of grid cells maintained after 8-OH-DPAT and vehicle infusion.

Measures of spatial firing after MS infusion of 8-OH-DPAT (top) and vehicle (bottom) for spatial information (left) and spatial correlation of rate maps (right). Each cell recorded across sessions is marked by a single colored line. The vertical black line represents the standard error of measurement.

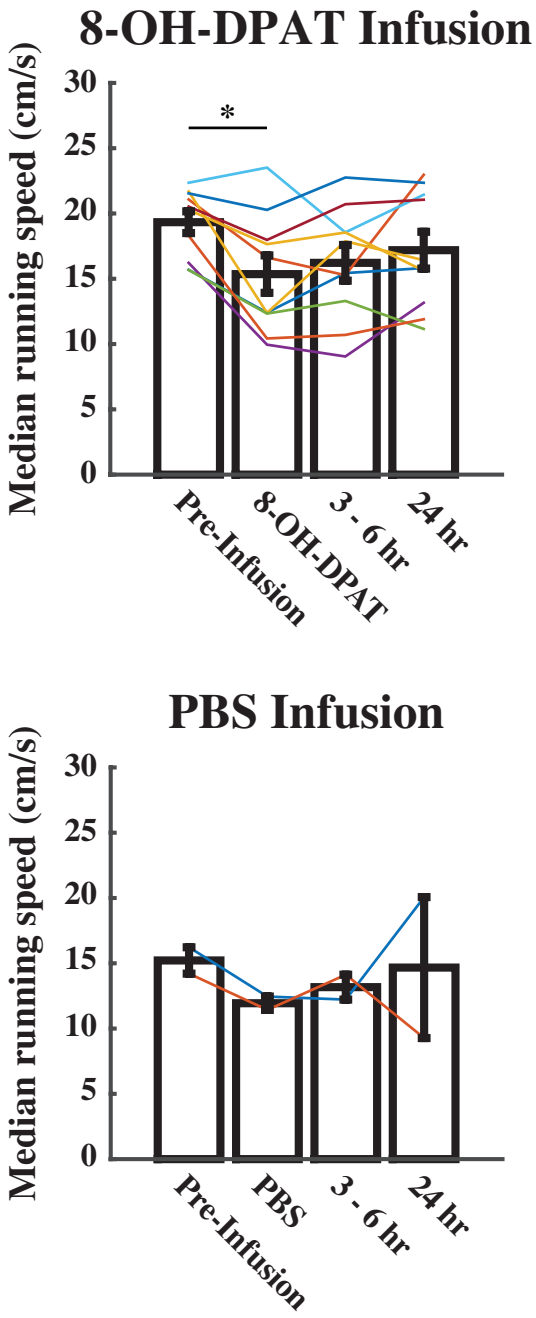

Figure 2.13. Median running speed (cm/s) across recording sessions.

Median running speed (cm/s) for 8-OH-DPAT infusion experiments (top) and PBS (vehicle) infusion experiments (bottom). There was a significant decrease in median running speed after 8-OH-DPAT infusion. Each session's median speed is marked by a single colored line. The vertical black line represents the standard error of measurement.

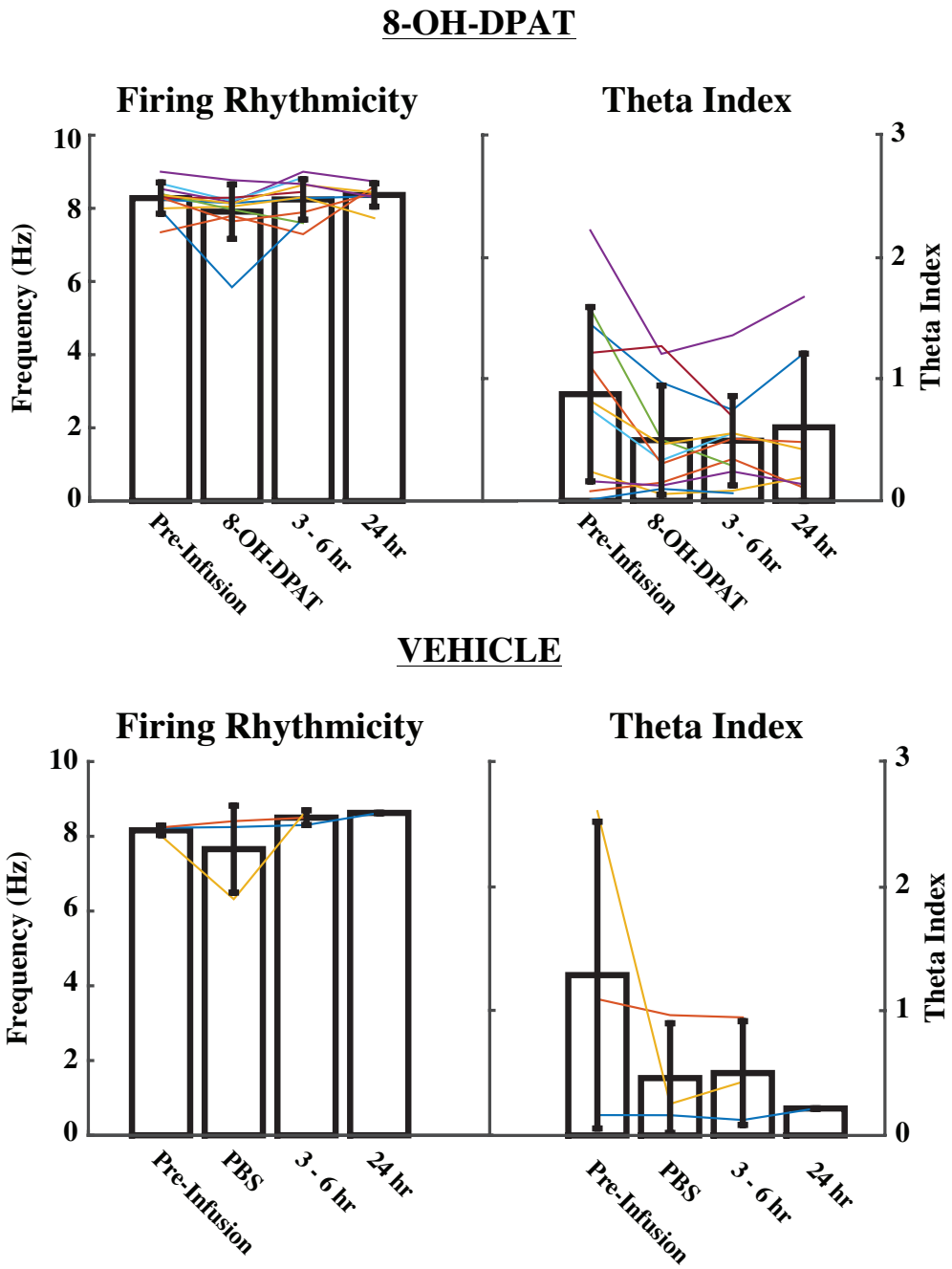

Figure 2.14. No significant differences seen in intrinsic firing rhythmicity after 8-OH-DPAT or vehicle infusion.

Firing rhythmicity (left) and theta index (right) for MS infusions of 8-OH-DPAT (top) and vehicle (bottom). Each cell recorded across sessions is marked by a single colored line. The vertical black line represents the standard error of measurement.

CHAPTER 3: Effects of systemic administration and MS infusion of a benzodiazepine on MEC activity[2]

[2]Monaghan, CK, Chapman IV, GW, Hasselmo, ME. In prep.

3.1. Introduction

Benzodiazepines (BDZs) are classic anxiolytics that have been well studied since their discovery decades ago. Similar to serotonergic anxiolytics, BDZs reduce hippocampal theta frequency in both awake, behaving animals and via reticular formation stimulation. However, despite the entorhinal cortex providing Type I theta to the hippocampus and the medial septum (MS) pacemaking both regions, little research has focused on the effects of BDZs on these areas. This is especially of interest as grid cells, neurons that are spatially modulated and periodic, are found in the medial entorhinal cortex (MEC) and have been correlated with theta rhythm in many ways (Giocomo et al., 2007; Jeewajee et al., 2008; Barry et al., 2012). Furthermore, input from the MS is necessary for maintaining the spatially periodic firing of grid cells and reduction of this is correlated with a disruption in theta (Brandon et al., 2011; Koenig et al., 2011). Grid scale has been correlated with theta frequency in a number of different ways and anxiolytics offer the opportunity to observe the effects of manipulating just the frequency without disrupting theta oscillations completely.

3.1.1. Dense GABAergic innervation throughout MS and MEC influences activity

GABA is the major inhibitory neurotransmitter and therefore GABA receptors are found ubiquitously throughout the brain. BDZs, such as diazepam, are positive allosteric modulators of GABA-A receptors and act by binding to the BDZ site, enhancing the effects of GABA (i.e. generally increasing chloride influx and pushing the cell toward the Nernst potential for chloride which is below the firing threshold) (Tan et al., 2011). The BDZ sites are found on GABA-A receptors between the alpha and gamma subunits

making up the receptor complex, and BDZs can affect different receptors made up of multiple subunit combinations, with only alpha4 and alpha6 isoforms being BDZ insensitive (Gao et al., 1995; Tan et al., 2011). One of the most common GABA-A receptor combinations accounts for over 40% of GABA-A receptors in the brain and is sensitive to BDZs (Gao et al., 1995). BDZ sensitive GABA-A receptors are present on both GABAergic and cholinergic neurons in the MS (Gao et al., 1995), and throughout cells in the MEC, suggesting BDZs could affect activity in these areas directly.

MS infusion of the GABA-A agonist muscimol severely disrupts both theta rhythm in the MEC and the spatial selectivity of grid cells (Mizumori et al., 1989; Brandon et al., 2011). However, since muscimol acts directly on GABA sites (as opposed to diazepam which has a positive modulatory effect through the BDZ site) it can still produce inhibition in cells without an afferent neuron releasing GABA (Gao et al., 1995). This could explain why theta power is nearly completely eliminated with muscimol infusions, whereas theta frequency and power are merely reduced with diazepam (Caudarella et al., 1987; Scheffzük et al., 2013).

3.1.2 Models provide testable predictions involving administration of benzodiazepines

Oscillatory interference models (OIMs) use interacting theta frequency oscillations to generate the spatially periodic firing of grid cells. Slight differences in theta frequency, as is seen in the subthreshold membrane potential oscillations recorded in layer II MEC stellate cells *in vitro* (Giocomo et al., 2007) and in the frequency of the rhythmicity of grid cell firing (Jeewajee et al., 2008), are hypothesized to be involved with the grid field size and spacing increase seen in progressively more ventrally

recorded grid cells in the MEC (Brun et al., 2008). Specifically, Burgess (2008) suggested that anxiolytics reduce the intercept, and not the slope, of the relationship between theta frequency and running speed. Therefore, while the mean theta frequency would decrease, grid scale would not be affected by anxiolytic administration.

The mechanisms underlying BDZ induced decreases in theta frequency are not well understood, and it is not known whether effects are mediated through the MS, which is necessary for theta rhythm in the MEC. Infusing a BDZ into the MS can test the involvement of this structure, along with a model prediction by John et al. (2014). In a septo-hippocampal model of the experimental results of anxiolytic effects on hippocampal theta shown by Wells et al. (2013), they predicted that introduction of BDZs into this system would be unable to produce a measurable effect on theta frequency. By comparing MEC recordings just before and following MS infusion of a BDZ to systemic experiments, this prediction can also be explicitly tested.

3.2. Materials and Methods

3.2.1. Subjects

Male Long-Evans rats (Charles River Laboratories) weighing between 350-450 grams at surgery were used for these studies. All experimental procedures were approved by the Institutional Animal Care and Use Committee for the Charles River Campus at Boston University. Rats were housed individually in plexiglass cages, maintained on a 12-hour light/12-hour dark cycle (testing always occurred during the light cycle), and were maintained at ~85% of their ad libitum weight. Prior to surgery, rats were

habituated to the experimenter and testing room. The animals were trained to forage in an open field environment (1 m by 1.5 m) for pieces of Froot Loops (Kellogg's). One wall of the otherwise black painted environment was white to provide stable landmark information; cues surrounding the environment were present to provide distal information as well.

3.2.2. Implant

Rats were implanted with recording drives housing up to 16 individually moveable tetrodes (four 12.7 μm nichrome wires spun together) and 4 reference tetrodes, aimed at the MEC. Tetrodes were gold plated to bring down the impedance to <150 kOhm. The exit of the drive was angled at ~25 degrees in the posterior direction in order to implant just anterior of the transverse sinus.

3.2.3. Surgery

Rats were anesthetized with isoflurane and given an injection of a ketamine/xylazine/acepromazine cocktail and buprenorphine; depth of anesthesia was monitored at least every 15 minutes by checking breathing and confirming lack of response to a toe pinch. An injection of atropine was given to prevent fluid buildup in the lungs. After the initial incision, the skull area was cleared of fascia and approximately 10 holes were drilled to attach anchor screws into the skull; 1-2 ground screws were placed over the cerebellum. Two craniotomies were performed: one to implant a drug delivery cannula (from Bregma: 0.5 mm anterior, 3.0 mm lateral; implanted at 25 degrees medially, lowered 6.0 mm from brain surface) and the second as the implant site (left

hemisphere; most lateral and posterior corner grazes where the left bone ridge and lambda suture meet). The implant was secured in place using Kwik-Sil and dental acrylic. Tetrodes were lowered 2-3 mm from the dorsal surface at surgery. Animals were allowed one week to fully recover after surgery before experiments began.

3.2.4. Neural recordings

Animals were tested daily in the open field during recordings to search for grid cells, conjunctive grid-by-head-direction cells, border cells, and theta rhythmic cells. Once theta rhythmic cells and theta oscillations in the LFP were recorded, tetrodes were lowered a maximum of ~35 μm/day; experiments were never done on days tetrodes were turned in order to maximize the likelihood of recording the same cells across sessions. Neural signals were preamplified by unity-gain operational amplifiers located on the head of the animal. Signals were linked to digital amplifiers and amplified (5,000-20,000X) and bandpass filtered (1-500 Hz) by the 64-channel Cheetah Digital Lynx acquisition system (Neuralynx Corp., Bozeman, MT). When a signal crossed threshold all four channels of the tetrode were digitized at 32 kHz and recorded. Position, head direction, and velocity data were calculated from a red (front) and green (back) diode positioned on the recording head stage and sampled at 30 Hz. Position was determined as the centroid of the diodes. LFP activity was collected at 32 kHz and downsampled to 508 Hz. LFP traces obtained from the MEC were recorded from a single lead of a tetrode and referenced to the animal ground or to a cortical electrode that did not show theta oscillations when referenced to ground.

3.2.5. Histology

When possible, final tetrode positions were marked before sacrificing the animal by passing current through tetrodes that had recorded grid cells. Animals were overdosed with isoflurane and perfused intracardially with saline followed by 4% paraformaldehyde. Brains were extracted and stored in 4% paraformaldehyde at 6 degrees C for at least 24 hours. Approximately 72 hours before slicing, brains were transferred into a 30% sucrose solution. The brain was cut to separate the MS and MEC portions; the MEC was sectioned along the sagittal plane to visualize tetrode tracks, while the MS was sliced along the coronal plane to confirm cannula placement. Sections were mounted on gelatin-subbed glass slides and stained with cresyl violet.

3.2.6. Experimental design

One to two 20-minute pre-drug recording sessions were performed prior to drug injection or infusion. After drug administration, recording sessions were performed up to 45 minutes in duration to ensure adequate coverage of the environment. This session began within 10 minutes following diazepam infusion, within 15 minutes of muscimol infusion, and at 30 minutes post diazepam injection. A twenty-minute recovery session was recorded 3-6 hours post-drug administration and 24 hours later, to confirm return to normal activity. Multiple experiments, including administration of different types of drugs, were performed in a rat for as long as a given grid cell could be well-isolated, however there was a minimum of 48 hours between all drug and vehicle administrations. When single units of interest could no longer be isolated, tetrodes were moved down and screening for cells of interest began again.

3.2.7. Drugs and drug administration

Drugs were administered either systemically through intraperitoneal injection or intracranially into the MS via the implanted guide cannula. Prior to an infusion, the dummy cannula was removed to allow access to the guide cannula. An injector cannula (33 gauge), extending 1 mm beyond the guide cannula, was filled with the drug or vehicle and lowered through the guide cannula and into the MS. A microinfusion pump infused 0.5 μL of the solution at a rate of 0.125 μL/min. The injector cannula was left inserted for two minutes after the infusion to allow the drug to diffuse throughout the tissue. The injector cannula was then removed and replaced with a sterilized dummy cannula.

Volume-matched vehicle controls were performed for both systemic injections (1 mL/kg) and infusions (0.5 μL). The BDZ diazepam (Sigma) was mixed in DMSO to make a concentration of 1.0 mg/mL and administered at 1.0 mg/kg systemically or infused between 5-30 μg. At this point, not enough DMSO (vehicle) infusion experiments had been performed to compare drug effects against so PBS was used for statistical testing for the time being. It is worth nothing that in the literature, lateral septum infusions of DMSO plus Cremophor and saline do not produce any behavioral effects (Stemmelin et al., 2005). Infusion of DMSO into the medial septum, hippocampus unilaterally or bilaterally, or intraventricularly did not have any effects on theta rhythm in the LFP, including looking at power and frequency (Leung and Shen, 2004; Sharifzadeh et al., 2005; Tronson et al., 2009).

Before commencing the first infusion experiment in a rat, a muscimol infusion (0.5 μL of 0.5 μg/μL) was performed once a grid cell was recorded and/or when theta oscillations were present in the LFP to confirm loss of theta power and grid cell spatial periodicity (when grid cells were being recorded) in order to verify correct cannula placement. If spatial periodicity and theta power were not disrupted, an injector cannula with a 2mm projection was tried, at least 48 hours later. If this was not successful, the rat was not used for collecting infusion data.

Diazepam systemic

Diazepam has been used widely in the literature and a small selection of representative doses can be found in Table 3.1. In this work, 1 mg/kg was administered as it was commonly found in the literature and did not greatly affect ambulation in most cases. In most reported cases, diazepam injection preceded experimental testing by 30 minutes; the same was done in these experiments as well.

Diazepam infusion

Literature review only yielded two groups reporting effects of infusing diazepam into the MS (Table 3.2). The amounts reported were quite a bit lower than what has been reported when infused into other areas of the brain (Table 3.3). Several infusion amounts were tested to help ensure any negative result was not due to insufficient concentration and included 2.5, 5, 10, and 15 μg. Experimental testing was performed ranging from immediately after diazepam infusion to 25 minutes post. Most recordings for this work were performed approximately 10 minutes after diazepam infusion.

3.2.8. Analyses

Cluster cutting across sessions

After the completion of each recording session, single units were isolated using cluster cutting software (Offline Sorter, Plexon Inc.). Single units were distinguished using peak amplitude and principal components for each waveform. Stability of units was confirmed by tracking waveform profiles across the four leads of the tetrode and cluster position across recording sessions, comparing to the baseline session.

Measurement of theta rhythm and running speed

LFP activity was collected at 32 kHz and downsampled to 508 Hz. Downsampled LFP was filtered using a second order butterworth bandpass filter with cutoff frequencies of 6-10 Hz for theta band. Phase was estimated using the angle of the Hilbert transform of the filtered signal and instantaneous amplitude was estimated as the amplitude of the Hilbert transform. The LFP channel used for analyses was chosen on an animal-by-animal basis for each set of four recording sessions based on spectral properties from the baseline recording (Brandon et al., 2013). For each channel the spectrum of LFP power was found, the peak within theta range determined, and divided by the mean signal, giving the relative power within the theta band. The LFP channel was then chosen as the channel with maximum theta to noise ratio for each rat's baseline session. Theta frequency, amplitude, and power were calculated for 2.5 cm/s running speed bins and plotted from 5-30 cm/s. Each rat's LFP signal was normalized to aid comparison between animals per Wells et al. (2013). In brief, for each measure (frequency, amplitude, and power), the overall mean across all animals during baseline was calculated. A

normalization factor was determined on an animal-by-animal basis as the mean difference in the animal's baseline signal from the population mean. This normalization factor was applied across all sessions for each animal, giving a normalized signal. This method accounts for a mean difference, but not speed modulated difference, in theta measures between animals.

Measurement of single unit properties

Spatial rate maps were constructed for a given unit by taking the number of spikes in 3.6 cm by 3.6 cm spatial bins and dividing by the amount of time spent in that bin. Rate maps were smoothed using a 5x5 bin pseudo-Gaussian kernel with a one-pixel standard deviation. The spatial periodicity of grid cells was quantified with a "gridness" score and computed from the spatial autocorrelation of the smoothed rate maps. For the gridness score calculated, "gridness 3," the center peak was removed from the autocorrelation and if present, the six surrounding peaks found and cut out to make a donut. If the grid shape was elliptical, it was distorted to create a circle. The correlation was calculated for each 3 degree rotation of the donut to itself. The gridness score is the difference between the correlation at the minimum peak of 60 or 120 degrees and the maximum trough at 30, 90, or 150 degrees. The grid field distance was determined from the spatial autocorrelation by calculating the average distance between the middle and six surrounding peaks, checked manually to ensure the proper fields were being detected and measured.

Head direction firing properties of units were calculated by constructing a polar histogram of firing rates by head direction. Spikes were put into bins of 6 degrees and

divided by the amount of time spent facing that direction. The mean resultant length (MRL) of the directionality of spiking was then calculated.

The spatial information (SI) score reflects the degree to which a cell's spiking can be used to predict the animal's location. It was calculated as in Cacucci et al. (2007) and expressed in bits/spike. Correlation of the spatial rate maps for cells were calculated by finding the Pearson's correlation coefficient between the baseline rate map and the following sessions for a given cell.

Spike time autocorrelograms were created with time bins of 10 ms and normalized and clipped to the peak in the theta range (6-10 Hz). Autocorrelograms were then fit with the equation:

$$y(t) = [a*(\cos(\omega*t)+1)+b]*\exp(-|x|/\tau_1)+c*\exp(-t^2/\tau_2^2))$$

Where y(t) is the normalized autocorrelogram value, t is the time lag, a is an amplitude of rhythmicity, τ_1 and τ_2 are fall off constants, b and c are coefficients for theta rhythmicity and theta skipping, and ω is the intrinsic frequency of the cell. The theta index was then defined as (a+b) over the mean of y, representing the relative amount of power in the theta range.

Classification of cells

Single units were classified as grid cells, head direction cells, spatially modulated non-grid cells, theta rhythmic cells, or interneurons. Grid cells were further divided into conjunctive (additionally head direction modulated) and non-conjunctive grid cells. To

determine gridness, head direction, and spatial information thresholds, shuffling was performed as in Bonnevie et al. (2013), for gridness 3, MRL, and SI content, respectively. Briefly, the sequence of spikes from a given cell was time shifted along the rat's path by a random interval between 20 s and 20 s minus session length, with the end wrapped to the beginning. A single unit was deemed a given cell type if the value exceeded the 95th percentile of all shuffled permutations. The thresholds for gridness3, MRL, and SI were 0.1902, 0.1586, and 3.2816, respectively. Cells not showing significant gridness, directionality, or SI content but were significantly theta rhythmic based on the measure described above, were deemed theta rhythmic cells. Cells with firing rates greater than 10 Hz were classified solely as putative interneurons (Savelli et al., 2008; Buetfering et al., 2014; Zheng et al., 2015). Somewhat surprisingly, shuffling to determine the SI threshold resulted in a very high number, suggesting the ease to which cells can be classified as spatially modulated, considering a common threshold used is 0.5, regardless of whether the cell's firing is based on actual spiking or shuffled data. Given this, and that few cells could be classified as spatially modulated, analyses were limited to grid cells, HD cells, theta rhythmic cells, and interneurons.

Data exclusion

If an animal did not cover at least 80% of the total number of position bins (3.6 cm x 3.6 cm) in the environment in the first 20 minutes of the recording session (length of most recordings) during the session immediately following drug administration, that set of experiments were excluded from analyses (Bjerknes et al., 2014). Histology was used to verify recording tracks to ensure they were positioned to record from the MEC

area; in one animal the recording drive was positioned too anteriorly and data from that animal were excluded. Single units were used for analyses if they were stable enough to be recorded across the first three recording sessions (Baseline, post-Drug/Vehicle administration, and 3-6 hour recovery), otherwise data for that cell were excluded and not analyzed.

Statistical tests of significance

All comparisons between baseline and other conditions used a Bonferroni correction for multiple comparisons with an alpha value of 0.05. This resulted in a p-value of 0.0016 for both LFP and single unit tests (0.05/(4*4*2) using an ANCOVA or repeated measures ANOVA, a p-value of 0.025 (0.05/2) for post-hoc t-tests, and a p-value of 0.05 for median speed tests.

For single unit analyses, a repeated measures ANOVA was performed for different measures (e.g. firing rate) to look at potential changes between baseline and after drug/vehicle administration, and tested for differences in the amount of change that occurred between the two groups. A significant result from this test suggests that the change that occurred from baseline to post-administration was different for the drug compared to the change that occurred after the vehicle. A non-significant result from this suggests that any change that might have occurred from baseline to post-administration for the drug was not significantly different from the potential change occurring after vehicle administration.

If the repeated measures ANOVA yielded a statistically significant result then a post-hoc paired t-test was performed to test for changes in the measure from baseline to

post-administration. A significant result from this suggests that after administration, the given measure changed significantly. A non-significant result implies that after administration, it cannot be rejected that the values are from the same distribution.

For LFP analyses, ANCOVAs were performed to examine changes in the intercept and slope of the relationship between LFP theta frequency, amplitude, and power across running speeds. Comparisons were made to vehicle, looking at potential differences in the change in the given measure from the baseline to second session (the recording following drug or vehicle administration). If an ANCOVA result was significant, a post-hoc ANOVA was performed to test for drug effects on the slope and intercept.

3.3. Results

3.3.1. Systemic administration of diazepam: LFP

Systemic administration of diazepam produced significant effects on theta frequency across a range of running speeds, similar to what has been reported in the hippocampus. ANCOVAs were performed to examine changes in the intercept and slope of the relationship between LFP theta frequency, amplitude, and power across running speeds. Comparisons were made to vehicle, looking at differences in the change in the given measure from the baseline to second session (the recording following drug or vehicle administration). If an ANCOVA result was significant, a post-hoc ANOVA was performed to test for drug effects on the slope and intercept.

After drug administration, the intercept of the relationship between theta frequency and running speed decreased from baseline compared to vehicle ($F(1,66)=43.11$, $p<9.51e-9$) (Figure 3.1, A1-2). This decrease was significant when looking at just the effect of drug from baseline as well ($F(1,76)=88.19$, $p<1e-10$) (Figure 3.1, A1). There were no significant differences found in the change in slope after drug administration compared to vehicle ($F(1,66)=0.46$, $p=0.5$) (Figure 3.1, A1-2).

Compared to vehicle, the change in intercept of theta amplitude across running speeds decreased after drug administration ($F(1,66)=29.02$, $p<1.03e-6$) while the difference in slope was not significantly different ($F(1,66)=0.02$, $p=0.88$) (Figure 3.1, B1-2). The decrease in the intercept was not significant when only looking at the change from baseline after diazepam injection ($F(1,76)=0.33$, $p=0.57$) (Figure 3.1, B1).

The intercept of theta power across running speeds was reduced after drug administration in comparison to vehicle ($F(1,66)=17.15$, $p<1.00e-4$) (Figure 3.1, C1-2). When looking at just the drug effect on the intercept of power from baseline, this was not significant ($F(1,76)=3.29$, $p=0.07$) (Figure 3.1, C1). No significant differences were seen in the changes in slope of theta power across running speeds when comparing drug and vehicle administration ($F(1,66)=0.79$, $p=0.38$) (Figure 3.1, C1-2).

3.3.2. Systemic administration of diazepam: single units

Repeated measures ANOVAs were performed to examine changes between baseline and the second recording session (following drug or vehicle administration), testing for differences in this change when comparing drug and vehicle. If the repeated

measures ANOVA was significant, a post-hoc paired t-test was performed to test for drug effects on the given measure from baseline to the post-administration second session.

In brief, no significant differences were seen in single unit firing properties after systemic administration of diazepam. After drug administration compared to vehicle administration, no differences were found in the change in mean firing rate between drug and vehicle for grid cells ($F(1,12)=1.42$, $p=0.26$), head direction cells ($F(1,27)=2.06$, $p=0.16$), theta rhythmic cells ($F(1,20)=0.21$, $p=0.65$), or interneurons ($F(1,5)=6.48$, $p=0.051$) (Figure 3.2).

No differences were found in the change between baseline and the second session in MRL for conjunctive cells ($F(1,7)=0.23$, $p=0.65$) or HD cells ($F(1,27)=8.10$, $p=0.008$) (Figure 3.3).

The differences in the change between drug and vehicle for gridness ($F(1,12)=0.63$, $p=0.44$) and grid field distance ($F(1,7)=6.11$, $p=0.04$) did not reach significance (Figure 3.4). Although qualitatively it looks like approximately half of the grid cells dropped in gridness score, most of those grid scores stayed below the threshold the remaining sessions. The rate maps and spatial autocorrelograms for all of the recorded grid cells can be seen in Figure 3.5.

There was no significant difference in the change seen in SI for grid cells when comparing drug and vehicle groups ($F(1,12)=2.84$, $p=0.12$) (Figure 3.6, left). Because the correlation of the baseline to itself is always 1, differences in spatial correlation of rate maps to baseline between the drug or vehicle session were compared to the 3-6 hour recovery session. No significant differences were seen when looking at the change in

spatial correlation when comparing drug and vehicle ($F(1,12)=0.78$, $p=0.39$) (Figure 3.6, right). Overall, systemic injection of diazepam did not have a significant effect on median running speed ($t(4)=-1.88$, $p=0.13$), nor did vehicle injection ($t(3)=-0.73$, $p=0.52$) (Figure 3.7).

No differences were seen in grid cells from baseline to the second session when comparing drug and vehicle groups in the change in intrinsic rhythmicity ($F(1,12)=1.03$, $p=0.33$) (Figure 3.8, left) or in theta index ($F(1,12)=0.03$, $p=0.86$).

3.3.3. MS infusion of diazepam: LFP

Across doses, MS infusion of diazepam did not produce any significant differences in the change in theta frequency across running speeds when compared to PBS vehicle infusion for either intercept ($F(1,56)=0.07$, $p=0.79$) or slope ($F(1,56)=1.21$, $p=0.28$) (Figure 3.9, A1-2), despite infusions of muscimol and the serotonergic agonist, 8-OH-DPAT producing effects within the same animals (Figure 3.10).

No significant differences between drug and vehicle were found in the change in amplitude of this relationship in the intercept ($F(1,56)=4.43$, $p=0.04$) or the slope ($F(1,56)=3.33$, $p=0.07$) (Figure 3.9, B1-2).

No significant differences were found in the change of theta power across running speeds comparing drug and vehicle for intercept ($F(1,56)=2.32$, $p=0.13$) or slope ($F(1,56)=0.001$, $p=0.97$) (Figure 3.9, C1-2).

3.3.4. MS infusion of diazepam: single units

In brief, no significant differences were seen in single unit firing properties after MS infusion of diazepam. After drug infusion compared to PBS infusion, there were no significant differences seen in the change in firing rates for grid cells ($F(1,11)=1.63$, $p=0.23$), head direction cells ($F(1,26)=0.01$, $p=0.91$), theta rhythmic cells ($F(1,26)=0.01$, $p=0.92$), or interneurons ($F(1,7)=9.75e-4$, $p=0.98$) when comparing changes seen in drug and vehicle groups (Figure 3.11).

No significant differences in changes between drug and vehicle groups in the MRL for HD cells ($F(1,26)=1.81$, $p=0.19$) (Figure 3.12, right) or conjunctive cells ($F(1,4)=0.05$, $p=0.83$) (Figure 3.12, left) were found.

Testing for differences in changes after infusion of diazepam or vehicle when comparing the two was not significant for gridness score ($F(1,11)=0.07$, $p=0.80$) or grid field distance ($F(1,7)=0.12$, $p=0.74$) (Figure 3.13).

No difference was seen in the change in SI between the two groups from baseline to the second session for grid cells ($F(1,11)=0.82$, $p=0.39$) (Figure 3.14, left). No significant difference emerged in the change of spatial correlation of spatial rate maps to baseline when comparing drug and vehicle effects between post-drug administration and the 3-6 hour recovery session ($F(1,11)=0.25$, $p=0.62$) (Figure 3.14, right). MS infusion of diazepam significantly decreased median running speed from baseline to post-infusion sessions ($t(6)=-6.43$, $p<6.71e-4$) while PBS vehicle infusion did not ($t(1)=-6.58$, $p=0.1$) (Figure 3.15).

No changes were seen from baseline to the second session when comparing drug and vehicle groups for grid cell intrinsic firing rhythmicity ($F(1,11)=1.94$, $p=0.19$) or theta index ($F(1,11)=1.68$, $p=0.22$) (Figure 3.16).

3.4. Discussion

In our results, the systemic administration of a benzodiazepine decreased theta frequency. Specifically, it decreased the y-intercept of the linear fit to the plot of theta frequency over different running speeds. Furthermore, systemic administration also decreased the intercept of the amplitude of theta oscillations across running speeds, suggesting theta rhythm became slower and smaller after systemic administration of diazepam. The systemic results from these experiments strongly corroborate the reported effects of anxiolytics on hippocampal LFP theta frequency (Wells et al., 2013), expanding detection to a new structure, the MEC.

MS infusion of diazepam did not produce any changes in MEC theta frequency, despite infusions of muscimol, a GABA-A agonist, disrupting theta oscillations in the same animals, as in previous reports (Mizumori et al., 1989; Brandon et al., 2011). This suggests that despite the MS being necessary for theta oscillations in both the MEC and hippocampus, the actions leading to a decrease in theta frequency in these areas by BDZs must be exerted outside the MS. In a septo-hippocampal model examining the effects of anxiolytic drugs on this circuit, it was suggested that increasing the maximal synaptic conductance of GABA-A receptors in this circuit had a negligible effect on mean theta frequency, predicting that introduction of BDZs into a septo-hippocampal circuit would not affect theta frequency (John et al., 2014). The septo-entorhinal circuit shares many

similarities with the septo-hippocampal circuit, including decreases in theta frequency after systemic administration of anxiolytics and if the John et al. (2014) prediction is extended to involve the MEC as well, this would lend support. John et al. (2014) suggest that the BDZ effect on theta frequency is mediated through medial hypothalamic sites, given that infusions of CDP into the medial supramammillary nucleus produce anxiolytic effects similar to systemic administration and reduce hippocampal theta frequency (Woodnorth and McNaughton, 2002; John et al., 2014). Future experiments involving BDZ infusions into the medial supramammillary nucleus while recording activity in the MEC could confirm this, but are beyond the scope of this work.

While median running speed was significantly lower after drug infusion, it is unlikely this affects the interpretation of the results. For one, the manner of examining changes in LFP theta minimizes the effects of differences in running speed across sessions by looking within bounded speed windows. Even given that a slower running speed would reduce theta frequency, the effect would be limited to lowering the average within a 2.5 cm/s bin, which is negligible. Furthermore, a drug effect on theta frequency was only found after systemic administration and not MS infusion, despite running speed being significantly altered during infusion trials.

Examining theta power across running speeds suggested a slight decrease in power through a change in the intercept and not the slope after systemic administration but not MS infusion. While Wells et al. (2013) did not see an effect on theta power after systemic BDZ administration, this small difference could be due to differences in calculating changes in power. They looked at subsets of data with similar median

running speeds while these results were calculated by finding the theta power within each speed bin and fitting a regression line to the data. However, this effect was relatively small in comparison to the change seen in theta frequency.

No changes were seen in the mean firing rates of any of the principal cell types or putative interneurons after systemic injection, similar to what was reported for principal cells in the hippocampus as well (Wells et al., 2013). MS infusion of diazepam did not elicit changes either. No significant differences were seen in any of the firing properties of the different types of neurons after either administration method of diazepam. Despite theta frequency in the LFP decreasing significantly, reflections of this could not be found in the spacing of grid fields. This is consistent with predictions made by Burgess (2008) that anxiolytics affect Type II theta due it being linked to arousal and anxiety (Sainsbury et al., 1987), which would not have an effect on the slope of theta frequency across running speeds and therefore grid cell field spacing. The lack of effects from diazepam administration on single unit firing properties highlights the resiliency of MEC cells to perturbations in the LFP. Future studies and analyses could look at LFP-related firing properties of grid cells, like seen in phase precession or phase locking, to examine if spiking slows down to maintain this relationship but might not be a large enough effect to be reflected in the intrinsic rhythmicity measures currently used.

3.5. Tables

Table 3.1. Selection of diazepam doses from the literature given via intraperitoneal injection.

Doses	Task	Effect	Timing	Citation
1.25 and 2.5 mg/kg	Social interaction test and elevated plus maze.	Both doses increased social interaction and open arm exploration and larger dose decreased motor behavior in both experiments.	30 minutes prior to testing.	Dunn et al. (1989)
1 and 2 mg/kg	Elevated plus maze.	Increased open arm traversals, decreased motor behavior.	30 minutes prior to testing.	Pellow et al. (1985)
1 mg/kg	Water maze.	Impaired retention of platform location (spatial information processing).	30 minutes prior to testing.	Brioni & Arolfo (1992)
0.3, 1, 3 mg/kg	Water maze.	1 and 3 mg/kg impaired place learning.	--	Arolfo & Brioni (1991)

Table 3.2. Literature review of diazepam concentrations infused into the medial septum or other areas of the brain.

Doses	Task	Effect	Timing	Citation
5, 10, and 15 pmol	Performed infusions and microdialysis to measure changes in hippocampal ACh.	Reduced hippocampal ACh release by 50%.	Maximal effect was 20 min post infusion, lasting up to 40 min.	Imperato et al. (1994)
1 ng	Step-down inhibitory avoidance task.	Infusion before training produced amnesia.	Infused 20 min before training.	Costa et al. (2010)

Table 3.3. Examples from the literature of infusions of diazepam into brain regions other than the MS.

Doses	Task	Effect	Timing	Citation
2 μg in ABLA bilaterally or dorsal periaqueductal gray	Anxiolytic effects measured with rat burying test (received shock) and effects on nociception effects evaluated.	Reduced burying behavior and had antinociceptive response.	Infused 15 min before burying behavior task.	Jimenez-Velazquez et al. (2010)
5 μg bilaterally in substantia nigra	Induced seizures via systemic administration of soman, which irreversably inhibits acetylcholinesterase.	Produced anticonvulsant effects.	Infused 20 min before soman injection.	Myhrer et al. (2006)
30 μg in amygdala and hippocampus	Negative contrast-- decrease in licking behavior when decrease sucrose concentration.	Infusion into amygdala but not hippocampus attenuated negative	Test conducted immediately after infusion.	Liao & Chuang (2003)

		contrast effect.		
20 ng, 100 ng, up to 5 µg unilaterally into locus coeruleus or intracerebroventricular infusion	Recorded sensory-evoked activity and spontaneous firing rates in LC; extracellular recordings under anesthesia.	Both infusion locations reduced spontaneous firing rates similar to systemic injections (though change very small); however unlike systemic injections did not attenuate evoked activity.	Infusion suggested to be just before post-drug recordings began.	Simson & Weiss (1989)
2 or 10 µg into raphe medianus in 1 ul, or 15 µg into dhipp in 3 µl	Examined effects on cerebral serotonin synthesis in hippocampus, cerebral cortex, striatum, cerebellum, and spinal cord.	Infusing 15 µg into hippocampus reduced 5-HT synthesis in that area. Infusion into raphe medianus did not affect hippocampal 5-HT synthesis.	Animals sacrificed 60 minutes after infusion to measure 5-HT synthesis.	Nishikawa & Scatton (1986)
30 µg into amygdala bilaterally	Tested post-shock freezing and hypoalgesia.	Infusing 30 µg bilaterally into basolateral amygdala attenuated both freezing and hypoalgesia.	Infusion (and formalin injection) occurred 25 minutes before behavioral testing.	Helmstetter (1993)

3.6. Figures

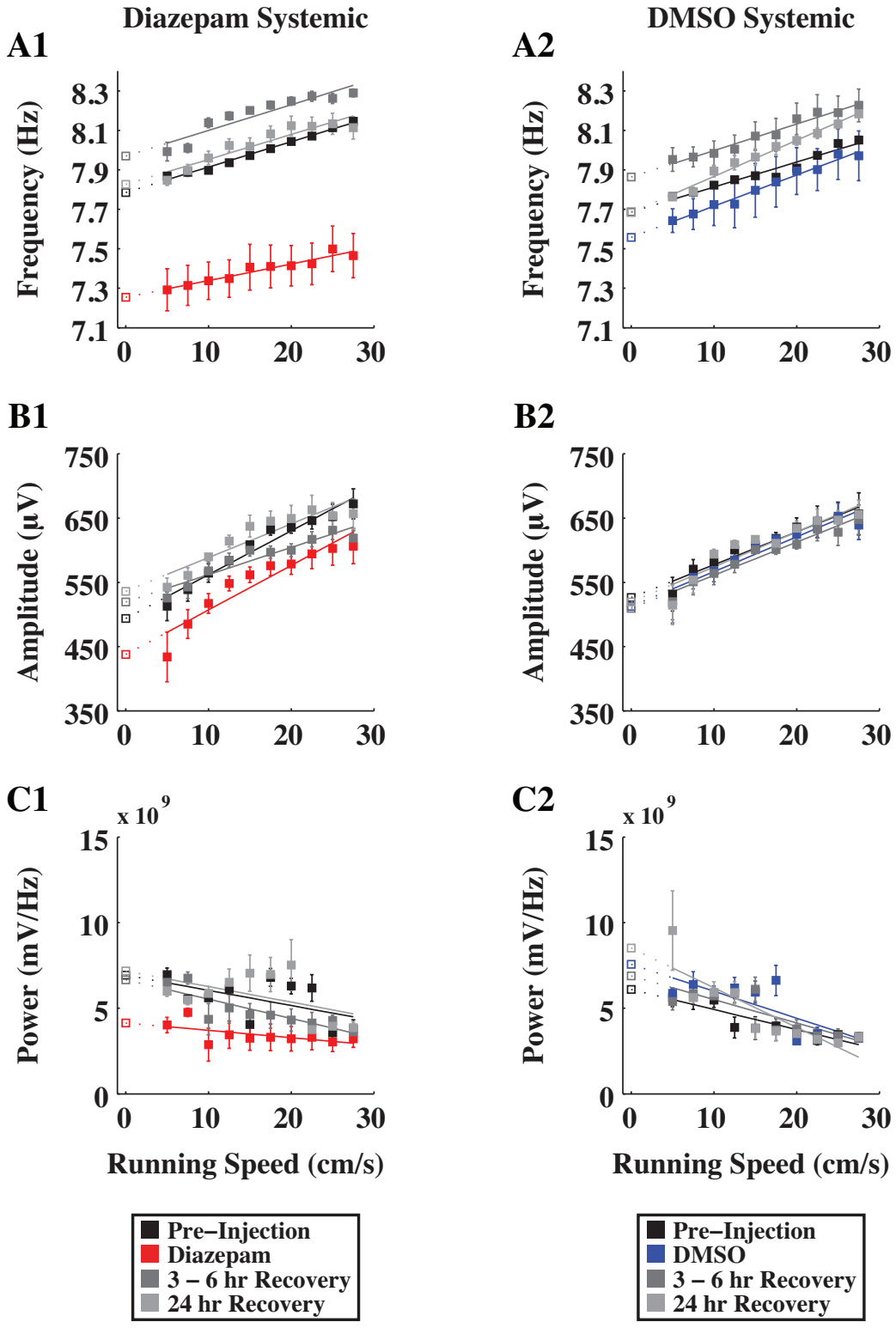
Diazepam Systemic
DMSO Systemic
A1
A2
B1
B2
C1
C2
Frequency (Hz)
Amplitude (µV)
Power (mV/Hz)
x 10^9
Running Speed (cm/s)
Pre–Injection
Diazepam
DMSO
3 – 6 hr Recovery
24 hr Recovery

Figure 3.1. Systemic injection of diazepam reduces the intercept of theta frequency and amplitude.

A. Effects of systemic injection (A1, red line) compared to baseline (black line) and recovery sessions (grey lines) on LFP theta frequency plotted across running speeds, and the same for vehicle (A2, blue line). B, C. Same as A but for theta amplitude and power, respectively.

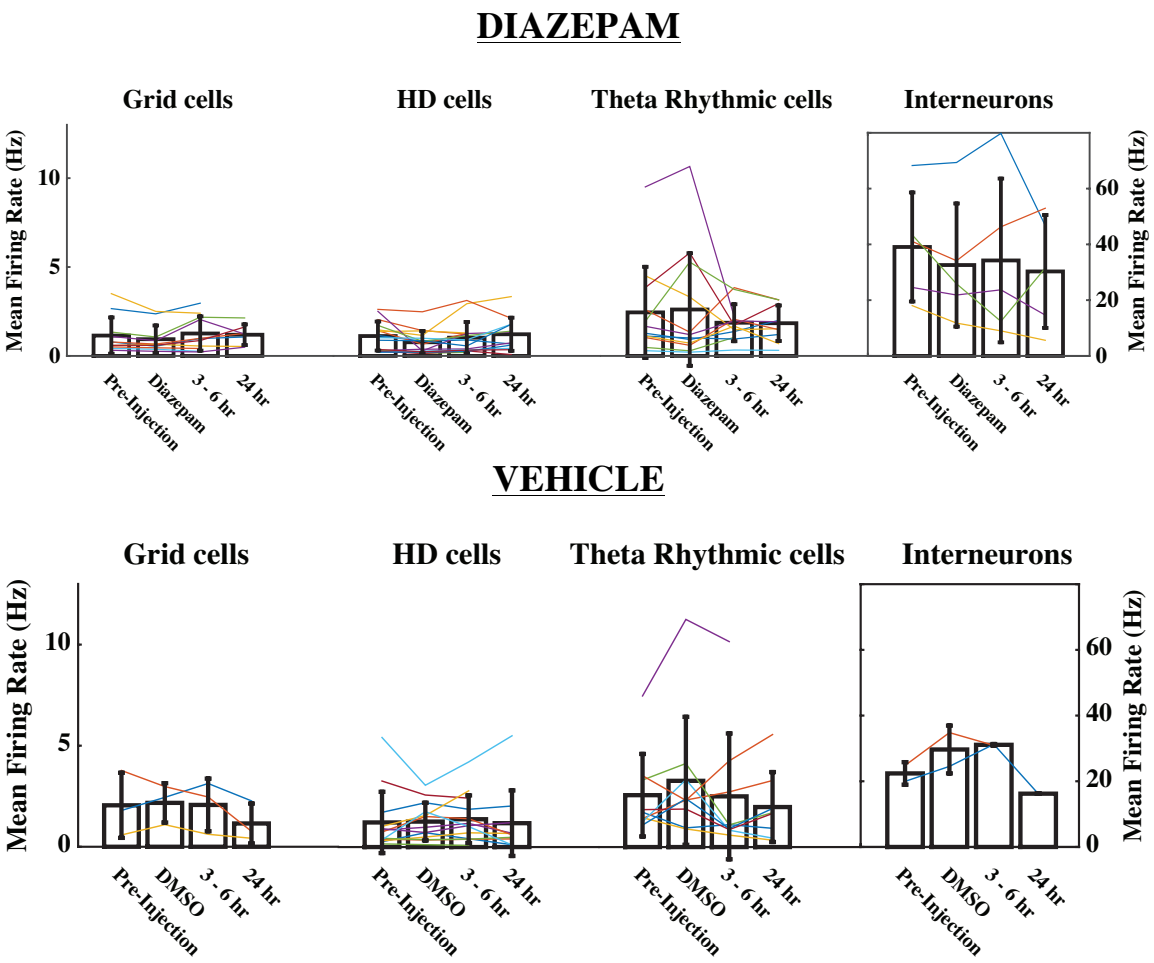

Figure 3.2. Mean firing rate for grid cells, HD cells, theta rhythmic cells, and interneurons across sessions.

No significant effects were seen after systemic injection of diazepam (top) and vehicle (bottom) on mean firing rate of grid cells, HD cells, theta rhythmic cells, or interneurons. Each cell recorded across sessions is marked by a single colored line. The vertical black line represents the standard error of measurement.

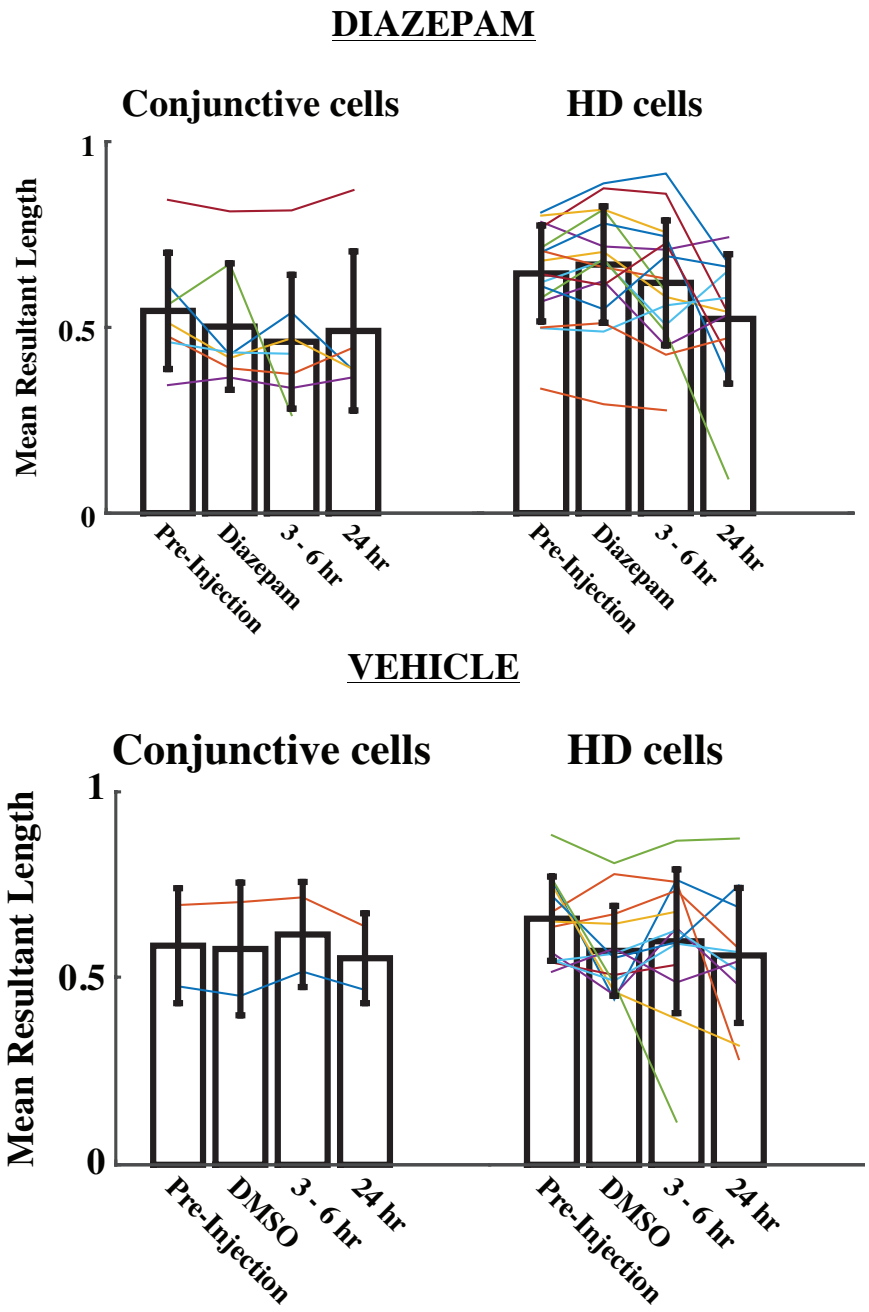

Figure 3.3. Mean resultant length of conjunctive and HD cells across sessions.

Directionality of cell firing across sessions for conjunctive grid cells and head direction cells after systemic injection of diazepam (top) and vehicle (bottom). No drug effects on directionality of firing for conjunctive head by grid cells or HD cells were seen. Each cell recorded across sessions is marked by a single colored line. The vertical black line represents the standard error of measurement.

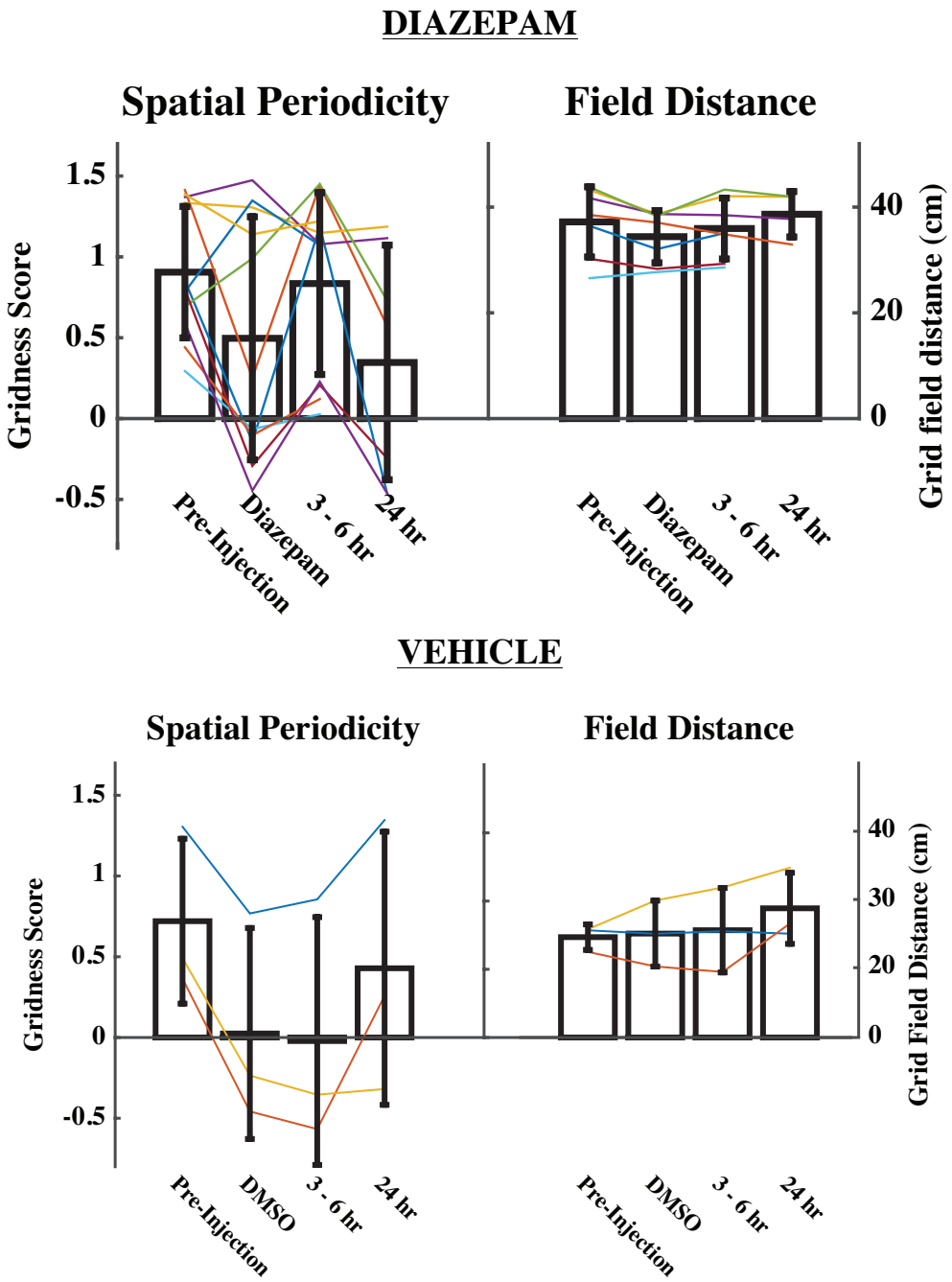

Figure 3.4. Spatial periodicity and grid field distances were unaffected by diazepam systemic administration.

Gridness score (left) and grid field distance (right) of grid cells after systemic injection of diazepam (top) and vehicle (bottom). Each cell recorded across sessions is marked by a single colored line. The vertical black line represents the standard error of measurement.

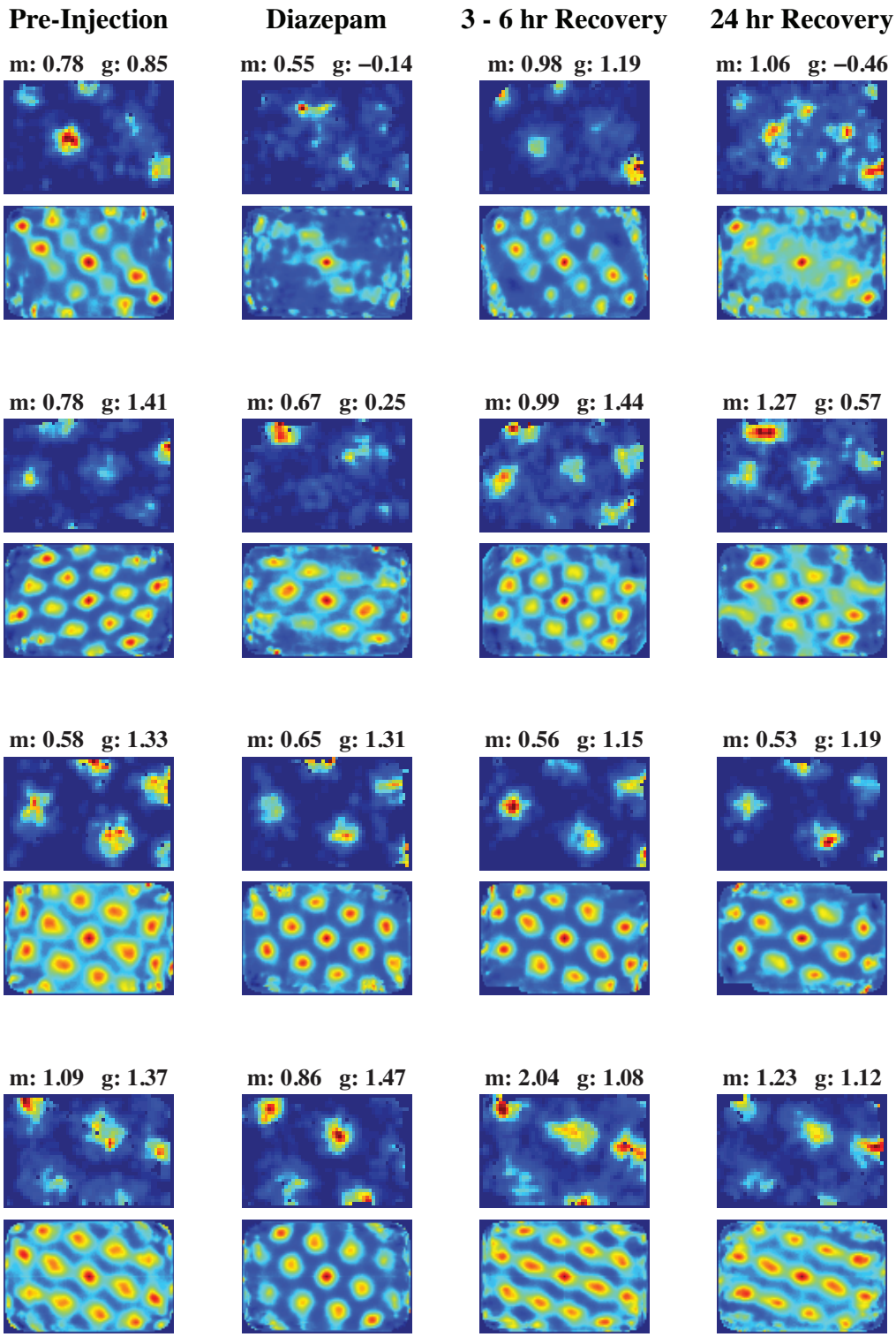
Pre-Injection
Diazepam
3 - 6 hr Recovery
24 hr Recovery
m: 0.78 g: 0.85
m: 0.55 g: –0.14
m: 0.98 g: 1.19
m: 1.06 g: –0.46
m: 0.78 g: 1.41
m: 0.67 g: 0.25
m: 0.99 g: 1.44
m: 1.27 g: 0.57
m: 0.58 g: 1.33
m: 0.65 g: 1.31
m: 0.56 g: 1.15
m: 0.53 g: 1.19
m: 1.09 g: 1.37
m: 0.86 g: 1.47
m: 2.04 g: 1.08
m: 1.23 g: 1.12

Pre-Injection	Diazepam	3 - 6 hr Recovery	24 hr Recovery
m: 1.34 g: 0.69	m: 1.07 g: 0.99	m: 2.18 g: 1.45	m: 2.14 g: 0.73
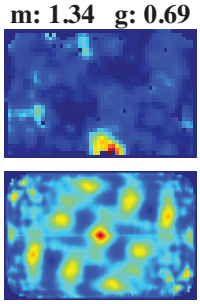	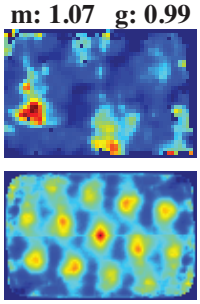	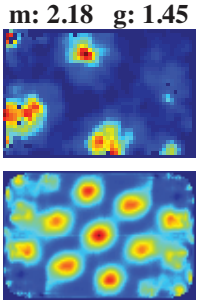	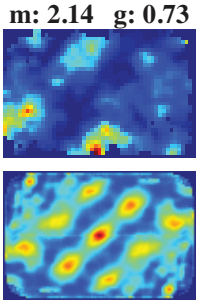
m: 0.42 g: 0.29	m: 0.37 g: –0.06	m: 0.25 g: 0.03	
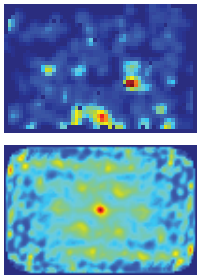	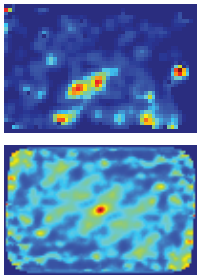	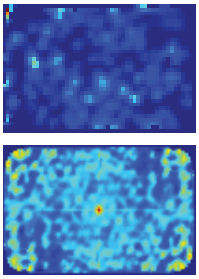	
m: 0.59 g: 0.80	m: 0.60 g: –0.29	m: 0.86 g: 0.21	m: 1.63 g: –0.25
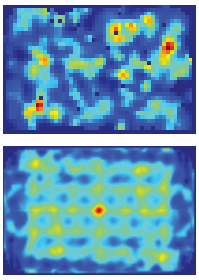	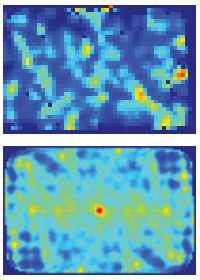	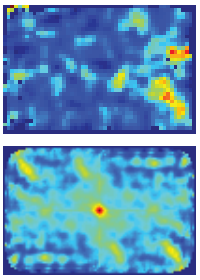	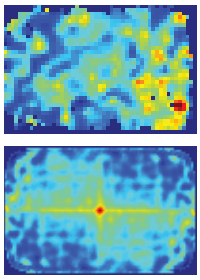
m: 2.66 g: 0.78	m: 2.37 g: 1.35	m: 2.97 g: 1.07	
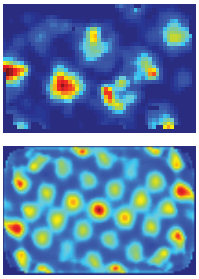	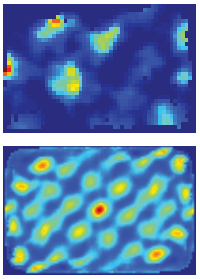	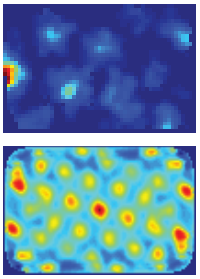	

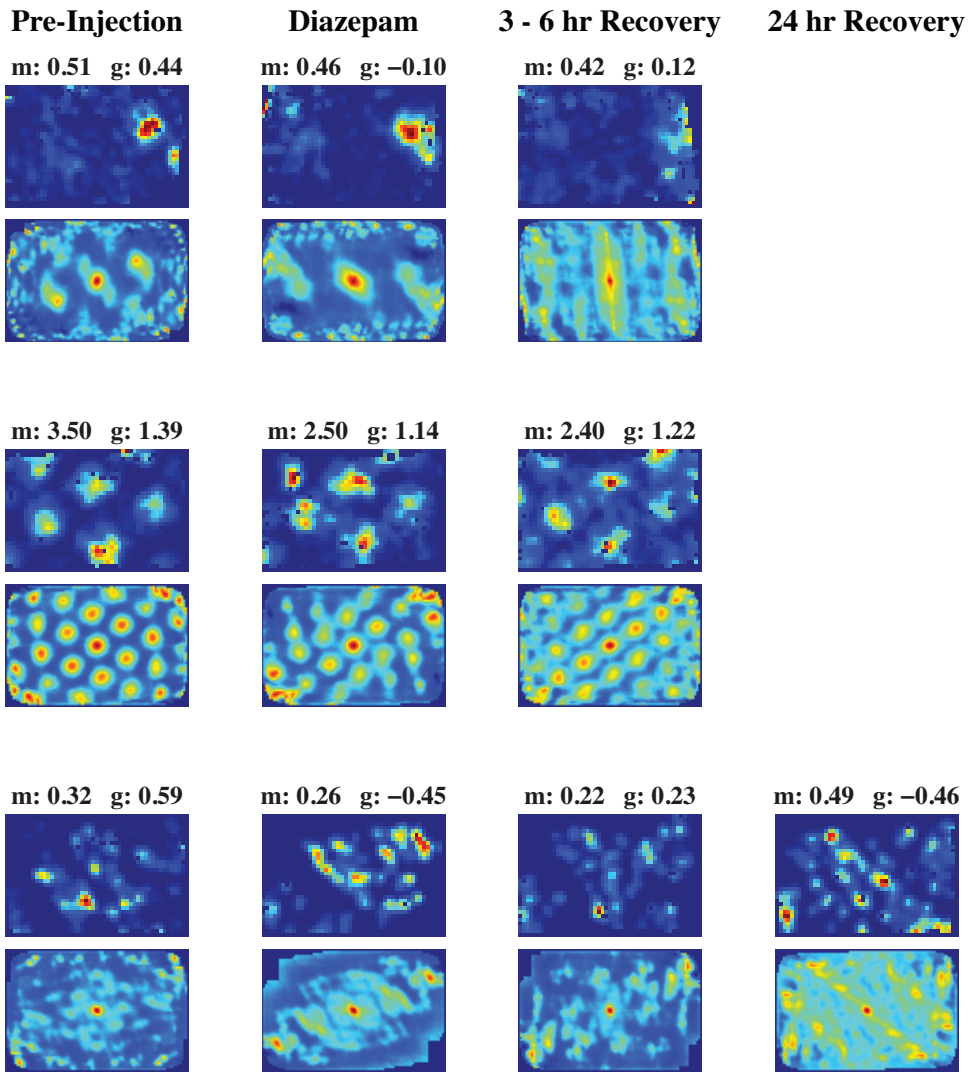

Figure 3.5. Rate maps and rate map autocorrelograms for all 11 grid cells for diazepam systemic experiments.

There was no statistical difference between gridness score before versus after administration of diazepam. Warmer colors in the plots indicate higher firing rates in the rate maps (top) and higher correlation in the spatial autocorrelation (bottom). Mean firing rate and gridness score are located on top of each plot. While the bar plot in Figure 3.4 suggests a number of grid cells lost their tuning after drug administration, qualitatively most appear to remain just as spatially periodic as before drug and during recovery sessions. Of note, the first two grid cells in the figure, recorded simultaneously, appear to undergo field remapping, returning to the original firing locations during recovery sessions. However, these are the only two examples of this phenomenon across all the experiments.

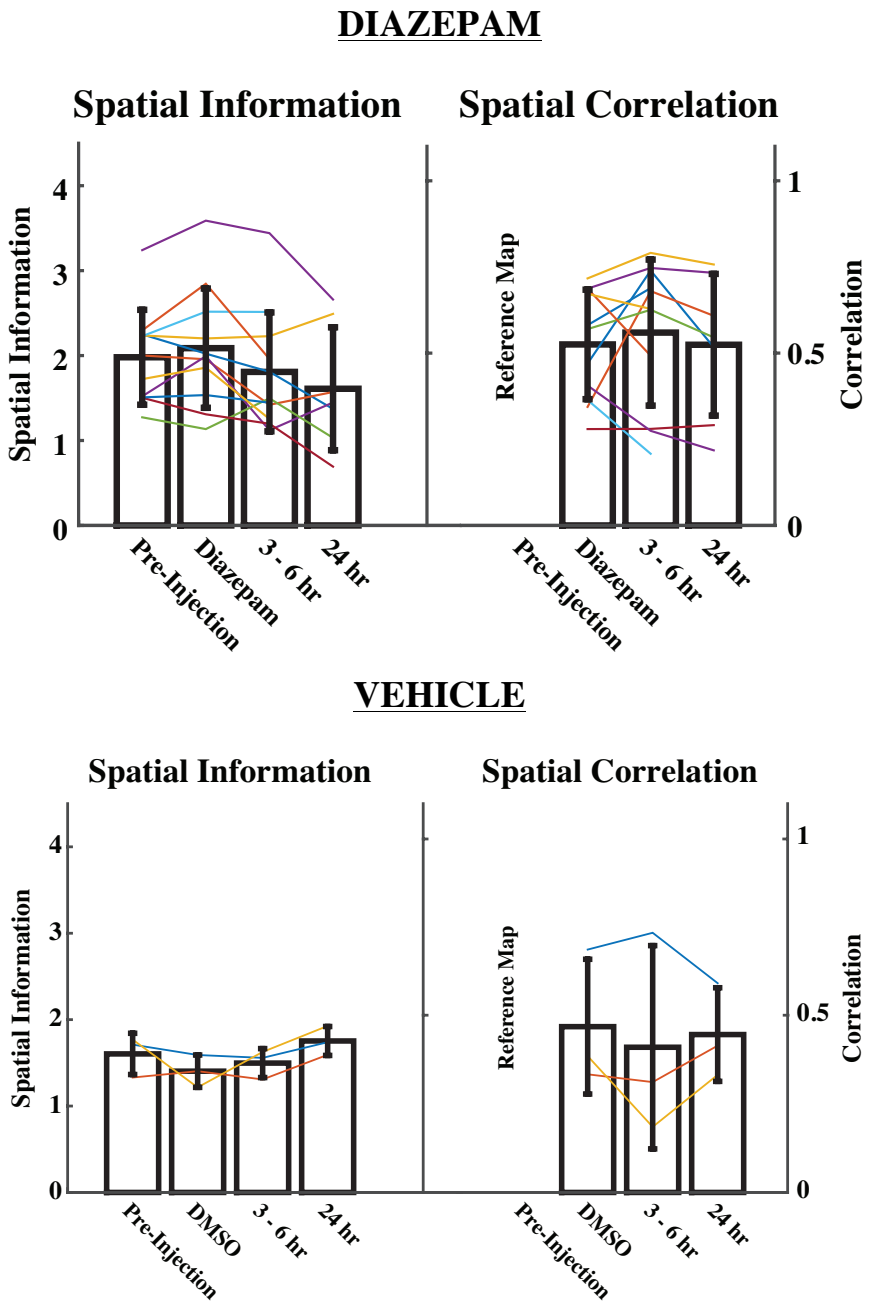

Figure 3.6. Spatial information score and correlation of rate maps of grid cells after systemic injection of diazepam and vehicle.

Measures of spatial firing after systemic injection of diazepam (top) and vehicle (bottom) for spatial information (left) and spatial correlation of rate maps (right). Each cell recorded across sessions is marked by a single colored line. The vertical black line represents the standard error of measurement.

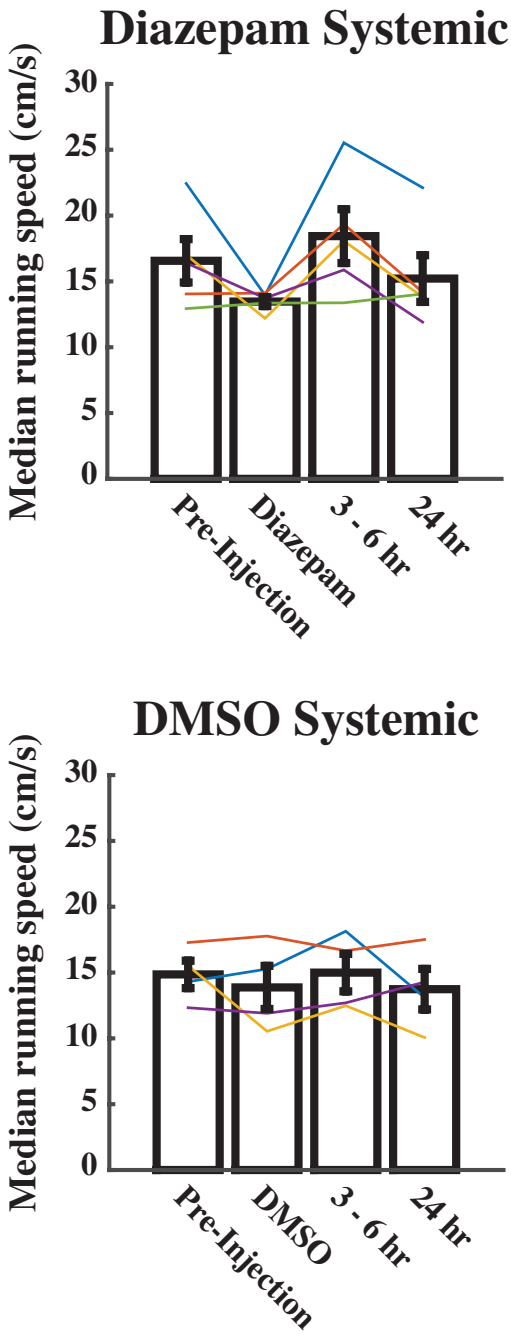

Figure 3.7. Median running speed (cm/s) across recording sessions.

No significant changes in median running speed from baseline to the second recording session were seen after administration of diazepam systemic (top) or PBS (vehicle) systemic experiments (bottom). Each session's median speed is marked by a single colored line. The vertical black line represents the standard error of measurement.

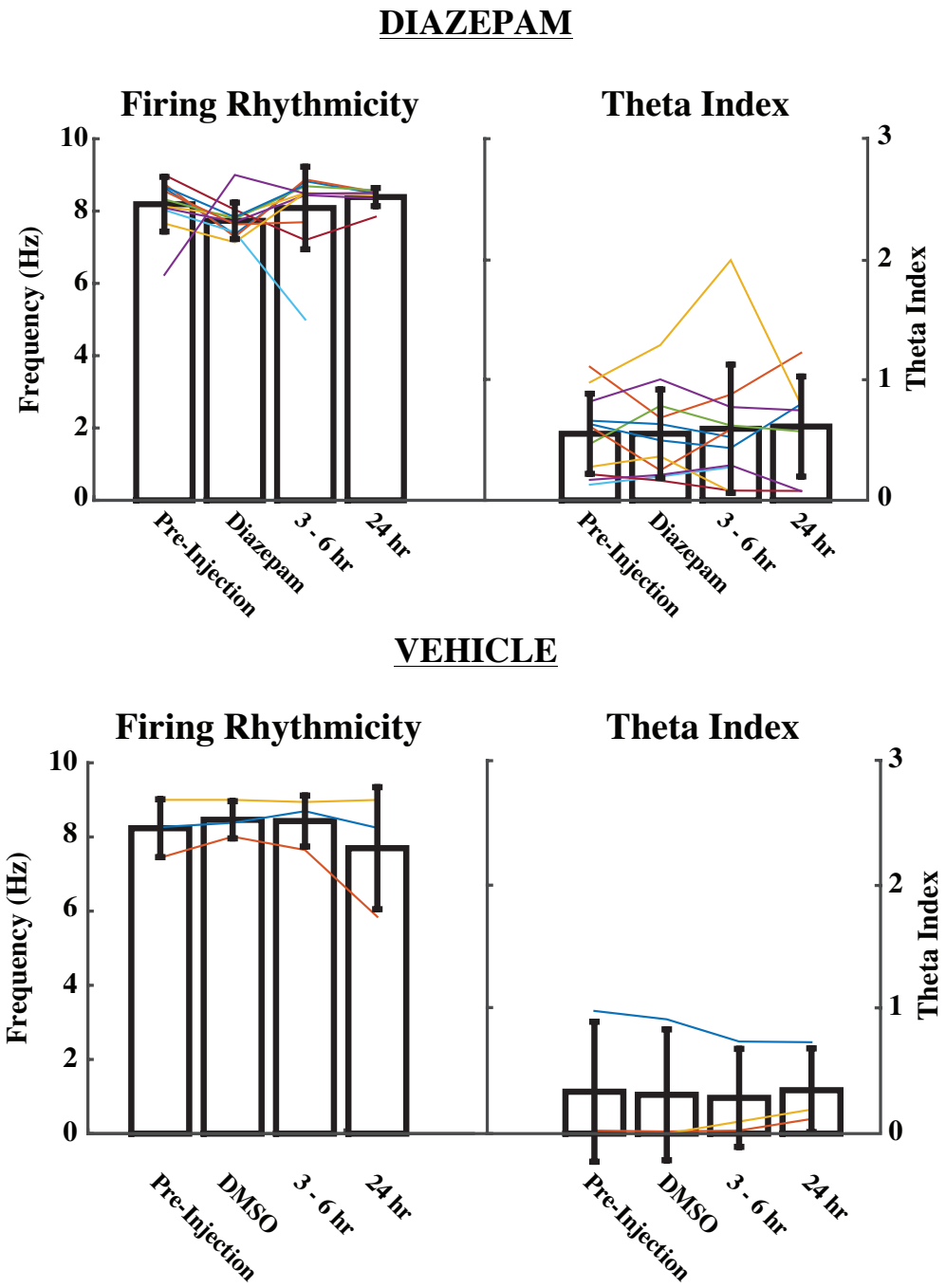

Figure 3.8. A decrease in intrinsic rhythmicity of grid cell firing did not reach significance after diazepam injection.

Firing rhythmicity (left) and theta index (right) for systemic injections of diazepam (top) and vehicle (bottom). Each cell recorded across sessions is marked by a single colored line. The vertical black line represents the standard error of measurement.

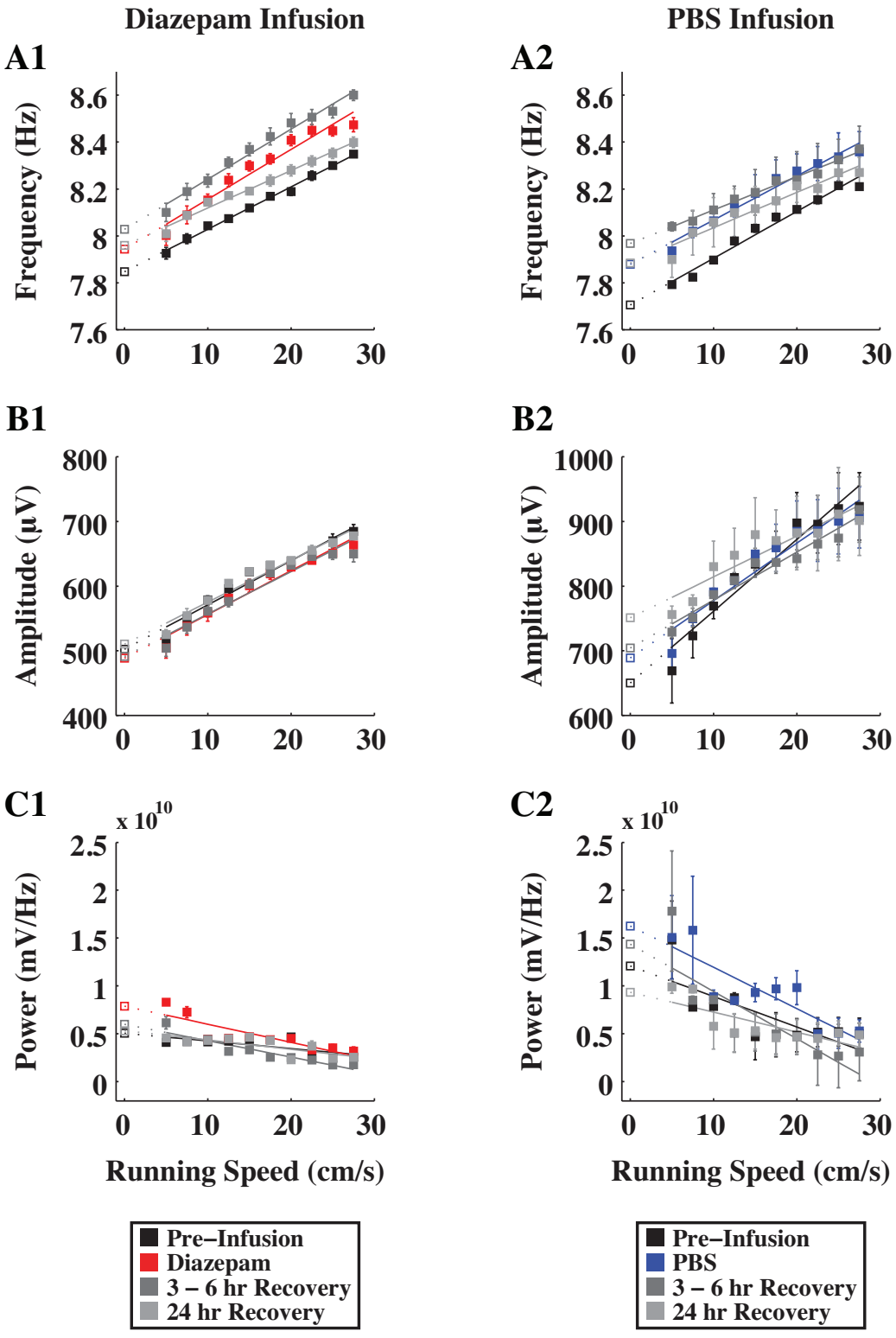
Diazepam Infusion
PBS Infusion
A1
A2
Frequency (Hz)
8.6
8.4
8.2
8
7.8
7.6
0
10
20
30
B1
B2
Amplitude (µV)
800
700
600
500
400
1000
900
800
700
600
C1
C2
x 10^10
Power (mV/Hz)
2.5
2
1.5
1
0.5
0
Running Speed (cm/s)
Pre–Infusion
Diazepam
3 – 6 hr Recovery
24 hr Recovery
Pre–Infusion
PBS
3 – 6 hr Recovery
24 hr Recovery

Figure 3.9. MS infusion of diazepam has no significant effect on LFP theta properties.

A. Effects of MS infusion (A1, red line) compared to baseline (black line) and recovery sessions (grey lines) on LFP theta frequency plotted across running speeds, and the same for vehicle (A2, blue line). B, C. Same as A but for theta amplitude and power, respectively.

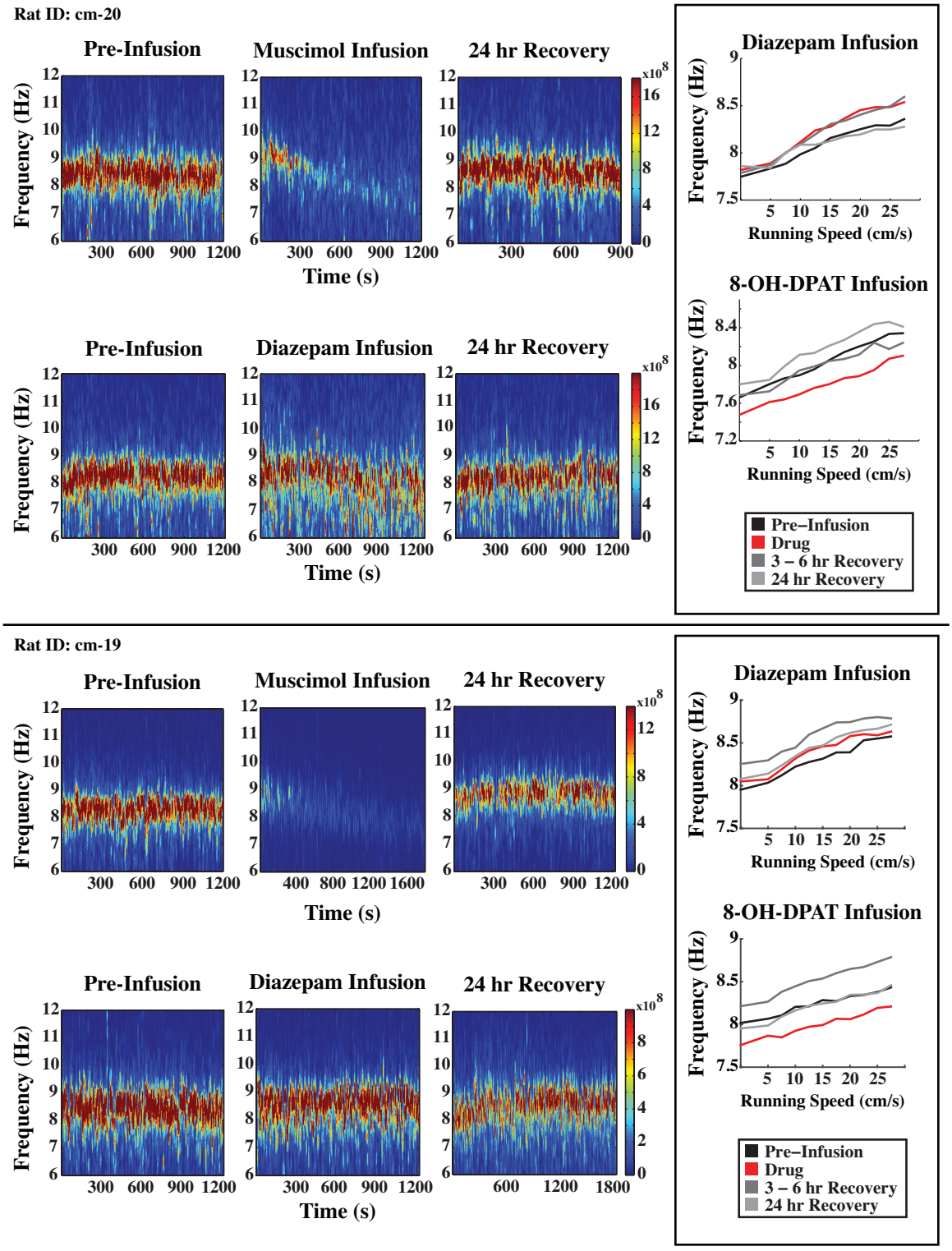
Rat ID: cm-20
Pre-Infusion
Muscimol Infusion
24 hr Recovery
Frequency (Hz)
Time (s)
x10^8
Pre-Infusion
Diazepam Infusion
24 hr Recovery
Frequency (Hz)
Time (s)
x10^8
Diazepam Infusion
Frequency (Hz)
Running Speed (cm/s)
8-OH-DPAT Infusion
Frequency (Hz)
Running Speed (cm/s)
Pre–Infusion
Drug
3 – 6 hr Recovery
24 hr Recovery
Rat ID: cm-19
Pre-Infusion
Muscimol Infusion
24 hr Recovery
Frequency (Hz)
Time (s)
x10^8
Pre-Infusion
Diazepam Infusion
24 hr Recovery
Frequency (Hz)
Time (s)
x10^8
Diazepam Infusion
Frequency (Hz)
Running Speed (cm/s)
8-OH-DPAT Infusion
Frequency (Hz)
Running Speed (cm/s)
Pre–Infusion
Drug
3 – 6 hr Recovery
24 hr Recovery

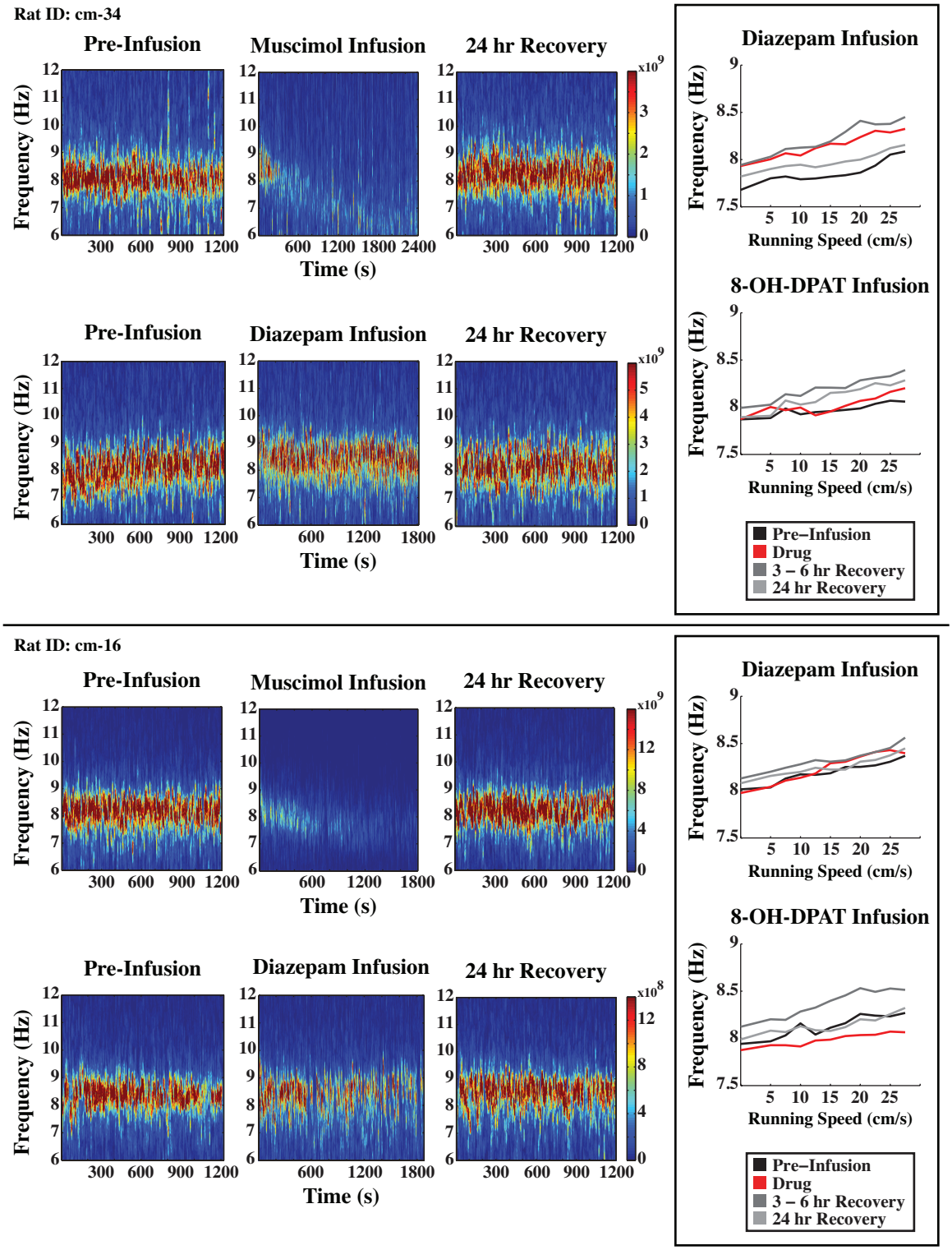

Figure 3.10. Spectrograms of the effects of infusions of muscimol and diazepam, and frequency versus speed plots after diazepam and 8-OH-DPAT infusion, for each of the four animals.

Spectrograms demonstrate loss of theta with muscimol but not with diazepam (left), and theta frequency versus running speed plots showing a decrease in the intercept of theta frequency after 8-OH-DPAT infusion but not diazepam.

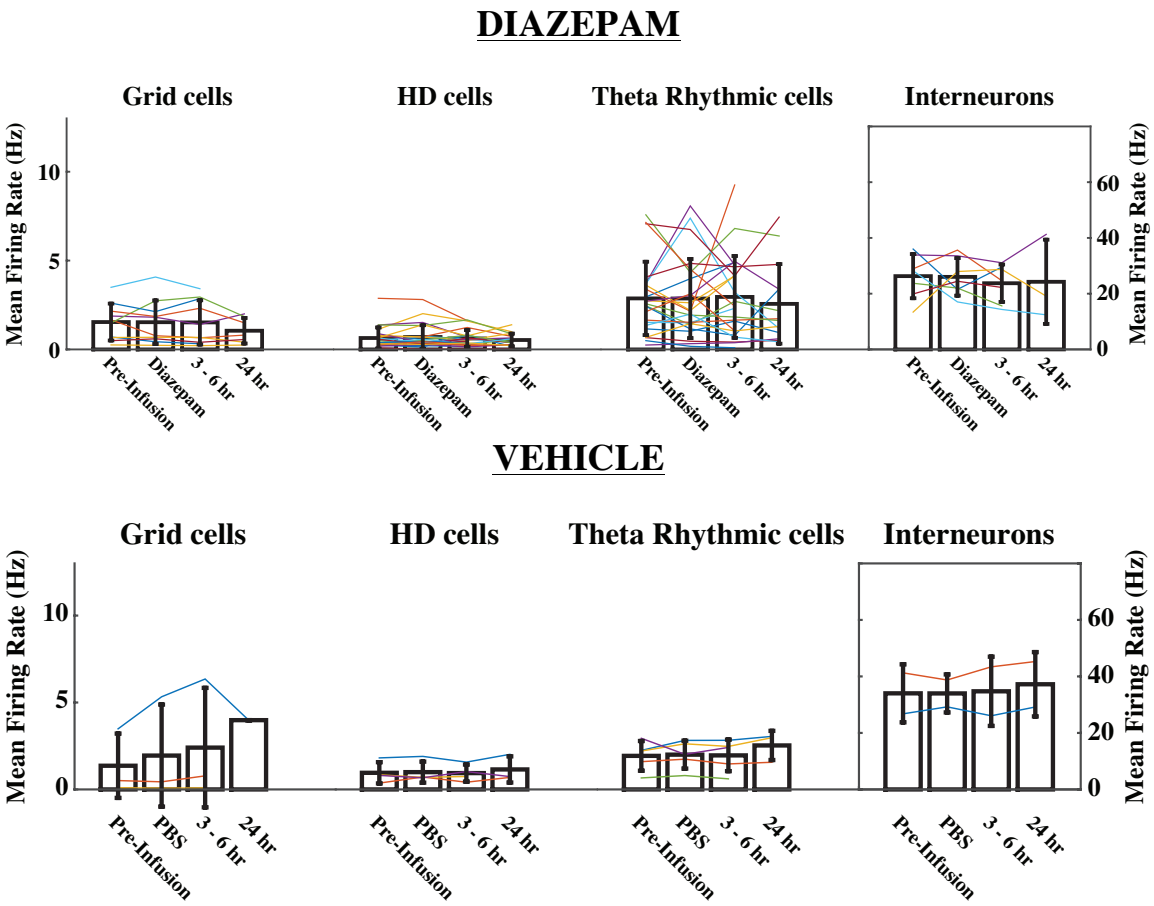

Figure 3.11. Mean firing rate for grid cells, HD cells, theta rhythmic cells, and interneurons across sessions.

No drug effects were seen after MS infusion of diazepam (top) or vehicle (bottom) on mean firing rate of grid cells, HD cells, theta rhythmic cells, or interneurons. Each cell recorded across sessions is marked by a single colored line. The vertical black line represents the standard error of measurement.

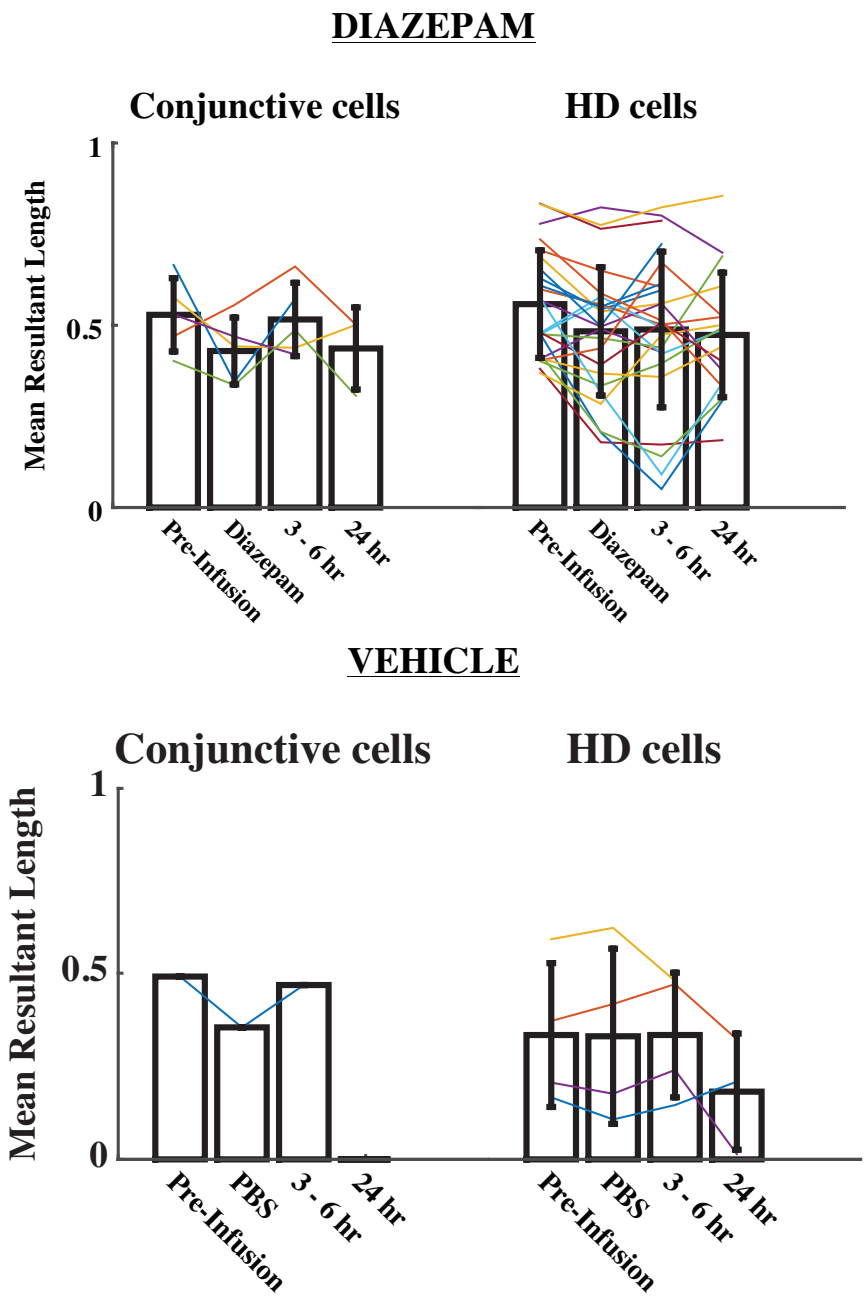

Figure 3.12. Mean resultant length of conjunctive and HD cells across sessions.

Directionality of cell firing across sessions for conjunctive grid cells and head direction cells after MS infusion of diazepam (top) and vehicle (bottom). No drug effects on directionality of firing for conjunctive head by grid cells or HD cells were seen. Each cell recorded across sessions is marked by a single colored line. The vertical black line represents the standard error of measurement.

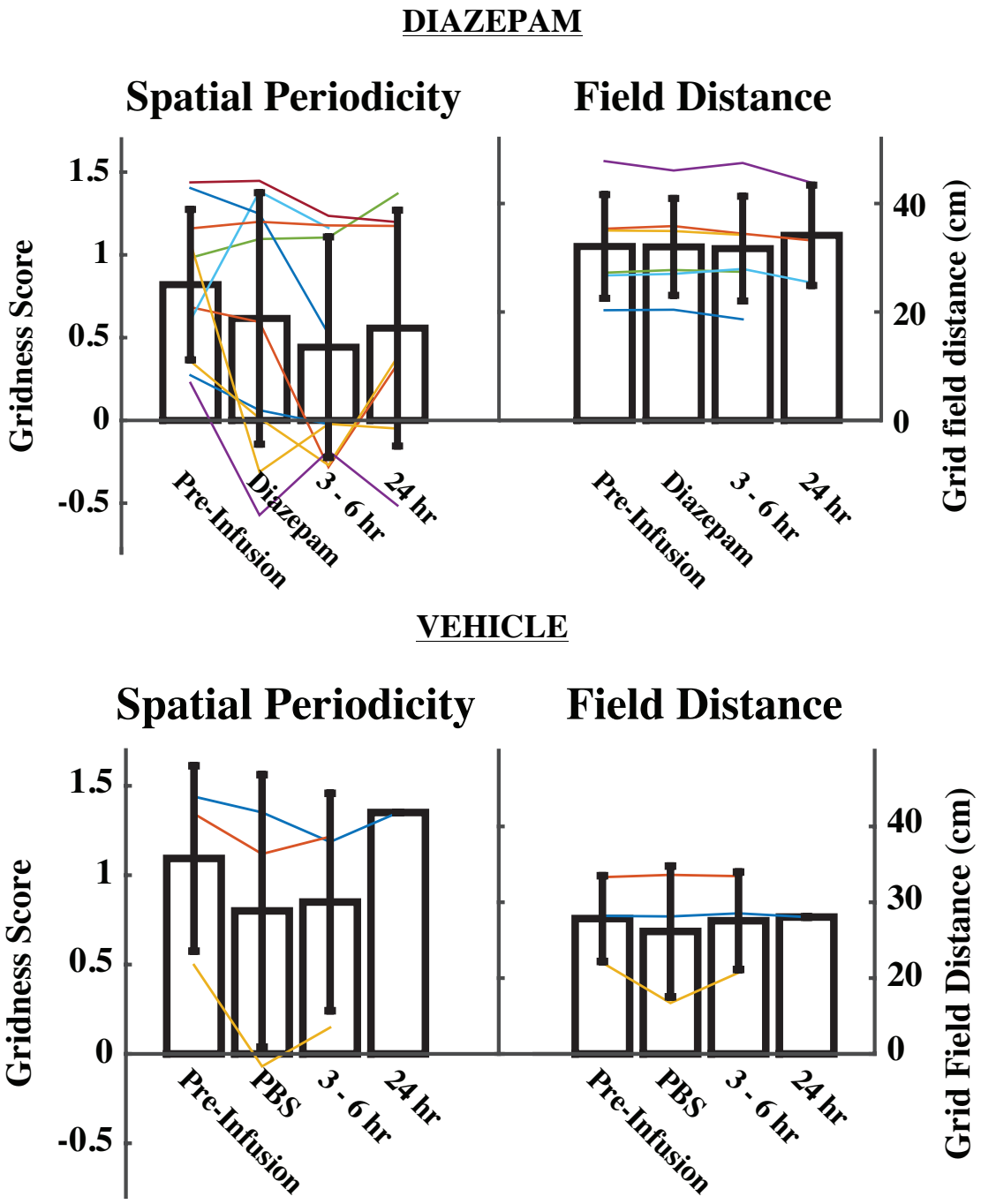

Figure 3.13. Spatial periodicity and grid field distances were unaffected by MS infusion of diazepam.

Gridness score (left) and grid field distance (right) of grid cells after MS infusion of diazepam (top) or vehicle (bottom). Each cell recorded across sessions is marked by a single colored line. The vertical black line represents the standard error of measurement.

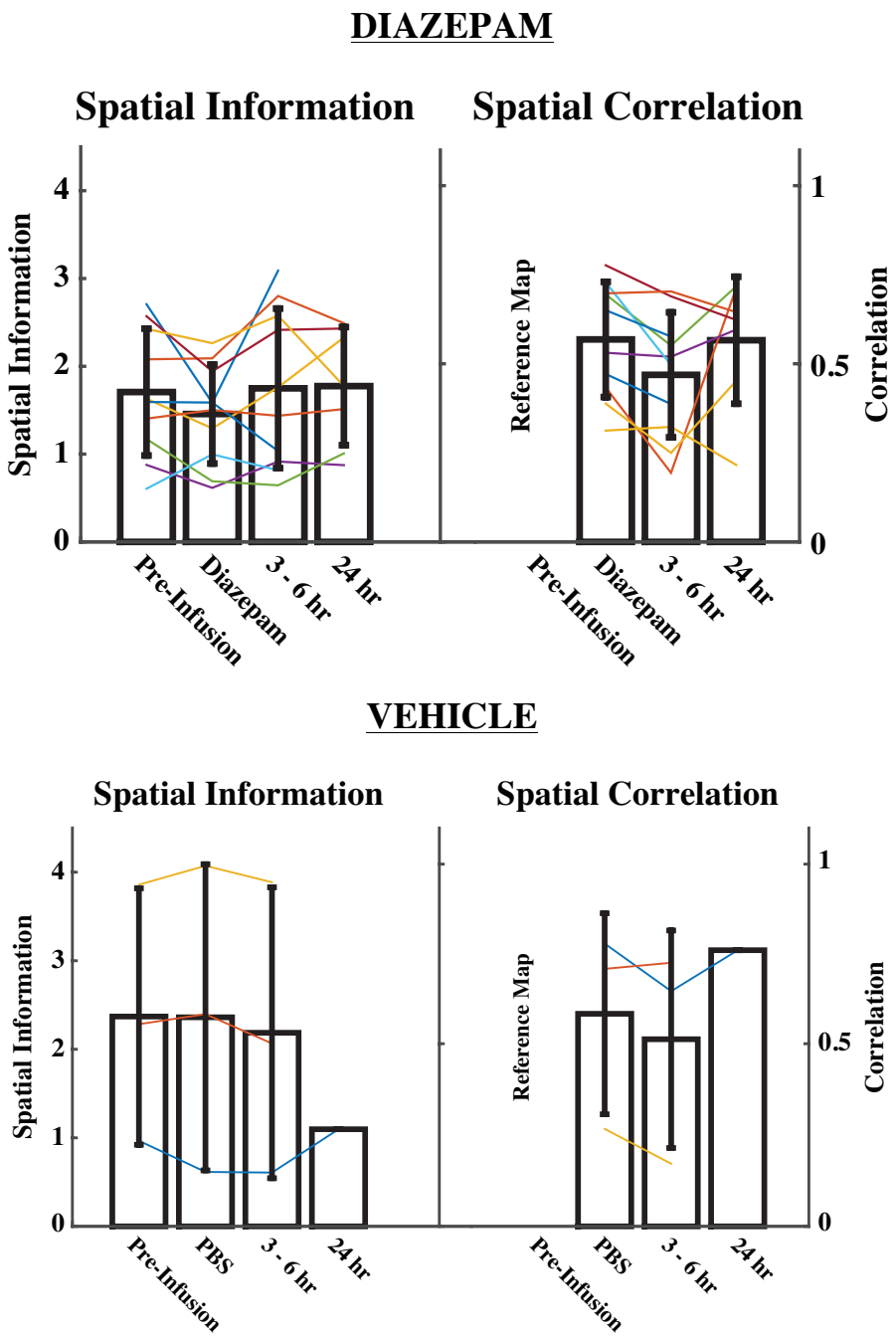

Figure 3.14. Spatial information score and correlation of rate maps of grid cells after MS infusion of diazepam or vehicle.

Measures of spatial firing after MS infusion of diazepam (top) or vehicle (bottom) for spatial information (left) and spatial correlation of rate maps (right). Each cell recorded across sessions is marked by a single colored line. The vertical black line represents the standard error of measurement.

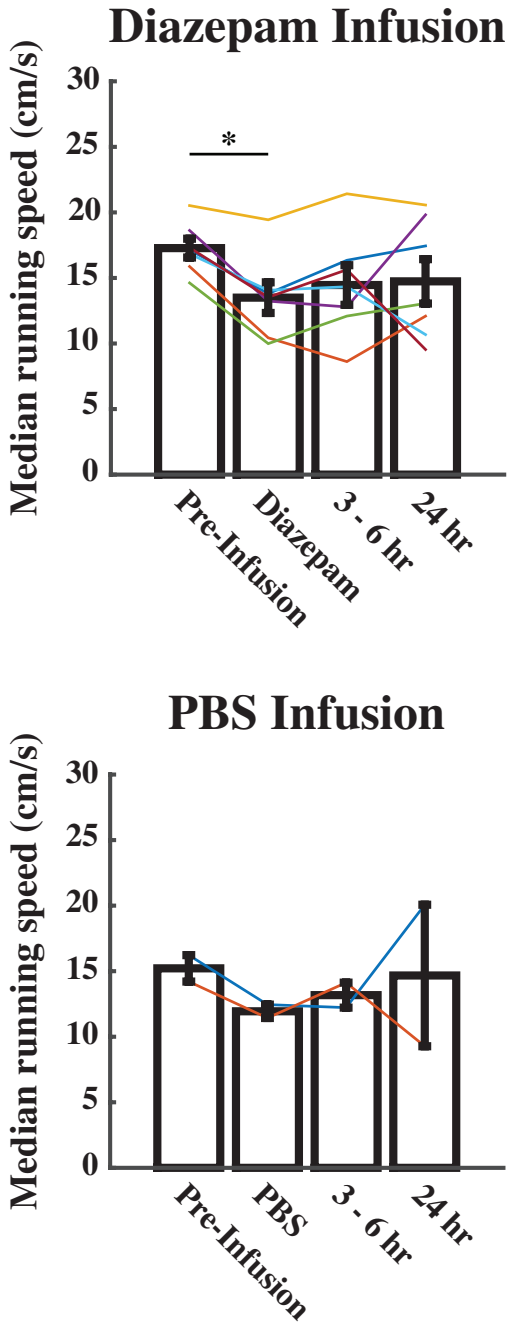

Figure 3.15. Median running speed (cm/s) across recording sessions significantly decreased after diazepam infusion.

A significant decrease in median running speed was seen after MS infusion of diazepam (top) in comparison to vehicle (bottom). Each session's median speed is marked by a single colored line. The vertical black line represents the standard error of measurement.

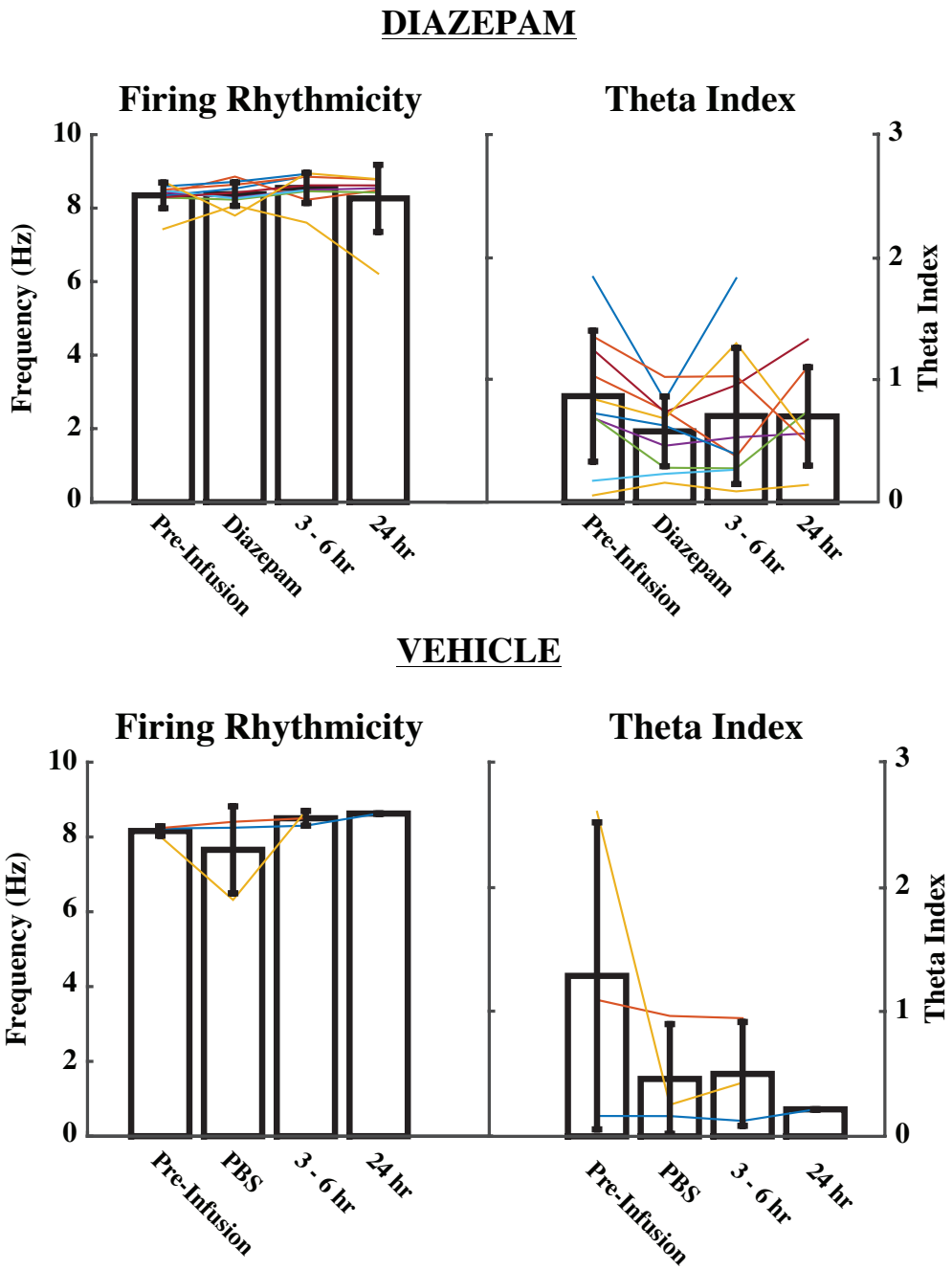

Figure 3.16. No significant differences were seen in intrinsic rhythmicity or theta index after diazepam infusion.

Firing rhythmicity (left) and theta index (right) for MS infusions of diazepam (top) and vehicle (bottom). Each cell recorded across sessions is marked by a single colored line. The vertical black line represents the standard error of measurement.

CHAPTER 4: Conclusion

4.1. Implications

Findings from this work suggest that the BDZ and serotonergic anxiolytic-induced decrease of theta frequency can be expanded from detection in hippocampal LFP theta to the MEC as well. There was a robust and significant decrease in the intercept of the regression line of the relationship between theta frequency and running speed as recorded in the LFP in the MEC for both types of anxiolytics when given systemically. The only effect seen on slope was after systemic administration of 8-OH-DPAT where it did not demonstrate an increase in slope common to multiple same day exposure sessions. However, it did not statistically differ from baseline and therefore was not outside a natural range of values. The effects of the drugs when given systemically on the intercept of theta frequency across running speeds largely corroborate recent data from Wells et al. (2013) from the hippocampus, despite recording in a different region and using different drugs within the two classes.

The findings that subthreshold membrane potential oscillations in layer II stellate cells are positively correlated with increasing depolarization, and the slope of the frequency versus depolarization relationship decreases for cells recorded at more ventral positions along the dorsoventral axis (also corresponding to changes in grid scale along the same axis) (Giocomo et al., 2007), has been used as evidence supporting the OIM (Burgess, 2008). Burgess (Burgess, 2008) also predicted a dissociation between the slope and intercept of the relationship between theta frequency and running speed and that specifically, changes in slope but not intercept would produce changes in grid scale. Given the evidence showing anxiolytics decrease not only theta frequency in general, but

also the slope of the relationship between frequency and the magnitude of stimulation in reticular stimulation evoked theta, it was thought that grid scale could be affected by anxiolytics as well. However, recent evidence specifically looking at the effects of anxiolytics on hippocampal theta frequency across running speeds has shown that the overall anxiolytic induced decrease in theta frequency comes from a decrease in the intercept of this relationship and not a change in slope (Wells et al., 2013). Therefore, if the same relationship holds true in the MEC then one would not expect a change in grid scale after administration of anxiolytics despite an overall decrease in theta frequency, based on this model. In line with this, these results support these predictions. Despite an overall decrease in mean theta frequency, no changes in grid scale were seen. Much like hippocampal results reported by Wells et al. (2013), systemic administration of both a serotonergic anxiolytic and a BDZ decreased the intercept of the relationship between theta frequency and running speed, but not the slope.

Results from this work did produce the novel finding that serotonergic anxiolytics could exert effects on theta frequency through the MS while BDZs cannot. Interestingly, in a septo-hippocampal model of the Wells et al. (2013) results, increasing synaptic conductance in the GABA-A mediated synapses was unable to produce changes in theta frequency, suggesting that systemic effects of BDZs on hippocampal theta might be mediated outside of the circuit (John et al., 2014). This could support the negative finding of a lack of effect after MS infusion of diazepam on MEC theta frequency despite a significant decrease following systemic administration. John et al. (2014) suggest the reduction could be mediated by medial hypothalamic sites, such as the medial

supramammillary nucleus, since infusion of a BDZ into that location mimics systemic administration results (Woodnorth and McNaughton, 2002). Future research could confirm this by recording MEC activity after infusing a BDZ into the supramammillary nucleus and comparing to systemic results.

Unlike infusions of diazepam, infusion of 8-OH-DPAT produced a statistically significant decrease in the intercept of theta frequency across running speeds, suggesting the mechanism of action underlying systemic effects of the drug could in some way be mediated through the MS. It is not clear if the MS is solely responsible for the drug action on theta frequency. While the decrease in theta frequency appears to be somewhat smaller than for systemic administration, this study did not look at the effects of different doses, which could affect the extent of the decrease in frequency. Furthermore, the median raphe nuclei provide dense serotonergic and non-serotonergic innervation of the MEC, hippocampus, and septal nuclei (Köhler and Steinbusch, 1982; Köhler et al., 1982), and manipulation of the median raphe can affect hippocampal theta rhythm (Kinney et al., 1994; Vertes et al., 1994). It is possible that systemic effects are mediated through the raphe nuclei and the MS is simply capable of, but not required for, producing effects on MEC theta frequency.

Systemic administration or MS infusion of diazepam did not appear to affect any single unit properties of grid cells, including spatial periodicity. MS infusions of the GABA-A agonist, muscimol, greatly reduce theta power and grid cell spatial periodicity (Brandon et al., 2011), however, it appears that despite positively modulating the same receptor, diazepam does not have the same effect. As diazepam is a positive modulator

of GABA-A receptors, working through the BDZ site, the extent of its effects are limited by the GABA release of an afferent neuron. Unlike muscimol, application of this drug to an area does not necessarily silence it through inhibiting local neurons and therefore its potential effects may be limited that way.

The only effect on a single unit firing property across all experiments was a decrease in the intrinsic rhythmicity found the firing of grid cells after 8-OH-DPAT systemic administration. It is possible this decrease is due to phase locking of grid cell firing to LFP theta. As LFP theta frequency decreases, if the cell maintains phase locking then it should slow its rhythmic firing slightly. That this effect is seen in systemic but not MS infusion of 8-OH-DPAT could reflect the magnitude of decrease necessary for the sensitivity of picking up this small change in firing. The figure showing the effects of MS infusion of 8-OH-DPAT does suggest a trend, but again does not reach significance (Figure 2.14, top left). While systemic administration of diazepam robustly decreased LFP theta frequency as well, there was not a significant change in the intrinsic rhythmicity of grid cell firing. However, the figure showing the change in rhythmicity (Figure 3.8, top left) does appear to show a trend, very similar to 8-OH-DPAT systemic administration, except for one cell. It could be that this outlier could be affecting what would otherwise be a significant effect, which increasing the sample size could address. Overall however, it appears that except in one single case, neither anxiolytic is able to produce changes in single unit firing properties—the mechanisms underlying their activity appear robust to anxiolytic-induced perturbations of the system.

4.2. Future directions

The data presented here are preliminary and increasing the sample size will help clarify and solidify effects. Furthermore, infusions of DMSO (diazepam vehicle) will be necessary to ensure the compound is not neutralizing any potential effects that might otherwise be seen, corroborating previously reported data in the literature that showed no effects from DMSO infusions on activity.

Ideally, it would also be interesting to observe effects on phase precession of grid cell firing, where spikes occur at earlier phases as an animal traverses through a grid cell's receptive field. However, due to the angle of approach toward the MEC, tetrodes pass through deeper layers first and make recording from phase precession-rich layer II less likely.

The finding that MS infusion of diazepam did not have an effect on MEC theta frequency supports the theory that benzodiazepines exert their frequency modulating effects through other nuclei, possibly the supramammillary nucleus (Woodnorth and McNaughton, 2002). An obvious next step from this would be to infuse a BDZ into the supramammillary nucleus and record MEC theta, looking for changes in frequency. An interesting addition to this might be to also test other anxiolytics, such as serotonergic-based ones. Since application of serotonergic 1A receptor agonists into the median raphe, which provides serotonergic input throughout the brain, disrupts hippocampal theta instead of modulating it, this suggests the anxiolytic-induced decrease in theta frequency by serotonergic anxiolytics could be mediated elsewhere. The medial supramammillary nucleus receives cholinergic input from medial septum and serotonergic input from

dorsal raphe (Gonzalo-Ruiz et al., 1999), so it is possible the effects of serotonergic anxiolytics could be mediated through this region.

REFERENCES

Acquas E, Wilson C, Fibiger HC (1996) Conditioned and unconditioned stimuli increase frontal cortical and hippocampal acetylcholine release: effects of novelty, habituation, and fear. Journal of Neuroscience 16:3089–3096.

Alonso A, García-Austt E (1987a) Neuronal sources of theta rhythm in the entorhinal cortex of the rat. I. Laminar distribution of theta field potentials. Experimental Brain Research 67:493–501.

Alonso A, García-Austt E (1987b) Neuronal sources of theta rhythm in the entorhinal cortex of the rat. II. Phase relations between unit discharges and theta field potentials. Experimental Brain Research 67:502–509.

Alonso A, Köhler C (1984) A study of the reciprocal connections between the septum and the entorhinal area using anterograde and retrograde axonal transport methods in the rat brain. Journal of Comparative Neurology 225:327–343.

Andersen P, Bland H, Myhrer T, Schwartzkroin P (1979) Septo-hippocampal pathway necessary for dentate theta production. Brain Research 165:13–22.

Arolfo MP, Brioni JD (1991) Diazepam impairs place learning in the Morris water maze. Behavioral and Neural Biology 55:131–136.

Baisden RH, Woodruff ML, Hoover DB (1984) Cholinergic and non-cholinergic septo-hippocampal projections: a double-label horseradish peroxidase-acetylcholinesterase study in the rabbit. Brain Research 290:146–151.

Barry C, Ginzberg LL, O'Keefe J, Burgess N (2012) Grid cell firing patterns signal environmental novelty by expansion. Proceedings of the National Academy of Sciences of the United States of America 109:17687–17692.

Barry C, Lever C, Hayman R, Hartley T, Burton S, O'Keefe J, Jeffery K, Burgess N (2006) The boundary vector cell model of place cell firing and spatial memory. Reviews in the Neurosciences 17:71–97.

Belchior H, Lopes-dos-Santos V, Tort ABL, Ribeiro S (2014) Increase in hippocampal theta oscillations during spatial decision making. Hippocampus 24:693–702.

Bjerknes TL, Moser EI, Moser M-B (2014) Representation of Geometric Borders in the Developing Rat. Neuron 7:1–8.

Blackstad TW, Kjaerheim A (1961) Special axo-dendritic synapses in the hippocampal cortex: electron and light microscopic studies on the layer of mossy fibers. Journal of Comparative Neurology 117:133–159.

Bland BH (1986) The physiology and pharmacology of hippocampal formation theta rhythms. Progress in Neurobiology 26:1–54.

Boccara CN, Sargolini F, Thoresen VH, Solstad T, Witter MP, Moser EI, Moser M-B (2010) Grid cells in pre- and parasubiculum. Nature Neuroscience 13:987–994.

Bonnevie T, Dunn B, Fyhn M, Hafting T, Derdikman D, Kubie JL, Roudi Y, Moser EI, Moser M-B (2013) Grid cells require excitatory drive from the hippocampus. Nature Neuroscience 16:309–317.

Bostock E, Muller RU, Kubie JL (1991) Experience-dependent modifications of hippocampal place cell firing. Hippocampus 1:193–205.

Brandon MP, Bogaard AR, Libby CP, Connerney MA, Gupta K, Hasselmo ME (2011) Reduction of theta rhythm dissociates grid cell spatial periodicity from directional tuning. Science 332:595–599.

Brandon MP, Bogaard AR, Schultheiss NW, Hasselmo ME (2013) Segregation of cortical head direction cell assemblies on alternating theta cycles. Nature Neuroscience 16:739–748.

Brioni JD, Arolfo MP (1992) Diazepam impairs retention of spatial information without affecting retrieval or cue learning. Pharmacology, Biochemistry & Behavior 41:1–5.

Brun VH, Solstad T, Kjelstrup KB, Fyhn M, Witter MP, Moser EI, Moser M-B (2008) Progressive increase in grid scale from dorsal to ventral medial entorhinal cortex. Hippocampus 18:1200–1212.

Buetfering C, Allen K, Monyer H (2014) Parvalbumin interneurons provide grid cell-driven recurrent inhibition in the medial entorhinal cortex. Nature Neuroscience 17:710–718.

Bullock TH, Buzsáki G, McClune MC (1990) Coherence of compound field potentials reveals discontinuities in the CA1-subiculum of the hippocampus in freely-moving rats. Neuroscience 38:609–619.

Burak Y, Fiete IR (2009) Accurate path integration in continuous attractor network models of grid cells. PLoS Computational Biology 5:e1000291.

Burgess N (2008) Grid cells and theta as oscillatory interference: theory and predictions. Hippocampus 18:1157–1174.

Burgess N, Barry C, O'Keefe J (2007) An oscillatory interference model of grid cell firing. Hippocampus 17:801–812.

Burwell RD, Amaral DG (1998) Cortical afferents of the perirhinal, postrhinal, and entorhinal cortices of the rat. Journal of Comparative Neurology 398:179–205.

Bush D, Burgess N (2014) A Hybrid Oscillatory Interference/Continuous Attractor Network Model of Grid Cell Firing. Journal of Neuroscience 34:5065–5079.

Buzsáki G (2002) Theta Oscillations in the Hippocampus. Neuron 33:325–340.

Buzsáki G, Anastassiou CA, Koch C (2012) The origin of extracellular fields and currents--EEG, ECoG, LFP and spikes. Nature Reviews Neuroscience 13:407–420.

Buzsáki G, Leung LW, Vanderwolf CH (1983) Cellular bases of hippocampal EEG in the behaving rat. Brain Research 287:139–171.

Cacucci F, Wills TJ, Lever C, Giese KP, O'Keefe J (2007) Experience-dependent increase in CA1 place cell spatial information, but not spatial reproducibility, is dependent on the autophosphorylation of the alpha-isoform of the calcium/calmodulin-dependent protein kinase II. Journal of Neuroscience 27:7854–7859.

Canto CB, Koganezawa N, Beed P, Moser EI, Witter MP (2012) All layers of medial entorhinal cortex receive presubicular and parasubicular inputs. Journal of Neuroscience 32:17620–17631.

Canto CB, Wouterlood FG, Witter MP (2008) What does the anatomical organization of the entorhinal cortex tell us? Neural Plasticity:1–18.

Caudarella M, Durkin T, Galey D, Jeantet Y, Jaffard R (1987) The effect of diazepam on hippocampal EEG in relation to behavior. Brain Research 435:202–212.

Chrobak JJ, Buzsáki G (1998) Gamma oscillations in the entorhinal cortex of the freely behaving rat. Journal of Neuroscience 18:388–398.

Climer JR, Newman EL, Hasselmo ME (2013) Phase coding by grid cells in unconstrained environments: two-dimensional phase precession. European Journal of Neuroscience 38:2526–2541.

Colom L, Nassif-Caudarella S, Dickson CT, Smythe JW, Bland BH (1991) In vivo intrahippocampal microinfusion of carbachol and bicuculline induces theta-like oscillations in the septally deafferented hippocampus. Hippocampus 1:381–390.

Coop CF, McNaughton N (1991) Buspirone affects hippocampal rhythmical slow activity through serotonin1A rather than dopamine D2 receptors. Neuroscience 40:169–174.

Coop CF, McNaughton N, Scott DJ (1992) Pindolol antagonizes the effects on hippocampal rhythmical slow activity of clonidine, baclofen and 8-OH-DPAT, but not chlordiazepoxide and sodium amylobarbitone. Neuroscience 46:83–90.

Costa JC, Costa KM, do Nascimento JLM (2010) Scopolamine- and diazepam-induced amnesia are blocked by systemic and intraseptal administration of substance P and choline chloride. Peptides 31:1756–1760.

De Almeida RMM, Giovenardi M, Charchat H, Lucion AB (1998) 8-OH-DPAT in the median raphe nucleus decreases while in the medial septal area it may increase anxiety in female rats. Neuroscience and Biobehavioral Reviews 23:259–264.

Deshmukh SS, Knierim JJ (2011) Representation of non-spatial and spatial information in the lateral entorhinal cortex. Frontiers in Behavioral Neuroscience 5:69.

Dolorfo CL, Amaral DG (1998) Entorhinal cortex of the rat: organization of intrinsic connections. Journal of Comparative Neurology 398:49–82.

Dunn RW, Corbett R, Fielding S (1989) Effects of 5-HT1A receptor agonists and NMDA receptor antagonists in the social interaction test and the elevated plus maze. European Journal of Pharmacology 169:1–10.

Elvander-Tottie E, Eriksson TM, Sandin J, Ogren SO (2009) 5-HT(1A) and NMDA receptors interact in the rat medial septum and modulate hippocampal-dependent spatial learning. Hippocampus 19:1187–1198.

Fox SE, Wolfson S, Ranck JB (1986) Hippocampal theta rhythm and the firing of neurons in walking and urethane anesthetized rats. Experimental Brain Research 62:495–508.

Freund T, Antal M (1988) GABA-containing neurons in the septum control inhibitory interneurons in the hippocampus. Nature 336:170–173.

Fuhs MC, Touretzky DS (2006) A spin glass model of path integration in rat medial entorhinal cortex. Journal of Neuroscience 26:4266–4276.

Fyhn M, Hafting T, Treves A, Moser M-B, Moser EI (2007) Hippocampal remapping and grid realignment in entorhinal cortex. Nature 446:190–194.

Fyhn M, Molden S, Witter MP, Moser EI, Moser M-B (2004) Spatial representation in the entorhinal cortex. Science 305:1258–1264.

Gao B, Hornung J, Fritschy J (1995) Identification of distinct GABA A-receptor subtypes in cholinergic and parvalbumin-positive neurons of the rat and marmoset medial septum—diagonal band complex. Neuroscience 65:101–117.

Gaykema R, van der Kuil J, Hersh L, Luiten P (1991) Patterns of direct projections from the hippocampus to the medial septum-diagonal band complex: Anterograde tracing with Phaseolus vulgaris leucoagglutinin combined with immunohistochemistry of choline acetyltransferase. Neuroscience 43:349–360.

Gaykema RP, Luiten PGM, Nyakas C, Traber J (1990) Cortical projection patterns of the medial septum-diagonal band complex. Journal of Comparative Neurology 293:103–124.

Giocomo LM, Zilli EA, Fransén E, Hasselmo ME (2007) Temporal frequency of subthreshold oscillations scales with entorhinal grid cell field spacing. Science 315:1719–1722.

Gogolák G, Stumpf C, Petsche H, Sterc J (1968) The firing pattern of septal neurons and the form of the hippocampal theta wave. Brain Research 7:201–207.

Gonzalo-Ruiz A, Morte L, Flecha JM, Sanz JM (1999) Neurotransmitter characteristics of neurons projecting to the supramammillary nucleus of the rat. Anatomy and Embryology 200:377–392.

Green JD, Arduini AA (1954) Hippocampal electrical activity in arousal. Journal of Neurophysiology 17:533–557.

Guanella A, Verschure PFMJ (2007) Prediction of the position of an animal based on populations of grid and place cells: a comparative simulation study. Journal of Integrative Neuroscience 6:433–446.

Hafting T, Fyhn M, Bonnevie T, Moser M-B, Moser EI (2008) Hippocampus-independent phase precession in entorhinal grid cells. Nature 453:1248–1252.

Hafting T, Fyhn M, Molden S, Moser M-B, Moser EI (2005) Microstructure of a spatial map in the entorhinal cortex. Nature 436:801–806.

Hargreaves EL, Rao G, Lee I, Knierim JJ (2005) Major dissociation between medial and lateral entorhinal input to dorsal hippocampus. Science 308:1792–1794.

Hasselmo ME (2014) Neuronal rebound spiking, resonance frequency and theta cycle skipping may contribute to grid cell firing in medial entorhinal cortex. Philosophical Transactions of the Royal Society B 369:1–11.

Hasselmo ME, Brandon MP (2012) A model combining oscillations and attractor dynamics for generation of grid cell firing. Frontiers in Neural Circuits 6:30.

Hasselmo ME, Shay CF (2014) Grid cell firing patterns may arise from feedback interaction between intrinsic rebound spiking and transverse traveling waves with multiple heading angles. Frontiers in Systems Neuroscience 8:201.

Helmstetter FJ (1993) Stress-induced hypoalgesia and defensive freezing are attenuated by application of diazepam to the amygdala. Pharmacology, Biochemistry & Behavior 44:433–438.

Heys JG, Giocomo LM, Hasselmo ME (2010) Cholinergic modulation of the resonance properties of stellate cells in layer II of medial entorhinal cortex. Journal of Neurophysiology 104:258–270.

Hoyer D, Hannon JP, Martin GR (2002) Molecular, pharmacological and functional diversity of 5-HT receptors. Pharmacology, Biochemistry, and Behavior 71:533–554.

Imperato A, Dazzi L, Obinu MC, Gessa GL, Biggio G (1994) The benzodiazepine receptor antagonist flumazenil increases acetylcholine release in rat hippocampus. Brain Research 647:167–171.

Inglis FM, Day JC, Fibiger HC (1994) Enhanced acetylcholine release in hippocampus and cortex during the anticipation and consumption of a palatable meal. Neuroscience 62:1049–1056.

Insausti R, Herrero MT, Witter MP (1997) Entorhinal cortex of the rat: cytoarchitectonic subdivisions and the origin and distribution of cortical efferents. Hippocampus 7:146–183.

Isayama S, Sugimoto Y, Nishiga M, Kamei C (2001) Effects of histidine on working memory deficits induced by the 5-HT 1A-receptor agonist 8-OH-DPAT. Japanese Journal of Pharmacology 86:451–453.

Jeewajee A, Barry C, O'Keefe J, Burgess N (2008) Grid cells and theta as oscillatory interference: electrophysiological data from freely moving rats. Hippocampus 18:1175–1185.

Jeffery KJ, Donnett JG, O'Keefe J (1995) Medial septal control of theta-correlated unit firing in the entorhinal cortex of awake rats. Neuroreport 6:2166–2170.

Jeltsch H, Bertrand F, Galani R, Lazarus C, Schimchowitsch S, Cassel J-C (2004) Intraseptal injection of the 5-HT1A/5-HT7 agonist 8-OH-DPAT and working memory in rats. Psychopharmacology 175:37–46.

Jiménez-Velázquez G, López-Muñoz FJ, Fernández-Guasti A (2010) Parallel anxiolytic-like and antinociceptive actions of diazepam in the anterior basolateral amygdala and dorsal periaqueductal gray. Brain Research 1349:11–20.

John T, Kiss T, Lever C, Érdi P (2014) Anxiolytic drugs and altered hippocampal theta rhythms: the quantitative systems pharmacological approach. Network 25:20–37.

Kamondi A, Acsády L, Wang XJ, Buzsáki G (1998) Theta oscillations in somata and dendrites of hippocampal pyramidal cells in vivo: activity-dependent phase-precession of action potentials. Hippocampus 8:244–261.

Kerr K, Agster K, Furtak S, Burwell RD (2007) Functional neuroanatomy of the parahippocampal region: the lateral and medial entorhinal areas. Hippocampus 17:697–708.

Kia HK, Brisorgueil MJ, Daval G, Langlois X, Hamon M, Vergé D (1996) Serotonin1A receptors are expressed by a subpopulation of cholinergic neurons in the rat medial septum and diagonal band of Broca--a double immunocytochemical study. Neuroscience 74:143–154.

King C, Recce M, O'Keefe J (1998) The rhythmicity of cells of the medial septum/diagonal band of Broca in the awake freely moving rat: relationships with behaviour and hippocampal theta. European Journal of Neuroscience 10:464–477.

Kinney GG, Kocsis B, Vertes RP (1994) Injections of excitatory amino acid antagonists into the median raphe nucleus produce hippocampal theta rhythm in the urethane-anesthetized rat. Brain Research 654:96–104.

Kinney GG, Kocsis B, Vertes RP (1995) Injections of muscimol into the median raphe nucleus produce hippocampal theta rhythm in the urethane anesthetized rat. Psychopharmacology 120:244–248.

Klancnik JM, Baimbridge KG, Phillips AG (1989) Increased population spike amplitude in the dentate gyrus following systemic administration of 5-hydroxytryptophan or 8-hydroxy-2-(di-n-propylamino)tetralin. Brain Research 505:145–148.

Klink R, Alonso A (1997) Muscarinic modulation of the oscillatory and repetitive firing properties of entorhinal cortex layer II neurons. Journal of Neurophysiology 77:1813–1828.

Koenig J, Cosquer B, Cassel JCJ (2008) Activation of septal 5-HT1A receptors alters spatial memory encoding, interferes with consolidation, but does not affect retrieval in rats subjected to a water-maze task. Hippocampus 18:99–118.

Koenig J, Linder AN, Leutgeb JK, Leutgeb S (2011) The spatial periodicity of grid cells is not sustained during reduced theta oscillations. Science 332:592–595.

Köhler C, Chan-Palay V, Steinbusch H (1982) The distribution and origin of serotonin-containing fibers in the septal area: a combined immunohistochemical and

fluorescent retrograde tracing study in the rat. Journal of Comparative Neurology 209:91–111.

Köhler C, Chan-Palay V, Wu J (1984) Septal neurons containing glutamic acid decarboxylase immunoreactivity project to the hippocampal region in the rat brain. Anatomy and Embryology 169:41–44.

Köhler C, Steinbusch H (1982) Identification of serotonin and non-serotonin-containing neurons of the mid-brain raphe projecting to the entorhinal area and the hippocampal formation. A combined immunohistochemical and fluorescent retrograde tracing in the rat brain. Neuroscience 7:951–975.

Kramis R, Vanderwolf CH, Bland BH (1975) Two types of hippocampal rhythmical slow activity in both the rabbit and the rat: relations to behavior and effects of atropine, diethyl ether, urethane, and pentobarbital. Experimental Neurology 49:58–85.

Krnjević K, Ropert N, Casullo J (1988) Septohippocampal disinhibition. Brain Research 438:182–192.

Leung LS (1984) Theta rhythm during REM sleep and waking: Correlations between power, phase and frequency. Electroencephalography and Clinical Neurophysiology 58:553–564.

Leung LS, Shen B (2004) Glutamatergic synaptic transmission participates in generating the hippocampal EEG. Hippocampus 14:510–525.

Leung SW (1979) Potentials evoked by alvear tract in hippocampal CA1 region of rats. II. Spatial field analysis. Journal of Neurophysiology 42:1571–1589.

Leutgeb S, Leutgeb JK, Barnes CA, Moser EI, McNaughton BL, Moser M-B (2005) Independent codes for spatial and episodic memory in hippocampal neuronal ensembles. Science 309:619–623.

Lever C, Burton S, Jeewajee A, O'Keefe J, Burgess N (2009) Boundary vector cells in the subiculum of the hippocampal formation. Journal of Neuroscience 29:9771–9777.

Liao R-M, Chuang F-J (2003) Differential effects of diazepam infused into the amygdala and hippocampus on negative contrast. Pharmacology, Biochemistry, & Behavior 74:953–960.

Lüttgen M, Ogren SO, Meister B (2005) 5-HT1A receptor mRNA and immunoreactivity in the rat medial septum/diagonal band of Broca-relationships to GABAergic and cholinergic neurons. Journal of Chemical Neuroanatomy 29:93–111.

Manns ID, Mainville L, Jones BE (2001) Evidence for glutamate, in addition to acetylcholine and GABA, neurotransmitter synthesis in basal forebrain neurons projecting to the entorhinal cortex. Neuroscience 107:249–263.

Manuel-Apolinar L, Meneses A (2004) 8-OH-DPAT facilitated memory consolidation and increased hippocampal and cortical cAMP production. Behavioural Brain Research 148:179–184.

McNaughton BL, Battaglia FP, Jensen O, Moser EI, Moser M-B (2006) Path integration and the neural basis of the "cognitive map". Nature Reviews Neuroscience 7:663–678.

McNaughton N, Coop CF (1991) Neurochemically dissimilar anxiolytic drugs have common effects on hippocampal rhythmic slow activity. Neuropharmacology 30:855–863.

McNaughton N, Kocsis B, Hajós M (2007) Elicited hippocampal theta rhythm: a screen for anxiolytic and procognitive drugs through changes in hippocampal function? Behavioural Pharmacology 18:329–346.

McNaughton N, Richardson J, Gore C (1986) Reticular elicitation of hippocampal slow waves: common effects of some anxiolytic drugs. Neuroscience 19:899–903.

Menard JL, Treit D (1998) The septum and the hippocampus differentially mediate anxiolytic effects of R(+)-8-OH-DPAT. Behavioural Pharmacology 9:93–101.

Mitchell S, Ranck JB (1980) Generation of theta rhythm in medial entorhinal cortex of freely moving rats. Brain Research 189:49–66.

Mitchell S, Rawlins J, Steward O (1982) Medial septal area lesions disrupt theta rhythm and cholinergic staining in medial entorhinal cortex and produce impaired radial arm maze behavior in rats. Journal of Neuroscience 2:292–302.

Mizumori SJ, Barnes CA, McNaughton BL (1989) Reversible inactivation of the medial septum: selective effects on the spontaneous unit activity of different hippocampal cell types. Brain Research 500:99–106.

Mizuseki K, Sirota A, Pastalkova E, Buzsáki G (2009) Theta oscillations provide temporal windows for local circuit computation in the entorhinal-hippocampal loop. Neuron 64:267–280.

Myhrer T, Nguyen NHT, Enger S, Aas P (2006) Anticonvulsant effects of GABA(A) modulators microinfused into area tempestas or substantia nigra in rats exposed to soman. Archives of Toxicology 80:502–507.

Naber PA, Lopes Da Silva FH, Witter MP (2001) Reciprocal connections between the entorhinal cortex and hippocampal fields CA1 and the subiculum are in register with the projections from CA1 to the subiculum. Hippocampus 11:99–104.

Navratilova Z, Giocomo LM, Fellous JM, Hasselmo ME, McNaughton BL (2012) Phase precession and variable spatial scaling in a periodic attractor map model of medial entorhinal grid cells with realistic after-spike dynamics. Hippocampus 22:772–789.

Newman EL, Gillet SN, Climer JR, Hasselmo ME (2013) Cholinergic blockade reduces theta-gamma phase amplitude coupling and speed modulation of theta frequency consistent with behavioral effects on encoding. Journal of Neuroscience 33:19635–19646.

Nishikawa T, Scatton B (1986) Neuroanatomical site of the inhibitory influence of anxiolytic drugs on central serotonergic transmission. Brain Research 371:123–132.

O'Keefe J (1976) Place units in the hippocampus of the freely moving rat. Experimental Neurology 51:78–109.

O'Keefe J, Burgess N (2005) Dual phase and rate coding in hippocampal place cells: theoretical significance and relationship to entorhinal grid cells. Hippocampus 15:853–866.

O'Keefe J, Dostrovsky J (1971) The hippocampus as a spatial map. Preliminary evidence from unit activity in the freely-moving rat. Brain Research 34:171–175.

O'Keefe J, Recce ML (1993) Phase relationship between hippocampal place units and the EEG theta rhythm. Hippocampus 3:317–330.

Pazos A, Palacios JM (1985) Quantitative autoradiographic mapping of serotonin receptors in the rat brain. I. Serotonin-1 receptors. Brain Research 346:205–230.

Pellow S, Chopin P, File SE, Briley M (1985) Validation of open : closed arm entries in an elevated plus-maze as a measure of anxiety in the rat. Journal of Neuroscience Methods 14:149–167.

Petsche H, Stumpf C, Gogolák G (1962) The significance of the rabbit's septum as a relay station between the midbrain and the hippocampus I. The control of hippocampus arousal activity by the septum cells. Electroencephalography and Clinical Neurophysiology 14:202–211.

Quirk GJ, Stewart M (1988) Neurons in entorhinal cortex of etherized rats exhibit rhythmic bursting correlated with the hippocampal EEG. Annals of the New York Academy of Sciences 529:310–313.

Ranck JB (1973) Studies on single neurons in dorsal hippocampal formation and septum in unrestrained rats. I. Behavioral correlates and firing repertoires. Experimental Neurology 41:461–531.

Rawlins JN, Feldon J, Gray JA (1979) Septo-hippocampal connections and the hippocampal theta rhythm. Experimental Brain Research 37:49–63.

Sainsbury RS, Bland BH (1981) The effects of selective septal lesions on theta production in CA1 and the dentate gyrus of the hippocampus. Physiology & Behavior 26:1097–1101.

Sainsbury RS, Harris JL, Rowland GL (1987) Sensitization and hippocampal type 2 theta in the rat. Physiology and Behavior 41:489–493.

Samsonovich A, McNaughton BL (1997) Path integration and cognitive mapping in a continuous attractor neural network model. Journal of Neuroscience 17:5900–5920.

Santucci AC, Shaw C (2003) Peripheral 8-OH-DPAT and scopolamine infused into the frontal cortex produce passive avoidance retention impairments in rats. Neurobiology of Learning and Memory 79:136–141.

Sargolini F, Fyhn M, Hafting T, McNaughton BL, Witter MP, Moser M-B, Moser EI (2006) Conjunctive representation of position, direction, and velocity in entorhinal cortex. Science 312:758–762.

Savelli F, Yoganarasimha D, Knierim JJ (2008) Influence of boundary removal on the spatial representations of the medial entorhinal cortex. Hippocampus 18:1270–1282.

Scheffzük C, Kukushka VI, Vyssotski AL, Draguhn A, Tort AB, Brankačk J (2013) Global slowing of network oscillations in mouse neocortex by diazepam. Neuropharmacology 65:123–133.

Schlesiger MI, Cannova CC, Boublil BL, Hales JB, Mankin EA, Brandon MP, Leutgeb JK, Leibold C, Leutgeb S (2015) The medial entorhinal cortex is necessary for temporal organization of hippocampal neuronal activity. Nature Neuroscience 18:1123–1132.

Sharifzadeh M, Sharifzadeh K, Naghdi N, Ghahremani MH, Roghani A (2005) Posttraining intrahippocampal infusion of a protein kinase AII inhibitor impairs spatial memory retention in rats. Journal of Neuroscience Research 79:392–400.

Simson PE, Weiss JM (1989) Peripheral, but not local or intracerebroventricular, administration of benzodiazepines attenuates evoked activity of locus coeruleus neurons. Brain Research 490:236–242.

Skaggs WE, McNaughton BL, Wilson MA, Barnes CA (1996) Theta phase precession in hippocampal neuronal populations and the compression of temporal sequences. Hippocampus 6:149–172.

Sławińska U, Kasicki S (1998) The frequency of rat's hippocampal theta rhythm is related to the speed of locomotion. Brain Research 796:327–331.

Solstad T, Boccara CN, Kropff E, Moser M-B, Moser EI (2008) Representation of geometric borders in the entorhinal cortex. Science 322:1865–1868.

Sprouse JS, Aghajanian GK (1987) Electrophysiological responses of serotoninergic dorsal raphe neurons to 5-HT1A and 5-HT1B agonists. Synapse 1:3–9.

Stemmelin J, Lukovic L, Salome N, Griebel G (2005) Evidence that the lateral septum is involved in the antidepressant-like effects of the vasopressin V1b receptor antagonist, SSR149415. Neuropsychopharmacology 30:35–42.

Stensola H, Stensola T, Solstad T, Frøland K, Moser M-B, Moser EI (2012) The entorhinal grid map is discretized. Nature 492:72–78.

Steward O (1976) Topographic organization of the projections from the entorhinal area to the hippocampal formation of the rat. Journal of Comparative Neurology 167:285–314.

Steward O, Scoville SA (1976) Cells of origin of entorhinal cortical afferents to the hippocampus and fascia dentata of the rat. Journal of Comparative Neurology 169:347–370.

Stewart M, Quirk GJ, Barry M, Fox SE (1992) Firing relations of medial entorhinal neurons to the hippocampal theta rhythm in urethane anesthetized and walking rats. Experimental Brain Research 90:21–28.

Tamamaki N, Nojyo Y (1995) Preservation of topography in the connections between the subiculum, field CA1, and the entorhinal cortex in rats. Journal of Comparative Neurology 353:379–390.

Tan KR, Rudolph U, Lüscher C (2011) Hooked on benzodiazepines: GABAA receptor subtypes and addiction. Trends in Neurosciences 34:188–197.

Taube JS (2007) The head direction signal: origins and sensory-motor integration. Annual Review of Neuroscience 30:181–207.

Taube JS, Muller RU, Ranck JB (1990) Head-direction cells recorded from the postsubiculum in freely moving rats. I. Description and quantitative analysis. Journal of Neuroscience 10:420–435.

Terrian D, Gannon R, Rea M (1990) Glutamate is the endogenous amino acid selectively released by rat hippocampal mossy fiber synaptosomes concomitantly with prodynorphin-derived peptides. Neurochemical Research 15:1–5.

Toth K, Borhegyi Z, Freund T (1993) Postsynaptic targets of GABAergic hippocampal neurons in the medial septum-diagonal band of broca complex. Journal of Neuroscience 73:3712–3724.

Tronson NC, Schrick C, Guzman YF, Huh KH, Srivastava DP, Penzes P, Guedea AL, Gao C, Radulovic J (2009) Segregated populations of hippocampal principal CA1 neurons mediating conditioning and extinction of contextual fear. Journal of Neuroscience 29:3387–3394.

van Groen T, van Haren FJ, Witter MP, Groenewegen HJ (1986) The organization of the reciprocal connections between the subiculum and the entorhinal cortex in the cat: I. A neuroanatomical tracing study. Journal of Comparative Neurology 250:485–497.

van Haeften T, Baks-te-Bulte L, Goede PH, Wouterlood FG, Witter MP (2003) Morphological and numerical analysis of synaptic interactions between neurons in deep and superficial layers of the entorhinal cortex of the rat. Hippocampus 13:943–952.

Vanderwolf C (1969) Hippocampal electrical activity and voluntary movement in the rat. Electroencephalography and Clinical Neurophysiology 26:407–418.

Vergé D, Daval G, Patey A, Gozlan H, el Mestikawy S, Hamon M (1985) Presynaptic 5-HT autoreceptors on serotonergic cell bodies and/or dendrites but not terminals are of the 5-HT1A subtype. European Journal of Pharmacology 113:463–464.

Vertes RP, Kinney GG, Kocsis B, Fortin W (1994) Pharmacological suppression of the median raphe nucleus with serotonin1A agonists, 8-OH-DPAT and buspirone, produces hippocampal theta rhythm in the rat. Neuroscience 60:441–451.

Vertes RP, Kocsis B (1997) Brainstem-diencephalo-septohippocampal systems controlling the theta rhythm of the hippocampus. Neuroscience 81:893–926.

Wainer BH, Levey AI, Rye DB, Mesulam M-M, Mufson EJ (1985) Cholinergic and non-cholinergic septohippocampal pathways. Neuroscience Letters 54:45–52.

Warburton EC, Harrison AA, Robbins TW, Everitt BJ (1997) Contrasting effects of systemic and intracerebral infusions of the 5-HT(1A) receptor agonist 8-OH-DPAT on spatial short-term working memory in rats. Behavioural Brain Research 84:247–258.

Wells CE, Amos DP, Jeewajee A, Douchamps V, Rodgers J, O'Keefe J, Burgess N, Lever C (2013) Novelty and anxiolytic drugs dissociate two components of hippocampal theta in behaving rats. Journal of Neuroscience 33:8650–8667.

Whishaw IQ, Sutherland RJ (1982) Sparing of rhythmic slow activity (RSA or theta) in two hippocampal generators after kainic acid CA3 and CA4 lesions. Experimental Neurology 75:711–728.

Whishaw IQ, Vanderwolf CH (1973) Hippocampal EEG and behavior: changes in amplitude and frequency of RSA (theta rhythm) associated with spontaneous and learned movement patterns in rats and cats. Behavioral Biology 8:461–484.

Witter MP, Amaral DG (1991) Entorhinal cortex of the monkey: V. Projections to the dentate gyrus, hippocampus, and subicular complex. Journal of Comparative Neurology 307:437–459.

Witter MP, Groenewegen HJ, Lopes da Silva FH, Lohman AHM (1989) Functional organization of the extrinsic and intrinsic circuitry of the parahippocampal region. Progress in Neurobiology 33:161–253.

Witter MP, Naber PA, van Haeften T, Machielsen WCM, Rombouts SARB, Barkhof F, Scheltens P, Lopes da Silva FH (2000) Cortico-hippocampal communication by way of parallel parahippocampal-subicular pathways. Hippocampus 10:398–410.

Woodnorth M-A, McNaughton N (2002) Similar effects of medial supramammillary or systemic injection of chlordiazepoxide on both theta frequency and fixed-interval responding. Cognitive, Affective & Behavioral Neuroscience 2:76–83.

Ylinen A, Soltész I, Bragin A, Penttonen M, Sik A, Buzsáki G (1995) Intracellular correlates of hippocampal theta rhythm in identified pyramidal cells, granule cells, and basket cells. Hippocampus 5:78–90.

Zheng C, Bieri KW, Trettel SG, Colgin LL (2015) The relationship between gamma frequency and running speed differs for slow and fast gamma rhythms in freely behaving rats. Hippocampus 25:924–938.

Zugaro MB, Monconduit L, Buzsáki G (2005) Spike phase precession persists after transient intrahippocampal perturbation. Nature Neuroscience 8:67–71.

CURRICULUM VITAE

Caitlin K. Monaghan
caitlinkmonaghan@gmail.com
66 Englewood Avenue, Apt. 1, Brighton, MA 02135
(503) 329-7402
YOB: 1986

EDUCATION

Boston University Boston, MA
Ph.D., Neuroscience 2016

University of Oregon Eugene, OR
Masters, Psychology 2010

University of Oregon Eugene, OR
B.S., Psychology 2008

RESEARCH EXPERIENCE

Boston University Boston, MA
Postdoctoral Fellow May 2016 – present
Graduate Student Sept. 2010 – May 2016
Thesis under Dr. Michael Hasselmo: "Effects of pharmacological manipulations on activity in the medial entorhinal cortex."

- Constructed implantable drives to record brain activity in rats.
- Performed brain surgery to implant recording drives and drug delivery cannulae.
- Executed *in vivo* electrophysiology recordings in awake, behaving rats.
- Administered drugs via intraperitoneal injection or intracranial infusion.
- Identified effects of anxiolytics in a novel brain region and ruled out one hypothesized region mediating this effect.

University of Oregon Eugene, OR
Masters Student Sept. 2008 – May 2010
Masters thesis under Dr. Clifford Kentros: "Neural correlates of the mouse anterior cingulate cortex."

- Conducted electrophysiological recordings in awake, behaving mice.
- Responsible for running experiments, analyzing data, and reporting results.
- Trained in histology, surgery, and electrode array manufacture.
- Investigated long-term mnemonic representations in single unit firing patterns.

University of Oregon Eugene, OR
Undergraduate Research Assistant Sept. 2007 – Sept. 2008

- Worked on adapting a human visual working memory change/no-change detection task into a rat version.
- Collaborated with other researchers on technical aspects of project.

University of Oregon Eugene, OR
Undergraduate Research Assistant April 2007 – Sept. 2007

- Performed research with human subjects in verbal working memory think/no-think paradigm.
- Worked on additional project using eye-tracking technology and analyzed data.

TEACHING EXPERIENCE

Boston University Boston, MA
Guest lecturer, Drugs and Behavior Nov. 2013

University of Oregon Eugene, OR
Graduate Teaching Fellow Sept. 2008 – May 2009

- Led lab sections for Psychology Mind and Brain Lab nearly every week over two terms for a total of 6 sections and approximately 180 students.
- Consulted with Professor regarding student concerns and provided feedback.
- Gave presentations, organized discussions, facilitated group projects, graded homework, and met with students individually.

University of Oregon Eugene, OR
Basic Teaching Skills Training Sept. 2008

- Attended and participated in workshop that focused on strategies for getting students to prepare and participate, facilitating discussions, promoting critical thinking, using group work, grading, managing the class, and preparing for exams.

ADDITIONAL EXPERIENCE

Employer: Dr. David Northway, Ph.D. Eugene, OR
Psychometrician May 2006 – Sept. 2008

- Administered numerous psychological and neuropsychological tests including intelligence, memory, developmental, and executive functions tests, among others.
- Worked with a wide range of people including Social Security Disability applicants, Veterans, head injury patients, children, and elderly.
- Completed standard office duties such as answering the phone, scheduling appointments, billing, and transcription.
- Did research on a variety of esoteric subjects to include in patient evaluations and legal proceedings.
- Fixed computer hardware or software problems that occurred in the office.

SKILLS

Laboratory: In vivo electrophysiology, aseptic survival surgery, histology, intracranial drug infusion.

Computer: Proficient in Macintosh and Windows operating systems, Microsoft Word, Microsoft Excel, Microsoft Powerpoint, Adobe Illustrator, Adobe Photoshop, MATLAB.

PUBLICATIONS

Monaghan, CK, Chapman IV, GW, Hasselmo, ME (in prep) "Systemic administration but not medial septal infusion of the benzodiazepine, diazepam, reduces theta frequency in the medial entorhinal cortex."

Monaghan, CK, Chapman IV, GW, Hasselmo, ME (in prep) "Systemic administration and medial septal infusion of serotonin 1A receptor anxiolytic, 8-OH-DPAT, reduces theta frequency in the medial entorhinal cortex."

Newman, EL, Gupta, K, Climer, JR, **Monaghan, CK**, Hasselmo, ME (2012) "Cholinergic modulation of cognitive processing: insights drawn from computational models." Frontiers in Behavioral Neuroscience 6: 1-19.

Weible, AP, Rowland, DC, **Monaghan, CK**, Wolfgang, NT, Kentros, CG (2012) "Neural correlates of long-term object memory in the mouse anterior cingulate cortex." Journal of Neuroscience 32: 5598-5608.

POSTERS

Monaghan, CK, Chapman IV, GW, Hasselmo, ME (2015) "Medial septal infusion of a serotonin 1A receptor agonist anxiolytic reduces theta frequency in the medial entorhinal cortex." Poster at Society for Neuroscience conference 2015. Saturday, October 17, 2015.

Monaghan, CK, Chapman IV, GW, Hasselmo, ME (2014) "Effects of a benzodiazepine and a serotonin 1A receptor agonist on neural activity in the rat medial entorhinal cortex." Poster at Society for Neuroscience conference 2014. Monday, November 17, 2014.

Weible, AP, **Monaghan, CK**, Rowland, DC, Kentros, CG (2010) "Anterior cingulate cortex neurons reflect prior experience." Poster at Society for Neuroscience conference 2010. Monday, November 15, 2010.

References available upon request.